Empirical and Numerical Evaluation of Mechanisms in Gas Production from CH_4-Hydrates

Emphasis on Kinetics, Electrical Resistivity, Depressurization and CO_2-CH_4 Exchange

Knut Arne Birkedal

Dissertation for the degree philosophiae doctor (PhD)

at the University of Bergen

2013

December 13th

Preface

This dissertation is submitted to the Department of Physics and Technology, Faculty of Mathematics and Natural Sciences, University of Bergen in the partial fulfillment of the requirements for the degree philosophiae doctor (PhD) and serves as documentation of my work during my PhD study. This work summarizes experimental work done in laboratories at the University of Bergen and at the ConocoPhillips Technology Center in Bartlesville, OK, USA. Numerical work has been performed at Lawrence Berkeley National Laboratory in Berkeley, CA, USA, during a 6-month research term funded by the Fulbright Scholar Program. The work has been funded by Statoil, ConocoPhillips' program for gas hydrates, and the Norwegian Research Council as part of the project "In-situ imaging of CO_2 flow, storage and entrapment in subsurface aquifers and hydrocarbon reservoirs". The latter project included studies of CO2 storage by various mechanisms, but only work related to the storage potential in hydrates has been included in the PhD dissertation.

Acknowledgements

First of all, a special thanks to my supervisor Professor Arne Graue for providing such an interesting and challenging topic for my PhD. Thank you for your guidance and for many possibilities over the years.

Thanks to Professor Bjørn Kvamme for your guidance and discussion on theoretical issues.

Thanks to Dr. Geir Ersland for all on- and off-topic discussions. It has been a pleasure!

A special thanks to Jim Stevens, Dr. James Howard and Dr. Keith Hester for your assistance in the laboratory and for many great experiences in Bartlesville. It will be missed.

I would like to thank my fellow students over the years for a good environment, inspiring discussions and lots of coffee. A special thanks to Jarle Husebø and Lars Petter Hauge for collaboration over the years.

A special thanks to Dr. Tim Kneafsey for arranging my stay at Lawrence Berkeley National Laboratory. Your work in the lab is inspiring. Thanks to Dr. George Moridis for your assistance and guidance through TOUGH+HYDRATE. Thanks to everyone who made my time at LBNL memorable!

Thanks to the Norwegian Research Council for funding this project. Thanks to the Fulbright Program for financial support during my stay at LBNL.

I would like to thank Kristian Ytre-Hauge for your friendship over the years. It is much appreciated!

Thanks to my family, especially Tove and Magne, for your support and love.

Finally, a special thanks to my beautiful and caring wife Marie for your understanding, undemanding patience and love. Your love has kept me sane during busy times. Jonathan Hjalmar, you make me proud and show me what life is all about!

List of papers

1) ERSLAND, G., **BIRKEDAL, K.A.**, GRAUE, A. 2009. *"MRI Characterization of Hydrate Growth Pattern and Production Scenarios in Sandstone"* International Conference Gas Hydrates Resources Development, Moscow, Russia, November 17-18.

2) **BIRKEDAL, K.A.**, ERSLAND, G., HUSEBØ, J., KVAMME, B., GRAUE, A. 2010. *«Geomechanical Stability during CH_4 Production from Hydrates – Depressurization or CO_2 Sequestration with CO_2-CH_4 Exchange"* 44th US Rock Mechanics Symposium, Salt Lake City, Utah, USA, June 27-30.

3) **BIRKEDAL, K.A.**, FREEMAN, C.M., MORIDIS, G.J., GRAUE, A. *"Numerical Reproduction of Empirical Methane Hydrate Dissociation and Reformation in Sandstone"* To be submitted to "Energy & Fuels".

4) **BIRKEDAL, K.A.**, HAUGE, L.P., ERSLAND, G., GRAUE, A. *"Electrical Resistivity Measurements in Sandstone during CH_4 Hydrate Formation and CH_4-CO_2 Exchange"* Submitted to "Journal of Geophysical Research: Solid Earth".

5) **BIRKEDAL, K.A.**, ERSLAND, G., HAUGE, L.P., GRAUE, A. *"Transport Mechanisms for CO_2-CH_4 Exchange and Safe CO_2 Storage in Hydrate Bearing Sandstone "* Submitted to "International Journal of Greenhouse Gas Control".

List of additional papers and talks

1. **BIRKEDAL, K.A.**, ERSLAND, G., HUSEBØ, J., KVAMME, B., STEVENS, J., HOWARD, J. & GRAUE, A. 2009 . *"Impacts from Salinity on Hydrate Growth Pattern and Induction Time in Porous Sandstone"* AGU Fall Meeting Abstracts, Abstract and oral presentation.

2. **BIRKEDAL, K.A**., HAUGE, L.P., ERSLAND, G., STEVENS, J., HOWARD, J., HESTER, K. & GRAUE, A. 2011. *"Electrical Resistivity Measurements of CH_4-Hydrate Bearing Sandstone during Formation"* 7th International Conference on Gas Hydrates. Edinburgh, Scotland. Proceedings paper and poster.

3. **BIRKEDAL, K.A.**, ERSLAND, G. & GRAUE, A. 2011. "*In situ imaging of CO_2 flow, storage and entrapment in subsurface aquifers and hydrocarbon reservoirs*". *CLIMIT Seminar.* Oslo, Norway. Poster.

4. **BIRKEDAL, K. A.**, ERSLAND, G. & GRAUE, A. 2011. "*Gas Production from CH_4 Hydrates – Depressurization or CO_2 Injection?*" *SPE One Day Seminar* Bergen, Norway. Abstract and presentation.

5. HAUGE, L.P., **BIRKEDAL, K. A.**, ERSLAND, G. & GRAUE, A. 2012. "*MRI of Hydrate Formation and Gas Production from Hydrates by CO_2 Injection*". *Transatlantic Science Week.* Houston, USA. Abstract and presentation.

6. **BIRKEDAL, K. A.**, ERSLAND, G., HAUGE, L.P. & GRAUE, A. 2012. "*Accessing Vast Gas Resources by CO_2 Sequestration in Hydrates*". *Transatlantic Science Week.* Houston, USA. Abstract and presentation.

7. **BIRKEDAL, K. A.**, MORIDIS, G.J., KNEAFSEY, T.J. & GRAUE, A. 2012. *"Experimental and Numerical Study of Methane Hydrate Dissociation in Bentheim Sandstone"*. *Transatlantic Science Week.* Houston, USA. Abstract and poster.

8. ERSLAND, G., GRAUE, A. & **BIRKEDAL, K.A.** 2012. *"Impact of Residual Water on CH_4-CO_2 Exchange Rate in Hydrate-Bearing Sandstone"*. *AGU Fall Meeting Abstracts.* Abstract and presentation.

9. HAUGE, L. P., **BIRKEDAL, K.A.**, ERSLAND, G. & GRAUE, A. 2012. *"Effects of Initial Saturation and Salinity on Methane Hydrate Growth in Bentheim Sandstone"*. *AGU Fall Meeting Abstracts.* Abstract and poster.

10. **BIRKEDAL, K.A.**, HAUGE, L. P., ERSLAND, G. & GRAUE, A. 2012. *"Electrical Resistivity Measurements in Sandstone During CH_4 Hydrate Formation and CH_4-CO_2 Exchange"*. *AGU Fall Meeting Abstracts.* Abstract and presentation.

    Paper award: *Outstanding Student Paper Award*

11. HAUGE, L.P., GAUTEPLASS, J., EIDE, Ø., **BIRKEDAL, K. A.**, ERSLAND, G. & GRAUE, A. 2013. *"In situ Imaging of CO_2 Flow, Storage and Entrapment in Subsurface Aquifers and Hydrocarbon Reservoirs*". *CLIMIT Seminar.* Oslo, Norway. Poster

12. HAUGE, L.P., GAUTEPLASS, J., **BIRKEDAL, K. A.**, ERSLAND, G. & GRAUE, A. 2013. *"Pore-scale Modeling and in situ Imaging of CO_2 Injection in Brine Saturated Sandstone*". *CLIMIT Seminar.* Oslo, Norway. Poster

13. **BIRKEDAL, K.A.**, HAUGE, L. P., ERSLAND, G. & GRAUE, A. 2013. *"Electrical Resistivity Measurements in Bentheim Sandstone during CH_4 Hydrate Formation and CH_4-CO_2 Exchange*". *SPE One Day Seminar.* Bergen, Norway. Abstract and presentation.

Summary

Focus is shifted towards renewable energy and sources of natural gas as the demand for cleaner energy continues to increase with global awareness on anthropogenic climate change. Methane (CH_4) provides advantages such as high enthalpy upon combustion and low carbon imprint compared to other fossil fuels. Natural gas is therefore predicted to play an important role as the world moves from coal dependency towards a cleaner and more sustainable energy future.

Natural gas hydrate is a solid state of gas and water, where water molecules interconnect through hydrogen bonding to form a cavity which is stabilized by a gas molecule through van der Waals interaction forces. This reaction occurs where water and CH_4 coexist at low temperature and high pressure. In nature, such conditions are typically found in permafrost and sub-marine environments. Vast energy resources are associated with gas hydrates, where different models suggest that hydrates contain 10^{15} to 10^{17} m^3 CH_4 at standard temperature and pressure (STP). In comparison, the annual gas consumption in the US is about $7 \cdot 10^{11}$ m^3. Gas hydrates may therefore become a significant contributor in the future energy mix. Current technological challenges are related to *in situ* characterization for accurate saturation estimates, further advances in production technologies and continuous improvements of available numerical models through comparison with actual field- and core-scale data.

A synergy between gas production and safe CO_2 storage is achieved through CO_2 sequestration in hydrate bearing sediments, where CO_2 replaces the existing CH_4 molecule within the hydrate crystal. The process occurs because CO_2 offers favorable thermodynamic conditions. Salt was observed to impact the hydrate formation rate and the amount of excess water in **Paper 1**. Depressurization and diffusion-driven CO_2 exchange were compared, where Magnetic Resonance Imaging (MRI) was used to monitor production *in situ*. CO_2-CH_4 exchange was more abundant for high residual brine, and therefore sensitive to initial salt concentration. Depressurization was assumed to be limited by permeability and heat transfer. Current opinion on geomechanical issues related to hydrate bearing sediments was addressed in **Paper 2**. Hydrate decomposition through depressurization resulted in production of associated water with potential loss of structural integrity, as gas

hydrates enhance sediment shear strength through mineral interaction. The sediment shear strength was assumed to be maintained during the CO_2-CH_4 exchange process based on minor intensity variations.

Depressurization is considered a promising production method for gas hydrates. The technology is yet available from the conventional oil and gas industry, and little energy is required to promote dissociation relative to thermal stimulation. Empirical dissociation data were compared with predictions utilizing TOUGH+HYDRATE in **Paper 3**. Accurate predictions of heat and fluid flow within the sample were achieved by discretizing the problem into a significant number of subdomains in a Cartesian 2D and a complex Voronoi 3D model. The problem was initialized based on MRI saturation data, while temperature measured in the confining fluid was used as a time-variable boundary. Empirical decomposition was successfully reproduced numerically by employing both the kinetic and equilibrium reaction model. Heat transfer was the main controlling mechanism. Kinetic limitations may be present in rapid small-scale dissociation tests, and the choice of reaction model should therefore reflect the physical geometry of the problem.

Some of the main conclusions from **Paper 1** - **Paper 3** were:

- Heat transfer was the most important mechanism for sustained hydrate dissociation during depressurization.
- Kinetic modeling was required for accurate numerical reproduction of small scale dissociation.
- The sediment shear strength was assumed to be maintained during CO_2-CH_4 exchange

Data logs such as resistivity and acoustics are often acquired during and after drilling through hydrate bearing intervals for evaluation of pore fluids. Accurate calibration is essential for correct interpretation of data. The complexity of the measurement is enhanced by competing processes, where increasing tortuosity increases the resistivity, while elevated ion concentration reduces the measured resistivity. These issues were addressed in **Paper 4**. Electrical measurements were compared to spatially resolved MRI saturation data for improved interpretation. The standard Archie model was insufficient for porosity and saturation estimates, and a dynamic empirical function that accounted for variable ion concentration was implemented. Changes in effective porosity were accurately described when employing the

dynamic function. *n* varied during growth and was dependent upon the hydrate growth pattern. Additional techniques for determining saturation should therefore preferentially aid in the resistivity interpretation.

The CO_2-CH_4 exchange process was maximized in **Paper 5** through constant volumetric injection rate in a fractured sample design which provided optimized flow conditions and a constant reaction interface. Five consecutive exchange sequences demonstrated enhanced exchange efficiency during constant injection, where negative effects of CO_2 dilution during CH_4 release were minimized. Final conversion efficiency was a function of saturation, non-uniformities and soaking time. 59-83% of the CH_4 was replaced by CO_2 during 2-5 days of injections.

Exchange efficiency was further addressed in non-fractured samples, where released CH_4 was continuously displaced towards the producer. The probability of plugging increased, and final mixed gas hydrate compositions were observed. Flow issues were addressed through CO_2/N_2 binary gas injection, which resulted in excellent flow conditions. CO_2-CH_4 exchange was substantiated during binary gas injection which was confirmed by in line Gas Chromatography (GC) measurements. The overall variation in hydrate saturation was not quantified, but significant resistivity decrease indicates partial dissociation or rearrangement of hydrate crystals.

Main conclusions from **Paper 4** and **Paper 5** were:

- Interpretation of saturation and porosity estimates during hydrate growth was improved by modifying Archie's resistivity model.
- 59-83% CO_2 was safely stored in gas hydrates through constant CO_2 injection while benefitting from CH_4 production.
- Binary gas injection (CO_2/N_2) promoted further exchange while maintaining permeability.

Collaborative experimental effort between the University of Bergen and ConocoPhillips resulted in co-injection of CO_2 and N_2 in a recent field test in Alaska (Ignik Sikumi). Several controlled laboratory experiments were conducted in preparation of the field test. Extended CO_2-CH_4 studies and electrical resistivity measurements were the main contributions from this work.

Table of Contents

1 NATURAL GAS HYDRATES

Gas hydrate is a solid inclusion compound of gas and water. The hydrate stability is governed by pressure, temperature and chemical potential of water and guests in co-existing phases, and the hydration reaction is commonly described as a pseudo reaction by

$CH_4 + n_H H_2O = CH_4 \cdot n_H H_2O + heat$

where the hydration number n_H is estimated to be 5.99 ± 0.07 for sI gas hydrate (Circone et al., 2005). CH_4 is typically concentrated by a factor of 164 relative to STP conditions.

There has been a proliferation in hydrate related research, where focus has shifted on gas hydrates from flow assurance perspective to potential energy resource. Even conservative estimates suggest that energy stored in gas hydrates is within the same order of magnitude as the sum of all conventional fossil fuels. The general consensus is that the resource is yet producible through existing technology applied in the oil and gas sector, but currently not at economic rates. Economic growth and development require access to clean and affordable energy. The last decade has seen a shift with increased gas hydrate research and several field tests for evaluation of production potential. These studies are motivated by the magnitude of the resource and the low carbon imprint of CH_4 upon combustion. Several comprehensive reviews are available on physical properties and challenges related to gas hydrates (Sloan and Koh, 2008, Makogon, 1997, Moridis et al., 2008, Waite et al., 2009), and Franks (1972) has given an extensive review of water properties which is useful for fundamental understanding of water and hydrate similarities. It is not within the scope of this work to give a detailed description of hydrate properties, but rather outline essential properties necessary for further discussions.

1.1 Hydrate structures

Gas hydrates consists of water molecules that interconnect through hydrogen bonding in an open structural lattice, where a hydrophobic guest molecule is suspended in the open space as a result of van der Waals interaction forces (also known as London dispersion forces). Several molecules are potential guests and will

result in different arrangement and structures of the water molecules. The polyhedral cavity which encapsulates the guest molecule are comprised by pentagonal and hexagonal faces, where pentamer is the most likely structure to spontaneously arise in water at different temperatures (Stillinger and Rahman, 1974). The different faces combine to form different polyhedrons, as illustrated in Figure 1. The pentagonal dodecahedron (5^{12}), which consists of twelve pentagonal faces, is a common polyhedron found in most hydrate structures. *Structure I* (sI) consists of two pentagonal dodecahedra and six tetrakaidecahedra, and is preferably stabilized by molecules with diameter ranging between 4.2-6 Å (e.g. CH_4, CO_2, C_2H_6). CH_4 is the most abundant guest molecule in natural gas hydrates (Milkov, 2005), and also the main target for natural gas production from hydrates. This study therefore emphasizes on sI gas hydrate.

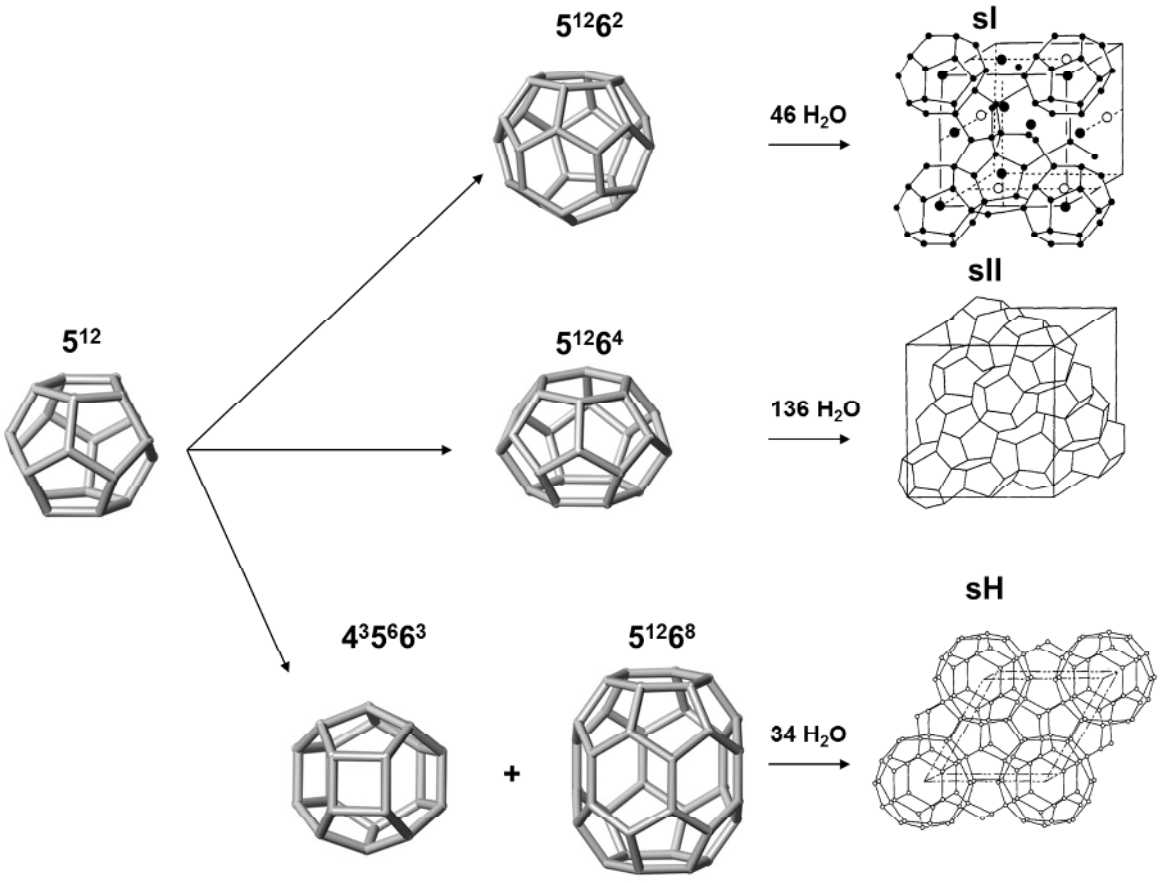

Figure 1 – Illustration of the most common polyhedra and hydrate structures. 5^{12} is a fundamental building block for all structures, and consists of twelve pentagonal faces. The polyhedron connects by sharing faces, and different combinations result in different structures. Figure modified from *Hester (2007)* and *Sloan and Koh (2008)*.

1.1.1 Guest molecules

A guest molecule that does not compete or interfere with the already existing hydrogen bonding is needed to stabilize the cavity. The preferred ratio of molecular to cavity diameter for a guest to stabilize a cavity is at least 0.76; however, this rule does not always apply. The cavity size and structure is dependent on the size of the guest molecule, where sI is stabilized by molecules with diameters between 4.2-6 Å in simple hydrate systems with only one guest molecule per crystal cell.

Raman and NMR spectroscopy are two common techniques used for identifying cavity occupancy. Different experiments (Sum et al., 1997, Lee et al., 2003) have demonstrated how empty cages may be present, which is more dominant for smaller cavities. Sum et al. (1997) used Raman spectroscopy and reported nearly complete filling of large cavities, while fractional occupation of small cavities were less than 1 (0.87-0.92, depending on the hydration number). This corresponded well with results using a statistical thermodynamic model. They also measured the guest occupancy in different cavities and were unable to detect any CO_2 in the small cavities. CH_4 is generally preferred guests in small cavities, but CO_2 occupancy is also a realistic scenario (Fleyfel and Devlin, 1988). Anderson (2003) reported increased CO_2 occupancy for higher pressure.

1.2 Hydrate kinetics

Fundamental understanding of mechanisms involved on microscopic and macroscopic scale during formation dissociation is essential from a production and flow assurance perspective. The following sections will outline processes and mechanisms involved during growth and dissociation.

1.2.1 Hydrate formation kinetics

Three conditions have to be met for gas hydrates to form (Makogon et al., 1999):

1. it has to be thermodynamically favorable ($\Delta G<0$)
2. access to hosts (water) and guests (gas)
3. heat released during the exothermic reaction has to be transported from the reaction site

1.2 Hydrate kinetics

The hydrate stability region is restricted to the upper left area in Figure 2, where different lines indicate stability for various gas compositions. The driving force, as most processes in thermodynamics, is related to Gibbs free energy. The thermodynamic potential is related to pressure, temperature and fluid composition. Hydrate deposits are therefore limited to permafrost and sub-marine environments because of the pressure/temperature restriction. This figure illustrates how CO_2 offers favorable thermodynamic conditions at temperatures below 10 °C from a Gibbs free energy point of view. The thermodynamic behavior of gas hydrates are described in detail elsewhere (Waals and Platteeuw, 1959).

If all conditions are met, hydrate growth will initiate as rearrangement of water and gas molecules in the water/gas phase once the system is within the hydrate stable region. Hydrate nucleation is not deterministic, and persistence of a non-equilibrium state (metastability) results in an induction time. This is a time-dependent

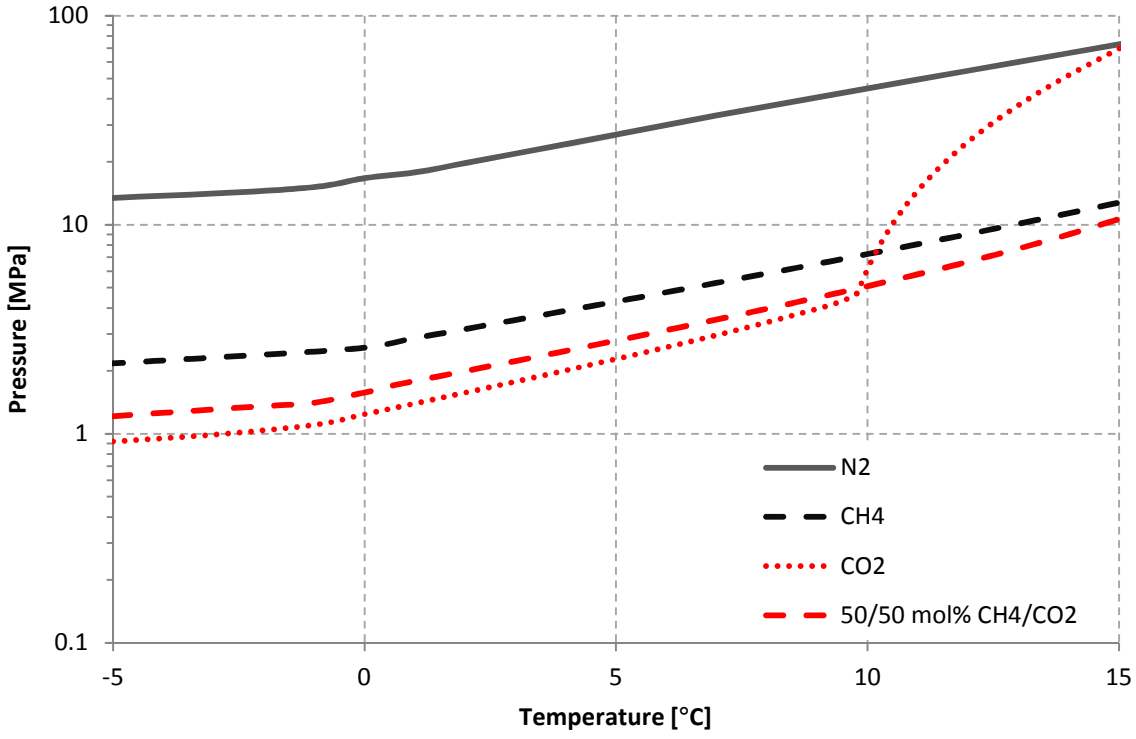

Figure 2 – Phase stability diagram for gas hydrate cavities occupied by different guest molecules. Experimental conditions were typically maintained at temperatures ranging between 0.5-10 °C, while pressure was maintained at 8.38 MPa during formation. N_2 will not be a stable hydrate former at the experimental conditions, but is included for comparison. Presence of salt ions would shift the hydration pressure and temperature upwards towards the left corner. Data was generated without presence of salts through CSMGem (Ballard and Sloan Jr, 2002).

random process, where water and gas molecules rearrange into labile clusters that agglomerate by sharing faces. The clusters may grow or collapse until it reaches a critical size where the free energy change overcomes the surface energy of the new interface (Clennell et al., 1999). The chemical potential will be further reduced with increasing nucleus radii, and progressive growth will therefore occur once critical size has been achieved. The induction time is dependent upon many variables, such as the experimental apparatus, dynamic (agitated) or static systems, presence of substrate material, the history of the water, water and gas composition, pressure and temperature and the degree of subcooling. The time-delay is a result of rearrangement of hydrate interfaces, solid surface effects and mass transfer through the hydrate film. The induction time initiates as the system reaches hydrate stable conditions, and concludes by the appearance of a detectable hydrate volume, as illustrated in Figure 3. Mechanisms involved during growth will be further elaborated later in this chapter.

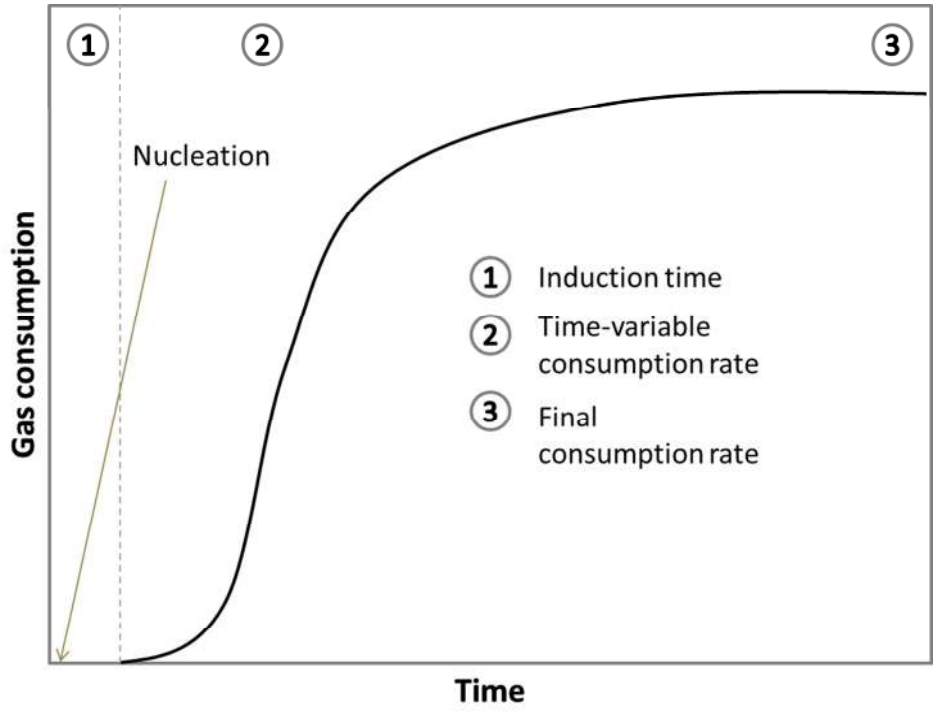

Figure 3 – Gas consumption during time-dependent hydrate formation. The induction time initiates as the system reaches hydrate stable conditions and concludes as the hydrate volume is detectable, where further growth occurs as a function of driving force. Figure modified and inspired from Lederhos et al. (1995).

Homogeneous and heterogeneous nucleation

The nucleation process depends on the physical state of the system and the fluids present. Homogeneous nucleation (HON) is a crystallization process occurring in absence of impurities, and is therefore not common. It also requires significant amounts of gas to be dissolved in the water phase, which is unusual for non-polar gases like CH_4.

Heterogeneous nucleation (HEN) occurs either at the interface between two different phases (Figure 4) or in presence of impurities such as micro-particles or minerals. The substrate, unless complete non-wetting, will increase the probability of growth and is therefore favored from a thermodynamic point of view (Kashchiev and Firoozabadi, 2002). Fluid interfaces provide abundance of both guests and hosts, and therefore increase the probability of growth as well. Nucleation usually occurs at the gas side of the interface in a CH_4/water system because of the inconsistency between hydration number of CH_4 hydrate (5.99) and the CH_4 solubility in water (750 moles of water per mole of methane at 4 °C (Lu et al., 2008)). The stability of the hydrate film formed at the interface is sensitive to the degree of solute saturation in contacting phases (Uchida et al., 1999). Solubility of vapor in gas is generally lower than solubility of gas in water, and the hydrate film will therefore typically propagate into the water phase. Gases with higher solubility, such as CO_2, will induce additional nucleation points in water solution.

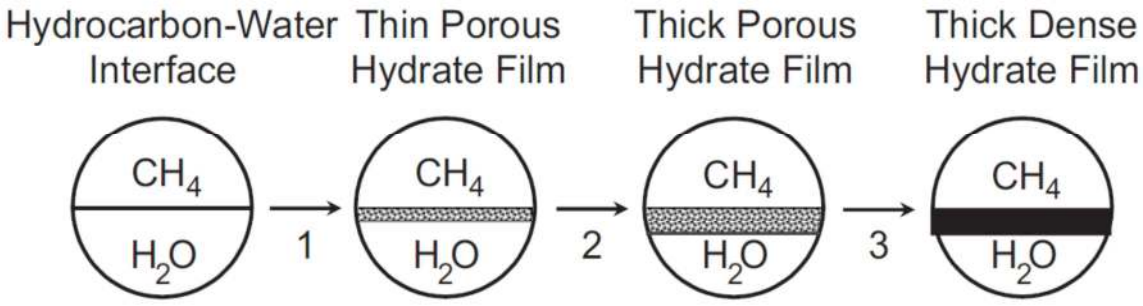

Figure 4 – Heterogeneous nucleation at the fluid interface, where nucleation and growth is more probable because both constituents (hosts and guests) can easily be accessed. A thin film will initially form at the interface, which will grow from the gas phase into the aqueous phase. Figure from Taylor et al. (2007).

Controlling mechanisms during growth

Limiting mechanisms during growth are related to the three conditions listed earlier (1.2.1). The general consensus is that growth limitations are related to intrinsic kinetics, mass or heat transfer.

A semi-empirical kinetic model was proposed by Vysniauskas and Bishnoi (1983) based on CH_4 formation studies using a semibatch stirred tank reactor. The model was later extended to include C_2H_6 and CO_2, and the driving force for the crystallization process was described by the fugacity difference (Δf) at experimental conditions (f_{exp}) and the three phase equilibrium fugacity (f_{eq}) (Englezos et al., 1987a, 1987b, Malegaonkar et al., 1997). The model is based on crystallization theory coupled with two-film theory to describe mass transport across the gas-liquid interface. The validity of a kinetic approach has been questioned (Sloan and Koh, 2008, Skovborg and Rasmussen, 1994), and kinetics may be less significant than anticipated during hydrate growth.

A simplified model was proposed by Skovborg and Rasmussen (1994), where hydrate growth was modeled as a mass-transfer-restricted process across the fluid interface. Later, heat transfer from the reaction site was suggested to be a controlling mechanism during hydrate growth, where subcooling determined the evolution of film growth (Uchida et al., 1999, Mori, 2001, Mochizuki and Mori, 2006, Freer et al., 2001). Both guest/host accessibility and heat transfer were listed as essential mechanisms required for hydrate formation. These processes are therefore expected to be more dominant than intrinsic kinetics during hydrate formation.

1.2.2 Hydrate dissociation kinetics

Mass transfer

Rehder et al. (2004) measured the dissolution rate of pure CH_4 and CO_2 hydrates at isothermal and isobaric conditions. Hydrate was exposed to under-saturated water, which initiated a decomposition process. Solubility of CO_2 in water is one order of magnitude higher than that of CH_4, which was reflected in the dissolution rate. Their data corresponded to a diffusive boundary layer model, thus indicating that dissociation was limited by diffusion/mass transfer. This mechanism will be the main controlling mechanism for gas hydrate deposits at the seabed and also in high water-flux areas such as fractures with high permeability and flow. This study clearly

demonstrated how hydrates contacted by under-saturated fluids decompose in an attempt to reach equilibrium conditions.

Intrinsic kinetics

Bishnoi and coworkers (1987, 2001, 2005) developed an intrinsic kinetic model for hydrate decomposition as well. The model and values were measured using a semi-batch stirred tank reactor with a particle size analyzer. The intrinsic rate was a function of particle surface area (A_S, surface area active during dissociation) and the fugacity difference between vapor and equilibrium pressure. The decomposition rate was described by

$$\left(\frac{\partial n}{\partial t}\right)_p = K_d A_p \left(f_g^v - f_{eq}\right), \tag{1}$$

where

$$K_d = K_d^0 exp\left(-\frac{\Delta E}{RT}\right). \tag{2}$$

The intrinsic rate (k_d^0) and activation energy (ΔE) was estimated to be 3.6E+04 mol/m^{2}Pas and 81 kJ/mol. The reported activation energy is higher than the enthalpy change during the reaction, and the physical interpretation of the model has been questioned. Gupta (2007) demonstrated how the data could be fitted equally well using a heat transfer model.

Heat transfer

The general consensus is that heat transfer is the dominant controlling mechanism during hydrate dissociation. In analogy to endothermic ice melting, hydrate dissociation also requires additional heat to break the hydrogen bonds. The latent heat of dissociation (500 J/g-water[1]) is higher relative to ice (334 J/g-water), as additional energy is required due to van der Waals interaction forces between the guest and the host molecules. Heat transfer, either through conduction or advection, is therefore necessary to maintain dissociation (Davies et al., 2006, Kamath et al., 1984). Hong et al. (2003) concluded in their analytical modeling study that dissociation occurs as a result of three driving forces; heat transfer, intrinsic kinetics and fluid flow. Initial dissociation was controlled by kinetics, but heat

[1] Joules per gram of water

transfer was the main controlling mechanism as the system reached the three-phase equilibrium line. Gupta et al. (2009) demonstrated how CH_4 hydrate decomposition followed the equilibrium three-phase curve, thus indicating that heat transport was a limiting mechanism. NMR spectroscopy revealed no cavity preference during dissociation, and decomposition progressed without presence of an activated state (Gupta et al., 2007). This also suggests that intrinsic kinetics does not play a major role during decomposition. However, the subject should be approached with caution, as different mechanisms may be active on various scales and time scales.

Presence of a porous medium adds further complexity to the hydrate formation and dissociation phenomenon. Physical and chemical properties of gas hydrates residing within porous media will be different from those observed in bulk. One evident effect is that presence of solid minerals affects the thermal properties of the composite system (Selim and Sloan, 1990). Capillary forces may also be described in terms of chemical potential (Nitao and Bear, 1996), where surface potential effects impact the pore water activity (Figure 5). A conceptual model of hydrate growth within porous media demonstrates the importance of capillary forces, where surface chemistry and intrinsic physical sediment properties affect the thermodynamic state, growth kinetics and spatial distributions of the reactants and products (Clennell et al., 1999). Models based on bulk experiments, especially for agitated systems, may not always be valid in a porous medium due to additional complex interaction forces.

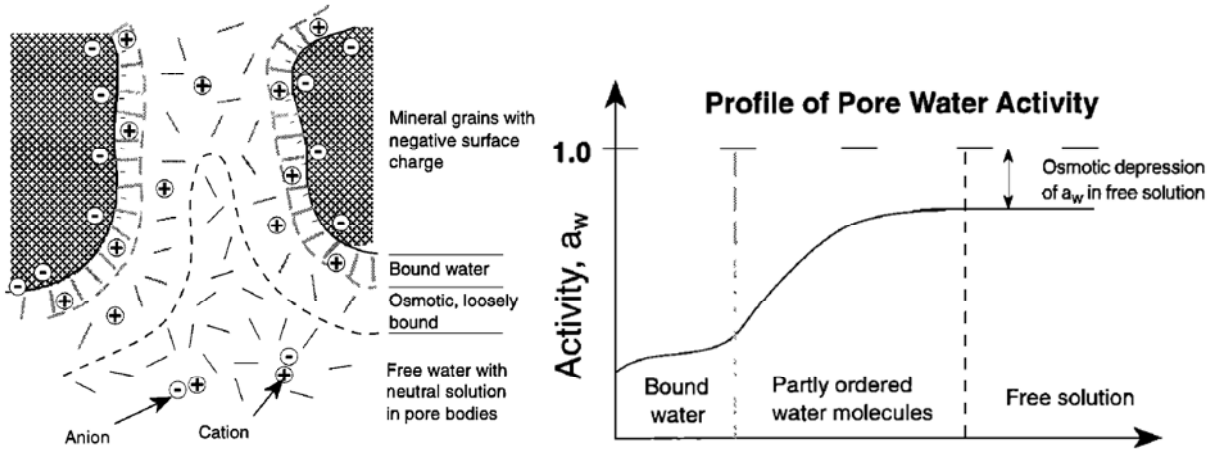

Figure 5 – Illustration of capillary effects on the water activity, where bound water has less contribution to reactions occurring within the pore space. Figure modified from Clennell et al. (1999).

Self-preservation effect

The "self-preservation" phenomenon, where gas hydrates are preserved for extended periods above their hydration temperature, has been reported by several researchers (Davidson et al., 1986, Stern et al., 1996, 2001, 2003, Takeya et al., 2002). Adiabatic cooling effects due to initial dissociation resulted in temperature reduction by 3-7 K, but additional temperature-dependent effects were observed. Figure 6 illustrates average times for 50% dissociation for a series of experiments. Deviation from expected dissociation rates were observed for the thermal regime ranging from 242 to 271 K. This may be due to a shielding effect of ice coating on the decomposing hydrate surface; however, non-uniform ice distribution was documented through X-ray analyses (Stern et al., 2001). Such phenomenon complicates the fundamental understanding of participating processes and numerical predictions.

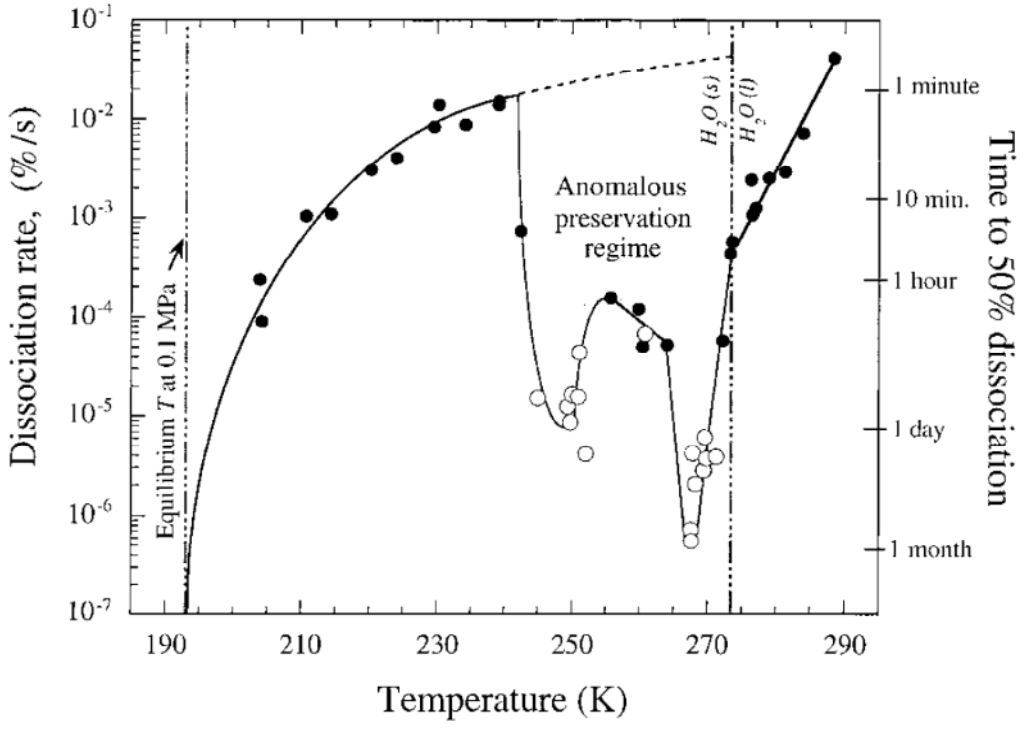

Figure 6 – Average time required for 50% dissociation of CH_4 hydrate. A thermal regime is observed where the dissociation rate deviates from the expected value by orders of magnitude (notice the logarithmic scale). Open data points were extrapolated, as the samples never converged towards 50% dissociation. Figure from Stern et al. (2001).

1.3 Gas hydrates in nature

The last decades have seen a significant increase in hydrate related research with focused effort towards gas production from hydrates. A population increase of 2 billion by 2050 and rapid economic growth in developing countries will likely elevate current energy consumption by 50% by 2035 (IEA, 2011). A sustainable energy future may be within reach (Chu and Majumdar, 2012); however, current energy consumption preserves our dependency on fossil fuels. Gas hydrates offer favorable conditions in terms of enthalpy upon combustion and carbon intensity, and may therefore be a potential energy resource for the future. Several countries have launched ambitious gas hydrate programs to determine the viability of the resource. This proliferation in focused gas hydrate research is motivated by the potentially vast energy resource, which is especially important for developing countries without access to hydrocarbon fuels. There are several challenges and current technology needs further refining and maturing; however, some hydrate deposits may yet be producible at economic rates with current technology. The following section will outline current challenges and opportunities and discuss motivations for hydrate related research.

1.3.1 Hydrate plugging in production and transportation pipelines

Flow assurance was the main driver for previous gas hydrate research due to plugging of production and transportation pipelines (Hammerschmidt, 1934). Abundance of water and gas in high pressure/low temperature environments makes hydrate formation inevitable. Significant effort is therefore made to avoid such temperature/pressure regimes. Hydrate agglomeration will eventually result in complete plugging with undesired downtime in production and potential hazards during removal. These plugs dissociate radially (Gupta, 2007, Davies et al., 2006), and differential pressure may result in high-velocity projectiles up to 300 km/hr as the plug becomes unattached from the pipe-wall surface (Sloan, 2003). Flow assurance is therefore frequently involved with injection of chemical additives that affect the hydrate formation ability through a range of different mechanisms.

Alcohols and glycols interact with the water molecules due to differences in electronegativity, which causes the inhibitors to compete with the hydrate crystal. These typically require high concentrations, and other chemicals, such as polymer

molecules, are therefore generally preferred. Salt, such as NaCl, is also an inhibitor, where the salt ionizes and interacts with a much stronger Coulombic bond than both the hydrogen bond and the van der Waals interaction forces. This is an efficient inhibitor, but issues such as corrosion makes salts unattractive for production and separation facilities.

A statistical mechanical model was developed by van der Waals and Platteeuw (1959), which describes the chemical potential of water molecules in hydrate cavities. The incipient hydrate formation conditions may be determined through this model, and the knowledge is transferred into pipeline and separation technology/facilities. The model is also applied in research related to hydrate mapping and gas production, and the majority of numerical modeling tools are based on the work of van der Waals and Platteeuw.

1.3.2 Evaluation of resource potential

Resource potential has been addressed through different models which indicate a potentially vast energy resource somewhere in the range of 10^{15} to 10^{17} m^3 CH_4 at standard temperature and pressure (STP) (Kvenvolden, 1988, Milkov, 2004, Klauda and Sandler, 2005). However, none of these estimates have made any prediction to what fraction of the resource is actually producible. The gas hydrate pyramid (Boswell and Collett, 2006) illustrated how different geologic features and technical challenges affects the potential commercialization. Moridis et al. (2011a) suggested that current studies should address issues such as; 1) what is the actual size of the resource, 2) what fraction is deposited in permeable high-quality sands, and 3) compiling this information with data from field tests and numerical work to enhance the quality of the prediction. Several studies have recognized the need for improved quality in resource potential assessments (Collett et al., 2008b, Frye, 2008). A range of hydrate deposits are located worldwide (Figure 7), but lack of field data makes evaluation of production potential difficult.

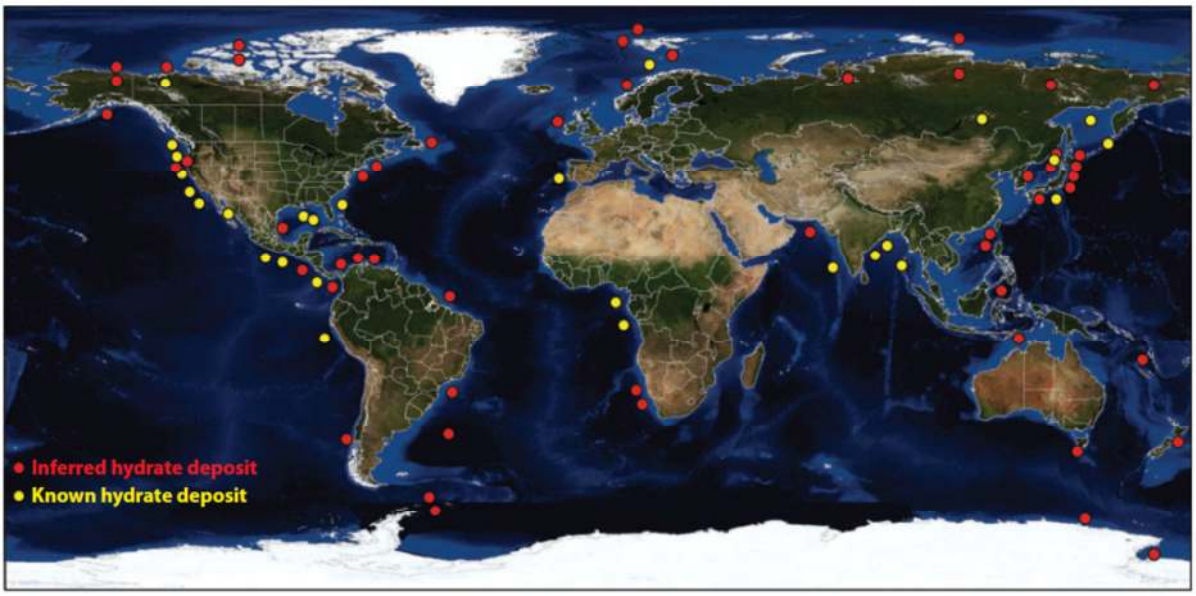

Figure 7 – Illustration of known and inferred gas hydrate deposits in the world. Inferred hydrate deposits are identified through indirect measures such as seismic reflectors or pore-water freshening in core samples. The distribution of hydrate deposits demonstrates how occurrence of hydrates is bound by thermodynamic restrictions. Figure from Hester and Brewer (2009).

A combination of accurate logging methods, geophysical surveys, geological models and numerical modeling is necessary for accurate estimates of *in situ* saturations and resource potential. There has been an advancement of technology and accuracy of estimations, where state-of-the-art measurements using integrated seismic and electromagnetic (EM) methods offer the latest within hydrate predictions (Edwards, 1997, Weitemeyer et al., 2006, Edwards et al., 2010). A comprehensive review of geophysical exploration techniques is given by Riedel et al. (2010) and will not be further elaborated here.

1.3.3 Well logging for saturation estimates

Logging is either performed as a wireline operation (borehole already exists) or as a logging while drilling (LWD) operation for high vertical resolution information about physical and chemical properties of the hydrate bearing sediment. Gas hydrates are sensitive to temperature, pressure and chemical changes, and LWD is therefore preferred as drilling-induced temperature increase or cooling by low-temperature drilling muds will corrupt the original state of the reservoir (Goldberg et al., 2010). In comparison, wireline measurements suffer from time-delay and data acquired may not be representative for the hydrate bearing interval. Common measurement

techniques include electrical resistivity logs in combination with supersonic logs for assessment of saturations within hydrate bearing intervals. Significant resistivity and acoustic velocities are associated with gas hydrates. Resistivity measurements in hydrate bearing sediments have been investigated in this study and will be further elaborated in Chapter 1.3.6.

1.3.4 Hydrate deposits and reservoir classes

Gas hydrates are deposited in a variety of different reservoir types, such as arctic and marine sands, fractured muds, mounds and un-deformed muds. For simplicity, the hydrate accumulations are often classified according to the conditions of hydrate bearing reservoir (Moridis and Collett, 2003). Class I accumulations have an underlying free gas zone, where the gas hydrate/free gas interface may coincide with the equilibrium line. Minor temperature or pressure changes will trigger decomposition due to proximity to the stability line, and production is further enhanced by presence of free gas. Class II deposits are underlain by a mobile water phase, whereas Class III is isolated from any mobile fluids. In terms of production, properties such as intrinsic permeability and fluid mobility will determine whether economic rates can be achieved. The feasibility will also depend on the reservoir temperature/pressure, as the entire hydrate interval may be well within the hydrate stable region and therefore require significant driving force to promote dissociation. The classes are illustrated in Figure 8. The more attractive deposits are typically less abundant.

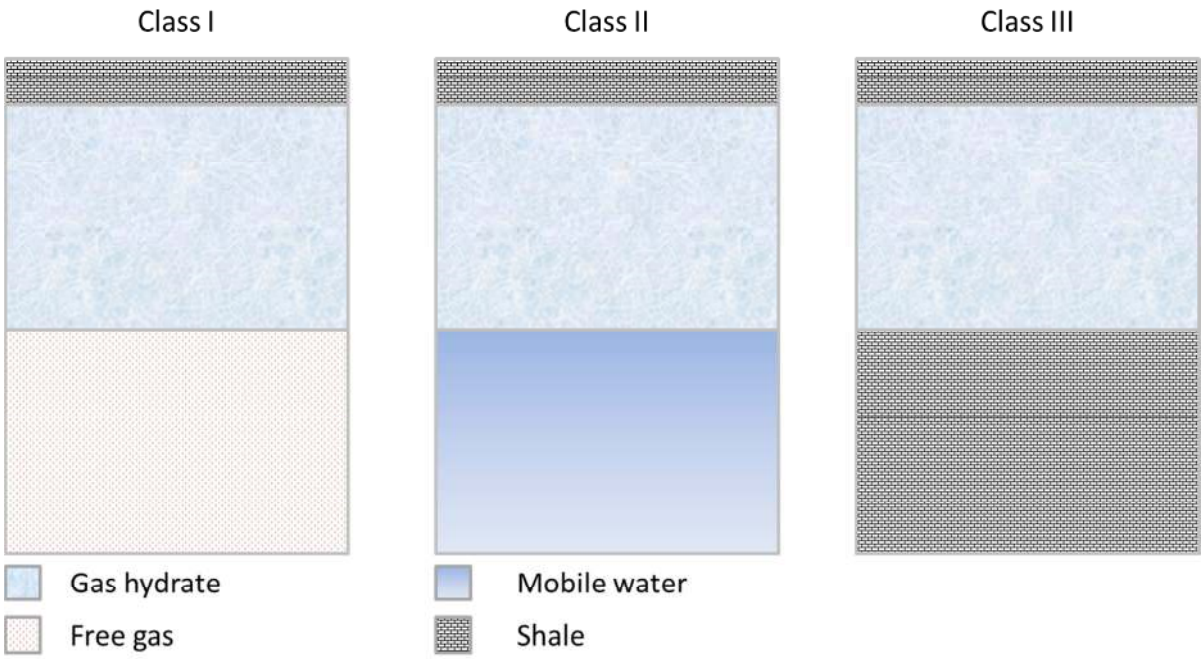

Figure 8 – Hydrate deposits classified according to properties of the geologic medium they reside in. In terms of production, Class I offers favorable conditions as only minor energy is required to promote dissociation. The free gas phase enhances gas production and the dissociation interface. Class II and III are sensitive to properties such as permeability and fluid mobility.

1.3.5 Hydrate configuration within the pore space

Most configurations of gas hydrates in unconsolidated sediments fall into the following categories (Sloan and Koh, 2008);

1. Finely disseminated hydrate that may dissociate rapidly
2. Nodular hydrate of up to 5 cm bulk hydrate
3. Layered hydrate separated by thin layers of sediment
4. Massive hydrates as thick as 3-4 m with maximum 95% hydrate saturation.

This study is mostly concerned with gas hydrates residing within the pore space and will therefore focus on mechanisms and forces involved on pore scale. Differences in hydrate growth pattern will affect some of the inherent properties. Helgerud (2001) measured wave speeds in gas hydrates and suggested four different hydrate growth patterns based on his study;

i. Hydrate preferentially forms at the grain contacts, thus cementing even at lower saturations
ii. Hydrate coats grains more or less uniformly, progressively cementing them as the hydrate volume increases

iii. Hydrate grows in the interior of the pores with partial support to the frame
iv. Hydrate grows without significant interaction with the frame

Several experiments have attempted to determine preferences in growth pattern. Ice Ih and gas hydrates exhibit similar properties, and ice growth in porous media has therefore been investigated through NMR measurements. These measurements indicate presence of a non-frozen water layer between the solid ice and the pore walls (Valiullin and Furo, 2002, Kleinberg et al., 2003, 2005). Water will usually be the wetting phase in a gas/water system. Experiments have demonstrated bulk growth in water wet samples or micro-models as capillary forces inhibit growth in the osmotic and bound layer (Clennell et al., 1999, Tohidi et al., 2001). Hydrate growth will therefore preferentially occur in larger pores due to extensive capillary forces in smaller pores (Torres et al., 2008). This is further enhanced in excess gas systems, where large pores have high accessibility of host and guest molecules. Crystallization in bulk is a slow process when considering the hydration number of CH_4 hydrate (5.99) and the solubility of CH_4 in water (750 moles of water per mole of methane at 4 °C (Lu et al., 2008)). Mass transfer and hydrate growth therefore preferentially occur at the interface between the two fluids in the larger pores (Kvamme, 2002), where the film propagates into the water phase (Uchida et al., 1999). Nucleation and growth on adsorbed fluid layers on mineral surfaces is also a realistic scenario, but we have to keep in mind that the hydrate nucleus is unable to attach to the mineral surfaces due to incompatibility between the surface hydrogen bonded water molecules and geometrical structures of partial charges on atoms in surfaces of minerals (e.g. theory from (Israelachvili, 2011)). Typically, 4-6 layers of water molecules will populate the Stern (or Helmholtz) layer and the diffuse electric double layer and separate the hydrate from the mineral surfaces. Presence of such layers may be of importance from a thermodynamic perspective, where hydrate can potentially be exposed to under-saturated fluids. These layers are also important from a mass-transfer perspective (Svandal et al., 2005) and for seismic interpretations.

Hydrate formation in laboratory synthesized samples

Accurate reproduction of natural processes and mechanisms are important from an experimental perspective, as differences in growth pattern will impact physical properties of the hydrate bearing sediment. Hydrate growth in laboratory

synthesized samples are often approached either through the ice-seeding method of Stern et al. (1996), (1998), partial water and gas saturation method (Stevens et al., 2007, Kneafsey et al., 2007) or by dissolving gas in water that is circulated through the sample (Spangenberg et al., 2005). The latter approach is not frequently applied, as it is a time-consuming process (up to 55 days was reported for CH_4 hydrate). The different approaches will impact how fluids are distributed within the pores and therefore also the hydrate growth pattern.

Variations in hydrate growth pattern

Ebinuma et al. (2005) measured mechanical properties of hydrate bearing sediments synthesized through ice seeding and excess gas. Low S_{wi} in the excess gas approach typically resulted in enhanced interaction with the mineral framework, as less $S_{h,CH4}$ was required to increase sediment stiffness. Less deviation was observed between the ice seeding and excess gas approach at higher S_{wi} because of increasing film thickness that separated the fluid interface (gas/water) and grain minerals.

Imbibition or drainage processes in porous media typically involves more or less smooth planar progressions due to interfacial tension between the fluids. Changes in hydrate saturation are more complex, both in terms of morphology and in pore habitat, as disconnected clusters may grow or decompose at different positions within the same pore. Hydrate morphology is important from a mass transfer perspective, and may also be important for interpretation of physical properties. Several studies have reported protrusion of dendrites or lobes which appear to be triggered by presence of saturated fluids (Uchida et al., 1999, Ohmura et al., 1999). The hydrate film surface acts as a nucleation site for growth of these geometric shapes due to favorable conditions in terms of Gibbs free energy. Growth is generally assumed to move in the direction of the water phase, but protrusions into the gas phase can also occur as a result of water volume expansion due to hydrate formation (Jung and Santamarina, 2012). The topology of lobes increases the reaction interface relative to planar progression and may therefore provide favorable mass transfer conditions. Additionally, imperfections such as tensile discontinuities and voids between polycrystals facilitate mass transport of guest molecules through the hydrate film. These mechanisms may be important when evaluating CO_2-CH_4 exchange in hydrates and resistivity measurements.

1.3.6 Electrical resistivity measurements for saturation estimates

Electrical resistivity logs are frequently acquired in combination with acoustic data when drilling through hydrate bearing intervals. The approach has been used extensively in the oil and gas industry and is well documented (e.g. (Archie, 1942, Serra, 1986, Ellis and Singer, 2007, Hearst et al., 2000)). The electrical properties of hydrate bearing sediments change with mineralogy, porosity, hydrate saturation, brine salinity, and the extent of occluded fluids. Reliable calibration data is therefore essential for correct interpretation. An introduction to Archie's law is given in **Paper 4**.

Resistivity measurements in hydrate bearing sediments

Several previous studies have documented resistivity logging in hydrate bearing intervals (e.g. (Mathews, 1986, Collett, 1998, Torres et al., 2008, Boswell et al., 2012, Collett et al., 2012b, Collett, 2001, Shankar and Riedel, 2011, Collett and Ladd, 2000, Sun and Goldberg, 2005, Chen et al., 2008, Pearson et al., 1983, Hyndman et al., 1999, Boswell et al., 2009, Anderson et al., 2008)). Saturation is estimated by measuring R_o at intervals below the hydrate stable region, while n=1.9386 (Pearson et al., 1983) is frequently applied.

Several laboratory experiments have attempted to evaluate the accuracy of the resistivity method. Pearson et al. (1986) combined acoustics and resistivity measurements on THF-hydrate-saturated Berea sandstone and Austin Chalk. Resistivity increased two orders of magnitude during growth, and they suggested that changes in ion concentration control the apparent resistivity. Ren et al. (2010) used similar methodology on CH_4 hydrate growth in quartz sand-packs, where resistivity dropped at the onset of formation and stabilized around 4 Ωm after growth. Similar trends have been reported by others, where values in the lower 1-20 Ωm range are more abundant (Li et al., 2010, Li et al., 2012). Some exceptions range one order of magnitude higher (Spangenberg et al., 2005), which suggest that the inherent resistivity is dependent upon intrinsic sediment properties and the conditions at which gas hydrates are synthesized.

Determining n for accurate saturation estimates

Saturation estimates through Archie's resistivity index are very sensitive to variations in the saturation exponent n, where minor changes result in significant

deflections in terms of saturation units (Worthington and Pallatt, 1992). The physical interpretation of *n* is related to interaction from the minerals and intrinsic sediment properties such as pore shape, connectivity and wettability. A literature survey suggested that *n* averages around 2 for water-wet samples (Anderson, 1986), and the value remains unaffected during drainage. However, the inherent resistivity increases as the medium moves from water-wet towards oil-wet conditions (Donaldson and Siddiqui, 1989, Worthington and Pallatt, 1992, Anderson, 1986) which is reflected in progressive resistivity and increasing *n* (Sweeney and Jennings, 1960, Wei and Lile, 1991, Zhou and Stenby, 1997, Morgan and Pirson, 1964). Archie's laws are therefore not valid at these conditions.

The interpretation of *n* for hydrate bearing sediments is related to hydrate configuration within the pore space, the hydrate geometry during growth and extent of interaction with mineral surfaces. Grain cementing growth yields strong resistance to electrical currents, as hydrate located in pore throats will efficiently reduce the connectivity of brine pathways. This will be reflected in high *n.* Hydrate growth within the center of the pore space will have less effect on the resistivity and therefore yields lower *n*.

A theoretical and network modeling study investigated how differences in growth pattern impact the intrinsic resistivity of hydrate bearing sediments, as illustrated in Figure 9 (Spangenberg, 2001). High capillarity resulted in *n* ranging between 0.5 and 4, where significant increase was observed for small variations in saturation units. Spangenberg later confirmed his predictions through experimental work (Spangenberg and Kulenkampff, 2006), but the majority of well log interpretations are still based on the value reported by Pearson et al. (1983).

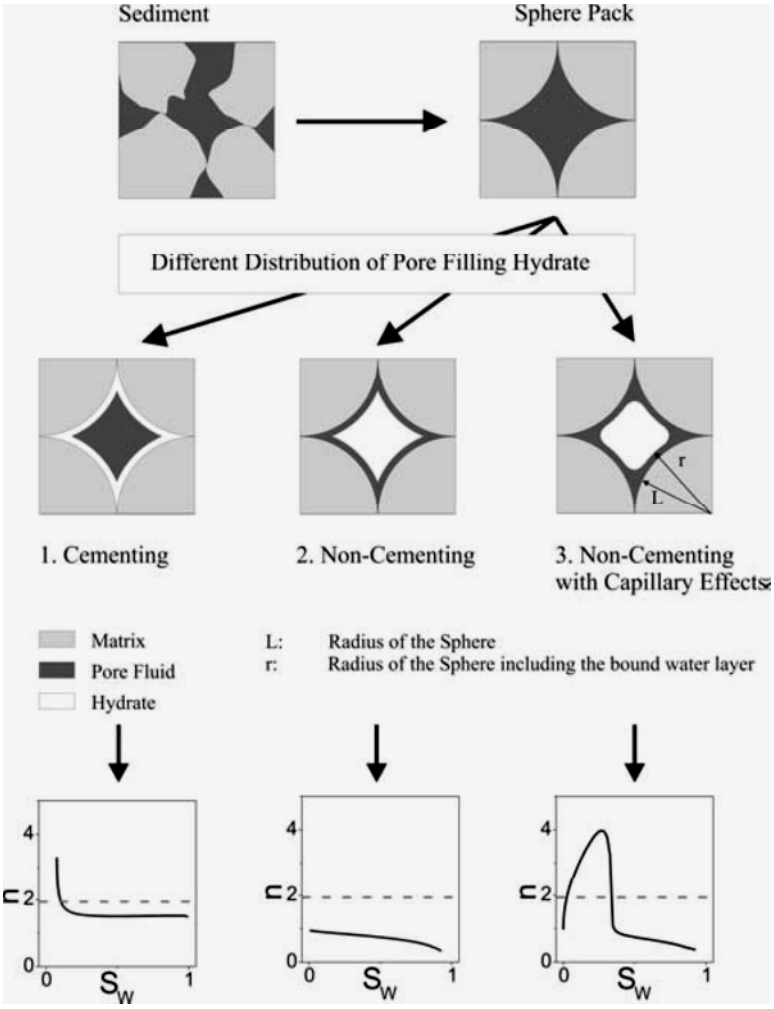

Figure 9 – Model for how various hydrate configuration within the pore space affect the inherent saturation exponent. A constant n is anticipated from the oil and gas industry, but varying growth pattern may affect the measured resistivity. Figure from Spangenberg and Kulenkampff (2006)

1.3.7 Geomechanical stability and environmental concerns

The stability and stiffness of unconsolidated sediment is enhanced by presence of gas hydrates that interact with the mineral framework and inhibit further consolidation. Subsidence due to continued sedimentation may eventually result in unfavorable temperature conditions due to the geothermal gradient. Decomposition results in locally higher pressure and may induce fractures where gas is vented. The hydrate no longer provides support to the under-consolidated sediment, and massive submarine landslides may occur. Hydrate decomposition is believed to have contributed to the Storegga slide on the Norwegian Continental Shelf (Bryn et al., 2005, Bugge et al., 1987, Sultan et al., 2004). Such landslides result in displacement

of large volumes of water and possible creation of subsequent tsunami (Dawson et al., 1988).

Other apparent disadvantages are release of CH_4, which is an aggressive greenhouse gas that may further enhance the greenhouse effect (Lelieveld et al., 1998). Gas hydrates represent a vast natural gas sink. For comparison, a 10% release of the CH_4 inventory would correspond to a tenfold increase in the global CO_2 concentration in terms of the Earth's radiation budget (Archer, 2007). Global temperature increase could substantially reduce the CH_4 hydrate inventory with accelerated positive feedback to global warming (Buffett and Archer, 2004, Kennett et al., 2003). The ocean will to some extent oxidize the CH_4 and reduce the negative feedback from CH_4 seeps into the atmosphere.

1.3.8 Gas production from gas hydrates

Production through decomposition

Gas production from natural gas hydrates has typically been approached through decomposition, where the physical or chemical conditions in the hydrate bearing reservoir are altered to promote dissociation. Figure 10 illustrates the three-phase equilibrium curve for CH_4 hydrates and the three methods applied for hydrate decomposition; depressurization, thermal stimulation and injection of inhibitors that compete or interfere with the hydrogen-bonded water molecules in the hydrate crystal. Depressurization is generally considered the most promising approach, as limited energy is required to promote dissociation (approximately 15%). The method is even more attractive for a Class I reservoir, where underlying free gas promotes high initial production rates and increases the decomposition surface area. Additionally, excess gas may indicate that the bottom of the hydrate deposits intersects the three-phase equilibrium line, where negative effects of the endothermic reaction are less substantial due to high reservoir temperature and low degree of subcooling.

Thermal stimulation is another method, where heat is added to the reservoir to promote dissociation. This approach is energy-intensive, as liquid must be heated and transported to the reservoir. The thermal properties of gas hydrates are also unfavorable, and the majority of heat will therefore be transferred to the rock matrix. Inhibitor concentration will be diluted during dissociation, and this approach

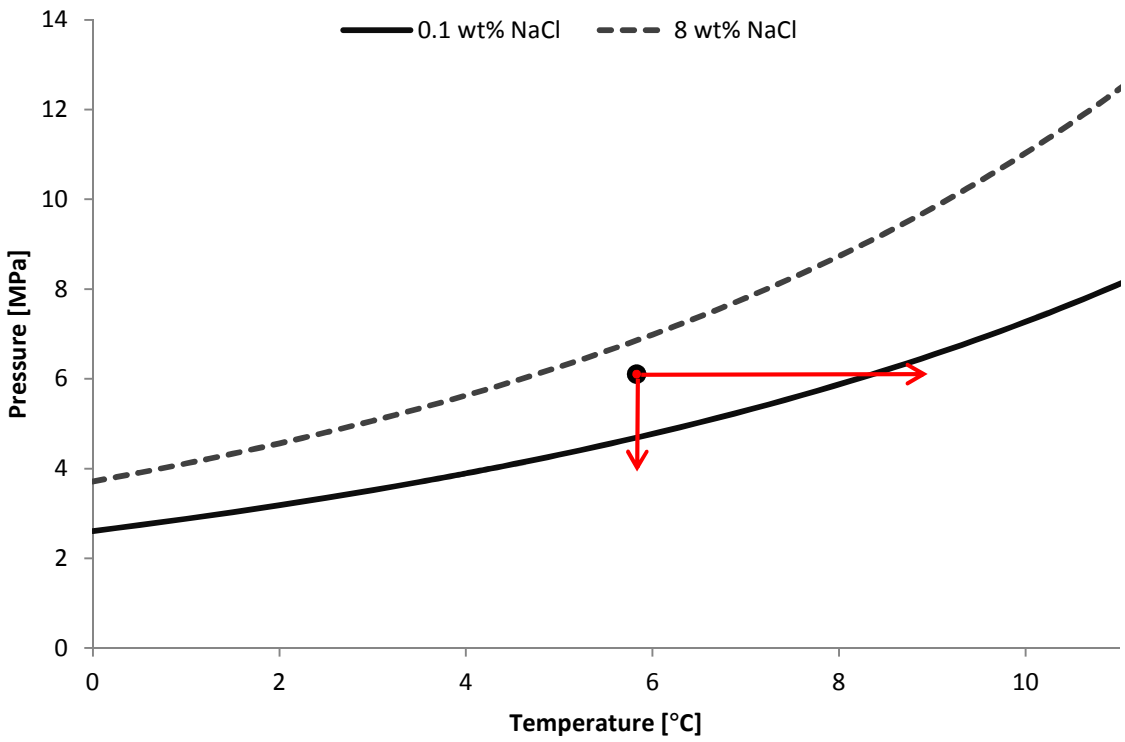

Figure 10 – Three-phase equilibrium line for CH_4 hydrates at different brine concentrations. The figure illustrates the three common approaches for hydrate decomposition; depressurization, thermal stimulation and injection of inhibitors that reduce the hydrate stable region.

is therefore not considered for full field stimulation. However, both thermal stimulation and inhibitor treatment in the near wellbore region are favorable to prevent ice and hydrate formation in the wellbore region due to Joule Thompson effects.

CO_2 replacement

CH_4 production from gas hydrates may also be approached through guest replacement where the injected gas provides a thermodynamically preferred gas hydrate (Svandal et al., 2006, Seo and Lee, 2001). Figure 2 demonstrated how different guests have inherently different stability regions, where the stability of CO_2 hydrate extends beyond that of CH_4 hydrate at specific temperature regimes. The potential energy of the system is reduced during the CO_2-CH_4 exchange process, where excess energy is released in form of heat (exothermic reaction). Liberated heat during CO_2 hydrate formation (Anderson, 2003) exceeds the requirement for CH_4 dissociation (Anderson, 2004). Liberated heat will therefore enhance the replacement process. Jung et al. (2010) suggested that liberated heat assists in the

exchange process for subcooling up to 10 K. However, the enthalpy contribution is sensitive to the fluids occupying the pores and the composite thermal conductivity of the HBS. Excess gas will reduce heat dissipation, where heat liberation efficiently facilitates additional CH_4 hydrate decomposition for accelerated exchange. Maintained sediment shear strength during exchange is an additional advantage (Espinoza and Santamarina, 2011).

The replacement technology has been demonstrated in bulk experiments (Lee et al., 2003, Lee et al., 2004, Park et al., 2008, Ota et al., 2005), in sediments (Graue et al., 2008, Kvamme et al., 2007, Yuan et al., 2013, Ersland et al., 2010, Jadhawar et al., 2005) and numerically (Phale et al., 2006, Kvamme et al., 2007, White et al., 2011). The exchange process is complex, where several variables complicate evaluation of final conversion efficiency.

Raman and NMR spectroscopy have been applied to measure hydration numbers for pure and binary phases. Inherent properties such as guest molecule affinity give a theoretical maximum recovery of 75% based on the 3:1 ratio of large to small cavities. This is based on the assumptions of complete hydration and replacement limited to large cavities. Recovery will increase by presence of empty cages and replacement in small cavities (Fleyfel and Devlin, 1988), which is possible from a theoretical perspective. Sum et al. (1997) used Raman spectroscopy and reported nearly complete filling of large cavities, while fractional occupation of small cavities was less than 1 (0.87-0.92, depending on the hydration number). This corresponded well with results using a statistical thermodynamic model.

Uchida et al. (2000) evaluated exchange by Raman spectroscopy and detected a 50-hour induction period without any reactions. 80% of the CH_4 molecules were replaced during the following 30 hours, while signal from small cavities disappeared completely after 100 hours. Lee et al. (2003) suggested that the bulk recovery was limited to 64%, however, exchange kinetics in sediments may not be comparable to bulk measurements because of the increased reaction interface area and presence of minerals. Chapter 1.3.5 discussed how hydrates and minerals are separated by a film with varying thickness. The diffusion coefficient of CO_2 and CH_4 in water (Thomas and Adams, 1965) are several orders of magnitude larger than in hydrate (Demurov et al., 2002, Davies et al., 2008). Mass transfer efficiency is therefore enhanced by the water layer, which is important from a replacement perspective

(Kvamme et al., 2007). Different geometric topologies may also be of importance for the exchange efficiency, as they increase the reaction interface. Overall, CO_2 replacement is a promising technological concept with positive feedbacks from increased hydrate stability and storage of a potent greenhouse gas.

1.3.9 Field evaluations and pilot tests

The last decade has seen an increase in the number of field evaluations and pilot tests, primarily driven by international gas hydrate R&D programs. Current national programs include India (the Krishna-Godavari basin (Collett et al., 2008a)), China (Yang et al., 2008), South Korea (Ulleung Basin(Park, 2008, Moridis et al., 2009)), Canada (Grace et al., 2008), and several active projects in the US (Frye et al., 2012, Boswell et al., 2012, Riedel et al., 2005). Extensive reviews and reports are available, and this section will therefore only give a brief summary of field tests in the open literature to demonstrate how the gas hydrate technology has advanced and becomes increasingly more focused for each field test.

Messoyakha

Messoyakha, located in the eastern Siberian permafrost, is an example of a Class I hydrate reservoir that has been produced through conventional depressurization since 1967 (Makogon, 1997). The base of the hydrate interval intersected the hydrate stable region and dissociation is therefore triggered through minor pressure changes. Production of free gas results in minor pressure drops that induce a constant gas flux from the hydrate interval. Gas hydrate decomposition may at least have contributed to additional 30% production.

Mallik

Conventional hydrocarbon exploration in the Mackenzie Delta-Beaufort Sea area accompanied by more than 200 wells have resulted in extensive knowledge of gas hydrate occurrences in the area. Three dedicated international scientific drilling programs have further enhanced the knowledge data base through data logs, several production tests, and sections of cored data (Dallimore et al., 1999, Dallimore and Collett, 2005, Yamamoto and Dallimore, 2008, Kurihara et al., 2010a). The Mallik 2007-2008 test was the most successful, where sustained production rates up to 4000 m^3/day were recorded (Grace et al., 2008). The production tests

provided data sets for calibration of existing hydrate numerical models through history matching (Kurihara et al., 2008, Moridis et al., 2004) and was therefore essential for evaluation of the model performance. Loss of geomechanical stability and sand and water production were obvious limitations during the production test.

Nankai Trough

A 16-year gas hydrate program was initiated in Japan in 2001 based on seismic data from the Nankai Trough-region. Japan does not have any natural sources of hydrocarbons and have therefore initiated a major research effort to assess the resource potential and to develop strategies for commercial gas production within 2018. Resource assessment suggested that a total of 40 tscf may be contained in gas hydrates in the Nankai Trough region, where 20 tscf is located in concentrated areas (Fujii et al., 2008). Two production tests are planned within 2015 (Masuda et al., 2009), where the first test was supposed to be initiated early 2013. Temperature response during the depressurization test will be monitored through two observation wells drilled in 2012 (Yamamoto et al., 2012). The Japanese programme is fairly advanced, and their scientists were involved in the Mallik field test. Results from Japan will probably not be published within the first years, but it has the potential to shape the gas hydrate future.

Mount Elbert

The USGS released an assessment of the North Slope gas hydrate potential in 2008 with a mean estimate of 85 tscf as technically recoverable (Collett et al., 2008b). The extensive well-network within the Milne Point-area has identified a range of potential hydrate prospects, where Mount Elbert is ranked highest (Collett et al., 2011). The BPXA-DOE-USGS Mount Elbert Gas Hydrate Stratigraphic Test Well was drilled in February 2007, where a 17 days joint effort resulted in a comprehensive dataset (Hunter et al., 2011). This study featured coring (Rose et al., 2011), evaluation of physical sediment properties (Winters et al., 2011, Kneafsey et al., 2011) and pore fluids (Torres et al., 2011, Stern et al., 2011). A full suite of logging tools were applied to determine the hydrate bearing intervals and saturations (Lee and Collett, 2011, Sun et al., 2011). The fluid flow potential was measured in four open interval flow tests that ranged from 6 to 12 hours each. These datasets were evaluated through history matching by several numerical models (Anderson et al., 2011a, Kurihara et al., 2011, Moridis et al., 2011b, Pooladi-Darvish and Hong, 2011)

and provided data for evaluation of potential long-term production (Anderson et al., 2011b, Collett et al., 2012a, Wilson et al., 2011). The stratigraphic well confirmed intervals with 60-75% S_h within reservoir quality sand.

Ignik Sikumi

This accumulation is also located on the Alaskan North Shore and was subject to a different approach. The University of Bergen developed a technology for gas production through CO_2 sequestration and CO_2-CH_4 exchange in the hydrate crystal in partnership with ConocoPhillips. A single well was drilled in April 2011 in proximity of the Prudhoe Bay Unit L-pad. The unit was chosen due to its low geologic risk and presence of multiple potential hydrate intervals. A full suite of logging tools were applied (including resistivity) in combination with a series of pressure tests (Schoderbek and Boswell, 2011). In 2012, 2609 kg CO_2 and 5479 kg N_2 (77/23 mol% N_2/CO_2) was injected into the Sagavanirktok "Upper C" sand with S_h averaging at 75% and a thickness of 30 ft (Schoderbek et al., 2012). Abundance of gas and water increases the plugging probability, and the wellbore conditions was maintained above 0 °C to avoid further complications by ice formation. Injection was initiated at February 15th, and the well was shut in after two weeks of injection. Flow-back was initiated March 4th and extended for 30 days, where the pressure initially was maintained above the hydration pressure for pure CH_4 hydrate. 998 mscf gas was produced and measured with a GC, which revealed 22 mscf CO_2, 155 mscf N_2 and 821 mscf CH_4. The final report is yet to come, but the pilot test has so far been considered a success (Parshall, 2012).

The five production tests reveal an evolving technological advance, both in terms of characterization and production methods. It also underlines the importance of data acquisition for further numerical evaluation and verification of numerical models and further refinement of production technologies.

2 EXPERIMENTAL DESCRIPTION

A range of different experiments have been performed during this study as part of an ongoing project between the University of Bergen and ConocoPhillips. This chapter will describe experimental techniques, setups and procedures for experiments performed at University of Bergen and at the ConocoPhillips Technology Center in Bartlesville.

2.1 Core properties and configurations

Core samples from hydrate reservoirs are rare and often corrupted during the retrieval and preservation process (Kneafsey et al., 2011). This study has therefore used an outcrop rock as an analogue to the reservoir. Bentheim sandstone is a consolidated and fairly uniform rock with 22-23% porosity, 1.1 D permeability and pore diameter averaging at 125 microns. The pore size distribution is unimodal, with grain density of 2.65 g/cm^3. The mineralogy typically showed 95-99% quartz with trace of the clay mineral kaolinite.

The core dimensions used in this study ranged from 6-15 cm in length and 3.81-5.15 cm diameter, where three different core configurations have been applied (Figure 11). Some samples had manufactured fractures along the longitudinal axis which were maintained open by a *polyoxymethylene* (POM) spacer. This spacer volume could be monitored *in situ* by MRI to verify CH_4 production. The spacer volume also increased the reaction area, and prevented flow issues during days and weeks of operation.

Figure 11 – Three different core configurations for different experiments. The single- and double-fracture designs were used during exchange studies, while non-fractured samples were used for resistivity, depressurization and additional exchange studies.

2.2 Magnetic Resonance Imaging

MRI was used to spatially resolve saturation changes *in situ*, either as 1D, 2D or 3D visualizations. This technique was used for all experiments conducted at the ConocoPhillips Technology Center, and these experiments therefore provide additional information regarding active mechanisms during hydrate growth or decomposition. The principles of Nuclear Magnetic Resonance (NMR) are based on quantum mechanics and Newtonian physics (Bloch, 1946, Purcell, 1946), and have been applied in the oil and gas industry for decades (e.g. (Coates et al., 1999, Dunn et al., 2002)). Previous effort has also documented the benefit of MR imaging and NMR spectroscopy for gas hydrate related studies (Baldwin et al., 2003, Ripmeester and Ratcliffe, 1999, Moudrakovski et al., 2004).

One of the advantages of MRI is that the signal intensity is proportional to hydrogen density and can therefore be used to substantiate presence of water and CH_4. Hydrogen in hydrate has short relaxation time which is not captured by the standard spin-echo sequence (Hahn, 1950). Drop in MRI intensity could therefore be quantified as hydrate formation. The magnetization $\mathbf{M}_0$ from Curie's law is inversely proportional to temperature. The signal strength will therefore increase during cooling processes for hydrate formation. MRI provided spatially resolved *in situ* saturation data during hydrate growth, exchange and decomposition. The MRI acquired a full 3D saturation image in 2 hours and 17 minutes and ran continuously during days or weeks of operation.

2.2.1 Processing data from the MRI

Unprocessed MRI data was structured into intensity averages and intensity profiles through an in-house IDL-based software (Husebø et al., 2007). ImageJ, a Java based image processing program, assisted in analysis and visualization of MRI data. T3D v.1.1.3 (Fortner Research, LLC) was also used for visualization purposes.

2.3 Experimental setups

The experimental concepts and techniques are similar for all experimental setups used in this study, where high precision equipment is assisted by a cooling system that provides temperature control during exo- and endothermic processes. The

experimental setup at the ConocoPhillips Technology Center is more complex because of the MRI. Five setups are currently available for gas hydrate studies at the University of Bergen, including a micro-model and a block setup that are briefly described in the Appendix A.

2.3.1 Experimental setup at ConocoPhillips Technology Center

The experimental setup took advantage of a superconducting "small body" Unity/Inova-Imaging 85/310 spectrometer MRI from Varian. The resonance frequency of 87.5 MHz corresponds to a 2 Tesla magnet, where three dimensional images were represented as 32x32x128 floating point arrays for the settings used in this study. A custom-made core holder with a composite fiberglass and resin housing was used, as described in Figure 12. All parts and equipment in vicinity of the MRI were made of non-magnetic components to ensure compatibility with the high magnetic field. This included titanium end caps, cobalt screws, POM spacers and *polyetheretherketone* (PEEK™) end pieces.

Two accurate Quizix C-6000-10K-HC-HT high pressure pumps were used for pore pressure (CH_4, CO_2, N_2 or binary gas mixtures). The pumps could operate at flow rates up to 200 ml/min at maximum 41.4 MPa with a resolution of 13.5 nl (nano-liters). Paroscientific Digiquartz pressure transducers measured inlet and outlet line pressure, while an additional transducer monitored the differential pressure at specified time intervals.

The confining system was combined with the cooling system because of restrictions presented by the MRI. Fluorinert FC-40 was used as confining fluid as it contains no hydrogen and minimizes RF loss due to its low dielectric properties. The Fluorinert was pressurized by a Quizix QX-6000 pump, while a recirculation pump ensured circulation of the fluid, as illustrated in the top of Figure 12 and in Figure 13. The system temperature was maintained constant at 4.0 ± 0.3 °C by circulating cooled confining fluid under pressure in lines inside a low-pressure PVC jacket that worked as an additional cooling loop outside the MRI. Antifreeze in the PVC jacket was cooled by a Termo Neslab RTE-221 refrigerated bath that provided constant heat exchange with the Fluorinert inside the high-pressure tubing. A type-T thermocouple was positioned within the cooling fluid, as illustrated in Figure 12, and was logged at specified time intervals using a HH506RA data-logger from Omega Engineering.

2.3 Experimental setups

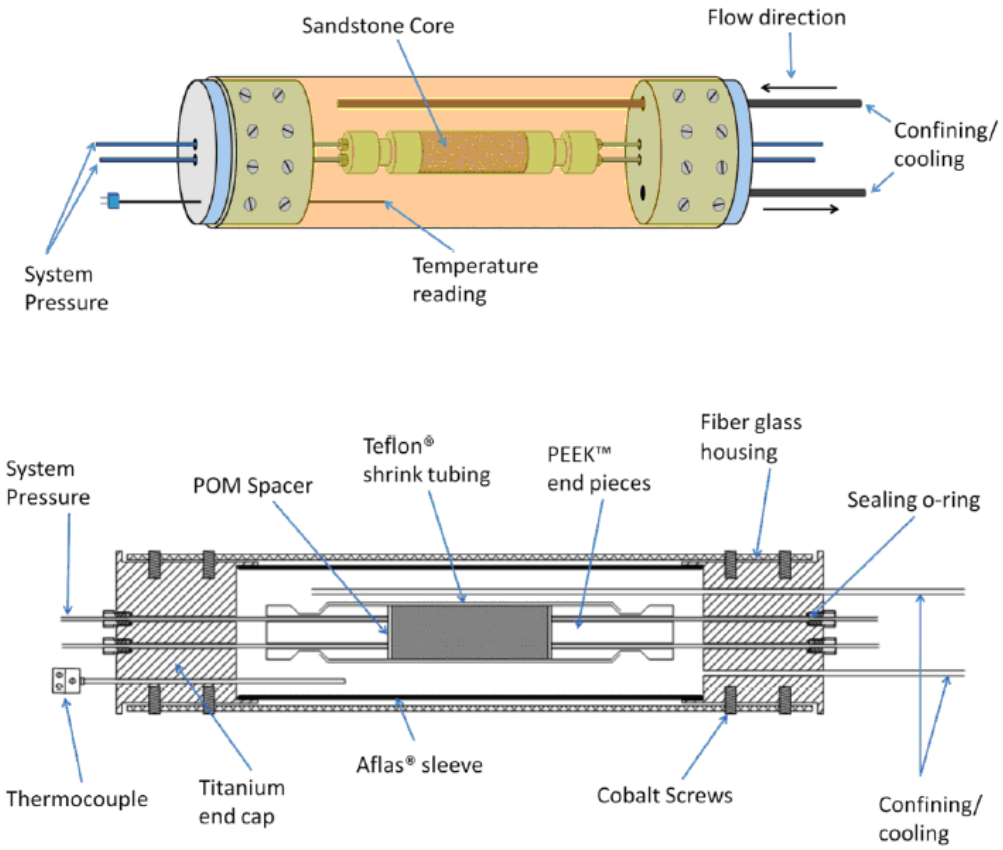

Figure 12 – Illustration of custom made pressure vessel for MRI experiments. All components were non-magnetic for compatibility with the magnet. Figure from Husebø (2008).

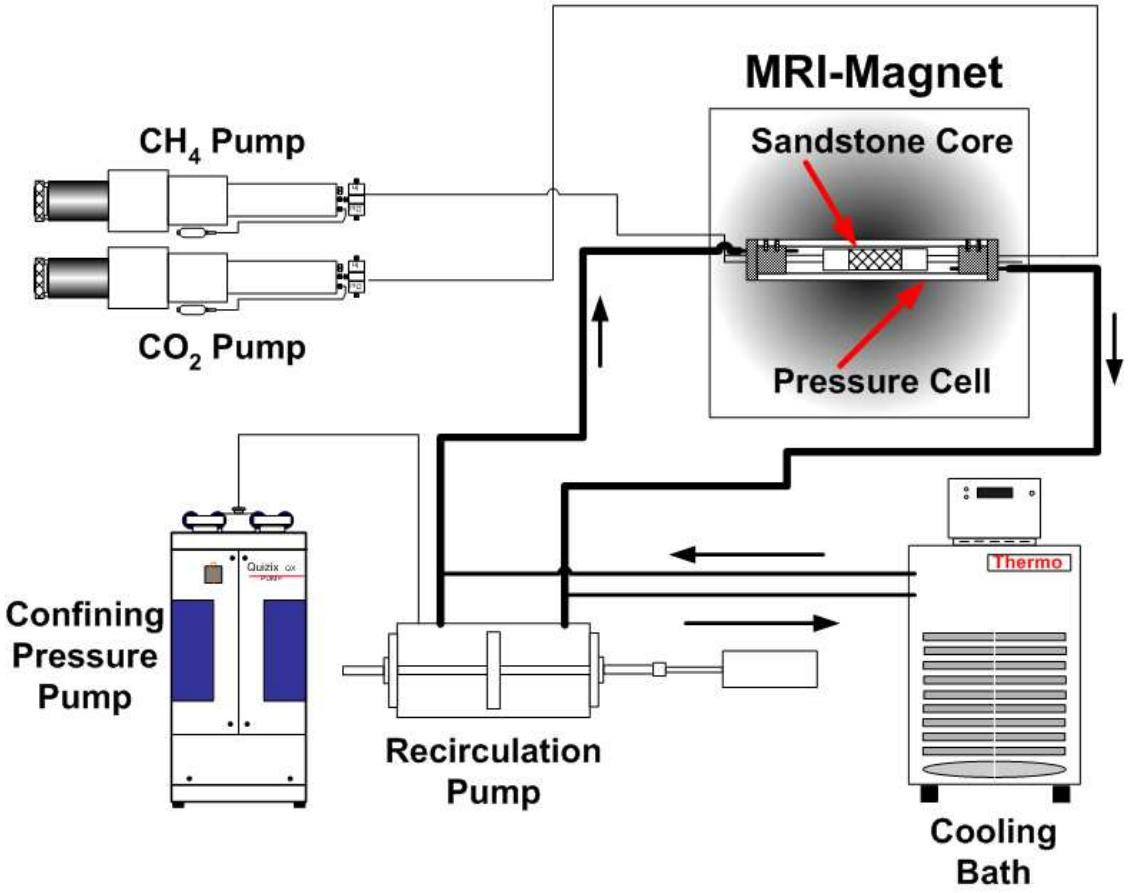

Figure 13 – Experimental setup at the ConocoPhillips Technology Center in Bartlesville. A combination of accurate high pressure pumps and in situ saturation information from MRI makes this setup ideal for investigation of mechanisms involved during hydrate growth, decomposition or exchange.

Resistivity setup

Slight modifications were made to the experimental setup to accommodate resistivity measurements. Silver filter papers were contacting the trans-axial core faces, as illustrated in Figure 14. A POM spacer was added to provide space for the wire attached to the silver paper. The paper and wire were held in place by the POM spacer. A pass-through fitting connected the electrodes to an external LCR meter through the PEEK end pieces. Resistivity and phase angle were measured with a HP 4263A LCR meter at specified time intervals for frequencies ranging between 100 Hz and 100 kHz.

Figure 14 – Silver filter paper, contacting both trans-axial core faces, were used as electrodes in the MRI system. A POM spacer was positioned on top to provide space for the wire, which was connected to a LCR meter through a pass-through connection.

2.3.2 Experimental setups at the University of Bergen

The main concept of experimental setups at the University of Bergen is illustrated in Figure 15. These setups are less complex in terms of imaging, which increases the overall flexibility as there is no magnetic field to take into consideration (e.g. time-delay in effluent profile was reduced from 5 to 0.3 hours as the GC could be positioned in proximity to the pressure vessel). RCH-Hassler type core holders with aluminum housing were provided from Temco (Figure 16). Chemical resistant sleeves (Nitrile rubber/Buna-N) were used to extend the lifetime during injection of reactive CO_2. The end-pieces were made of SS-316 with three NPT connection ports for each distribution plug. These were either connected to high pressure tubing for pore pressure or thermocouples that measured temperature at the core surface and/or within the sample. Accurate high pressure pumps (either Quizix C-5000-2.5K-HC, Teledyne Isco 100 DM or 260 D, or Sanchez Technology Stigma 300, 500 or 1000 pumps) were used for pore pressure (gas or water). Custom designed Druck UNIK 5000 pressure sensors were monitoring differential, inlet and outlet line pressure (0.04 % FS). Pressure was recorded at specified time intervals by an in-house built Labview program. Quizix QX, C-5000-10K-SS or air-driven Haskel MS-71/MS-188 liquid pumps in combination with gas-loaded accumulators were used for constant overburden pressure.

The core outlet could be routed through a complex effluent-evaluation loop consisting of several elements. Two back pressure regulators were put in series for improved flow control. Line pressure was first reduced from 8.38 MPa by a gas-loaded Hastelloy Equilibar EB1ZF1 Zero Flow Precision back pressure regulator equipped with Hastelloy diaphragm and Merkez Z1602 o-rings for chemical

compatibility. The line pressure was reduced to 0.1 MPa by the second pressure control unit, a spring-loaded Swagelok KLF High-Sensitivity back pressure regulator. The gas composition could then be determined by an in line Agilent 3000A Micro GC with a TCD detector at one minute time resolution. This setup has recently been modified with an additional mass flow meter in combination with a large gas accumulator for improved interpretation accuracy.

Cylindrical cooling jackets were designed and built in-house, where cooled antifreeze was circulated in a low pressure cooling system for heat exchange with the core holder and sample. Temperature was measured using T-type thermocouples which were logged at specified time intervals using a HH506RA data-logger from Omega Engineering (0.1 °C resolution).

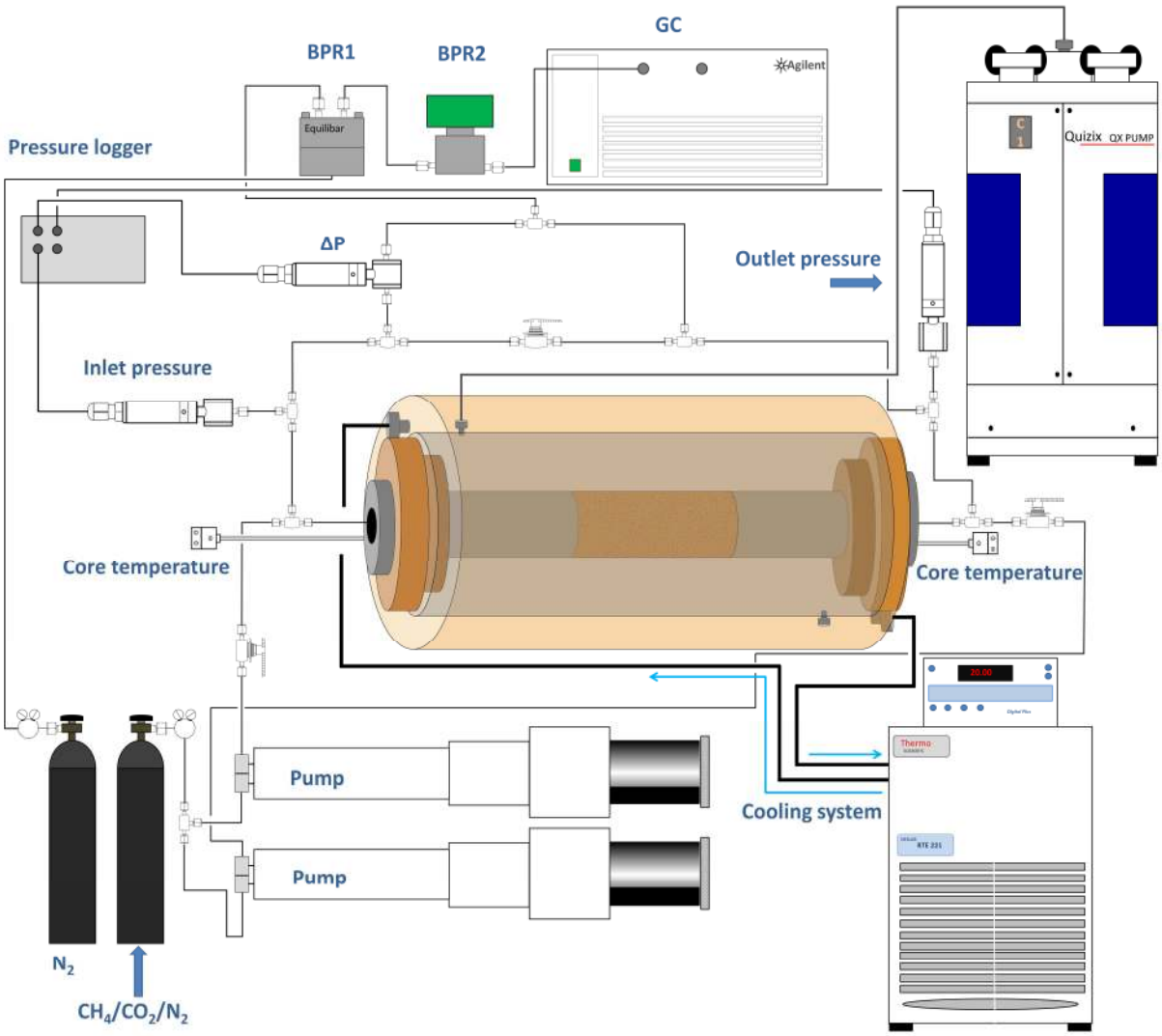

Figure 15 – Description of main principles of the three experimental setups at the University of Bergen. The core outlet (right side) was either routed to a receiving pump (lower) or through an in-line GC for evaluation of gas composition.

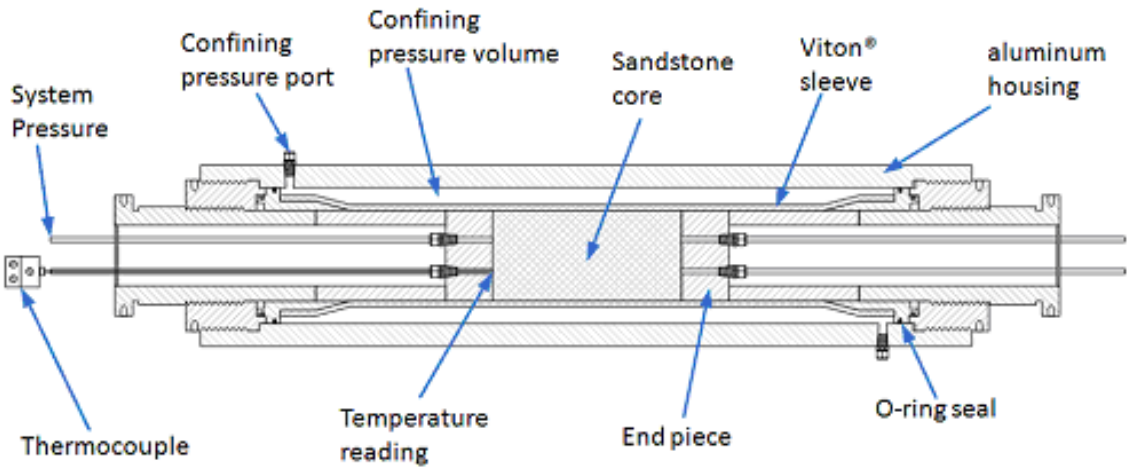

Figure 16 – Illustration of Hassler-type core holder used at the University of Bergen. Two pressure ports were available for confining pressure, while six connections were available for temperature readings and pore pressure control. Figure from Husebø (2008).

Resistivity setup

A Temco EHCH four-electrode core holder was used to bypass the contact impedance between the current electrodes and sample. Four-electrode setups have been detailed elsewhere (Bona et al., 2008). The core holder was equipped with a floating distribution plug which allowed radial and axial confining stress, as illustrated in Figure 17. The inner end piece faces were coated with a high conductivity silver layer contacting the trans-axial core faces. Two circular electrodes were embedded in a Buna-N sleeve with 2.54 cm spacing. These were connected to a HP 4262A LCR meter that measured resistivity between the electrodes using 1 kHz and 1 V. Dielectric fittings were used to avoid bypass during measurements. The core holder was equipped with a cylindrical cooling jacket where cooled antifreeze was circulated by a Thermo Neslab RTE-17 refrigerated bath.

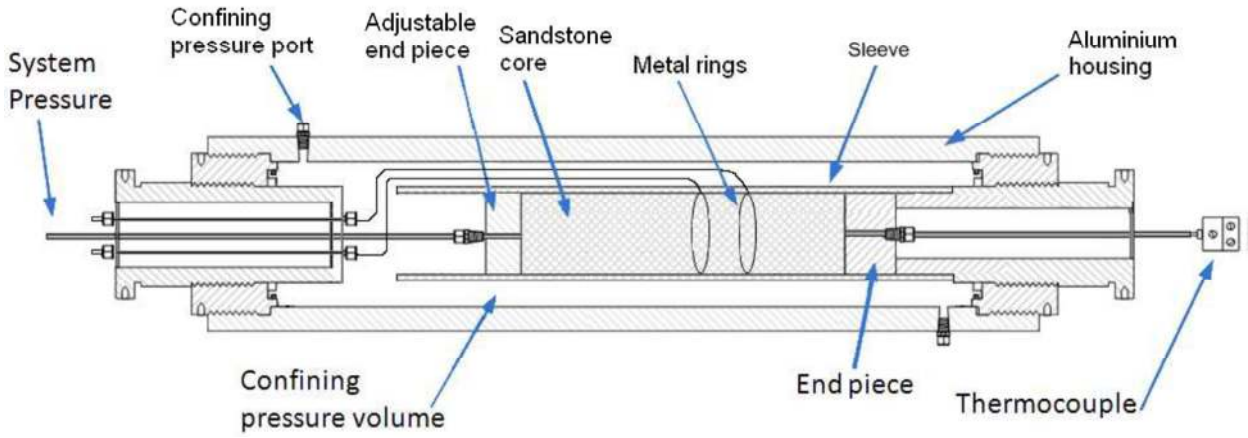

Figure 17 – Four electrode core holder used for hydrate resistivity experiments. The electric potential was measured across the two electrodes embedded in the sleeve. Figure from Odland (2009).

2.4 Experimental procedures

2.4.1 General procedures at ConocoPhillips Technology Center

Each sample was evacuated and saturated with a NaCl concentration ranging between 0.1 and 5 wt% ranging from fully saturated (1.0) to partial water saturation of 0.3. The core was assembled between two POM spacers and PEEK end pieces, which were held in place by Teflon shrink tubing. Figure 18 illustrates the saturation process for an assembled sample, where water imbibes from right. Partial vacuum assisted in distributing the water. The sample was positioned inside the composite core holder and centered inside the MRI. Fairly homogeneous longitudinal water saturation was confirmed through 1D profiles. The pore- and overburden pressure was then increased in a stepwise manner to 8.38 MPa and 10.44 MPa, respectively. The system was cooled to 4 °C while 3D MRI data were acquired continuously every 2 hours and 17 minutes.

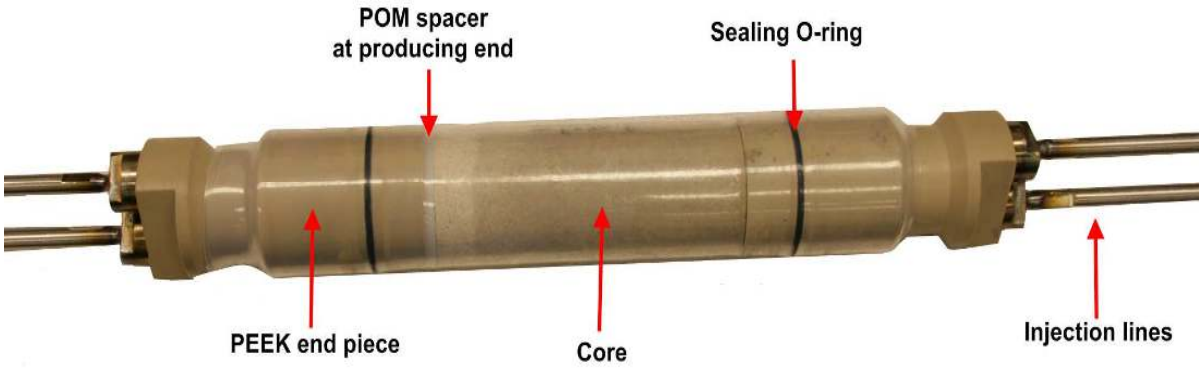

Figure 18 – Demonstration of core assembly and saturation process, where a water front is moving from right towards left. A single POM spacer is located at the left side for this specific test. The Teflon shrink tubing is confining all parts and isolating the sample from the confining fluid.

2.4.2 General procedures at the University of Bergen

The samples were saturated through spontaneous imbibition by positioning each sample horizontally in contact with a thin water film. Bentheim has a fairly high spontaneous imbibition potential, and samples were typically evacuated post saturation to achieve desired saturation. MRI has confirmed that this induces relatively uniform saturation conditions. The sample was positioned between two circular open-volume POM spacers and mounted into the core holder, where pore- and overburden pressure was increased in a stepwise manner to 8.38 MPa and 10.44 MPa, respectively. The system was then cooled to 4 °C.

2.4.3 Experimental procedure for resistivity measurements

The silver paper or end-pieces were saturated with brine prior to assembly to minimize contact impedance. This was the only deviation from the general procedure.

2.4.4 Experimental procedure during depressurization

The pressure was reduced at constant volumetric rate once no further changes in S_h were detected. Pressure was maintained above the hydration pressure, and the system was given time to equilibrate. The pore pressure was then further reduced and maintained below the hydration pressure, where dissociation was quantified

through volume changes (pump log) and changes in S_w (MRI). Two experiments were performed at three sequential pressure steps (3.96, 3.89 and 3.82 MPa), where the pore pressure was reduced once no further decomposition was detected. A third experiment was performed at 3.2 MPa, where gas hydrate decomposed at a single pressure step.

2.4.5 Experimental procedure for CO_2 exchange

The sample was wrapped in several layers of heavy duty plastic wrapping and aluminum foil (Bergen) to minimize negative effects of carbonic acid that forms during CO_2 injection. Two different approaches were then applied.

Huff and puff

CO_2 was injected through the open spacer volume to displace excess CH_4 while the effluent was evaluated *in situ* by the in line GC. The system outlet was isolated once only traces of CH_4 were observed, and the inlet was maintained at constant pressure for days or weeks of CO_2 soaking. CH_4 production and accumulation in the spacer volume was monitored and quantified by the MRI. A sequential flush displaced the produced CH_4 and replenished CO_2 once minor intensity changes were observed. This procedure was repeated for the second flush.

Constant volumetric injection

The sample was isolated after hydrate formation commenced. Inlet and outlet lines were evacuated and pressurized by CO_2. Sample valves were opened simultaneously, and injection was initiated at 0.033 ml/min. The in line GC measured composition of the produced gas at specified time intervals.

2.4.6 Depressurization for determining hydration pressure

The intrinsic hydration pressure is dependent upon the guest composition, as illustrated in Figure 19. Variations in dissociation pressure can therefore be used for evaluation of guest composition if we assume that the hydrate and gas phase are in equilibrium. This concept was applied in this study, where hydrate dissociation was quantified through changes in MRI intensity or pump volume data. The approach is susceptible to variations in free gas composition and is therefore only valid as an approximation towards final conversion efficiency. This method was used to

evaluate mixed hydrate composition in a joint experimental study to address CO_2-CH_4 exchange kinetics (Hester et al., 2011), which will be elaborated in Chapter 4.4.3.

The depressurization process was initiated by CH_4 injection to displace excess CO_2 and thus limit reformation during decomposition. The flush continued until only traces of CO_2 were observed in the effluent. The depressurization sequences were performed in a stepwise manner, where pressure was reduced in 0.07-0.21 MPa steps while monitoring pump data and MRI. Pressure was then maintained constant during the next two consecutive MRI acquisitions (4 hours and 34 minutes) where decomposition was quantified through volume and intensity changes.

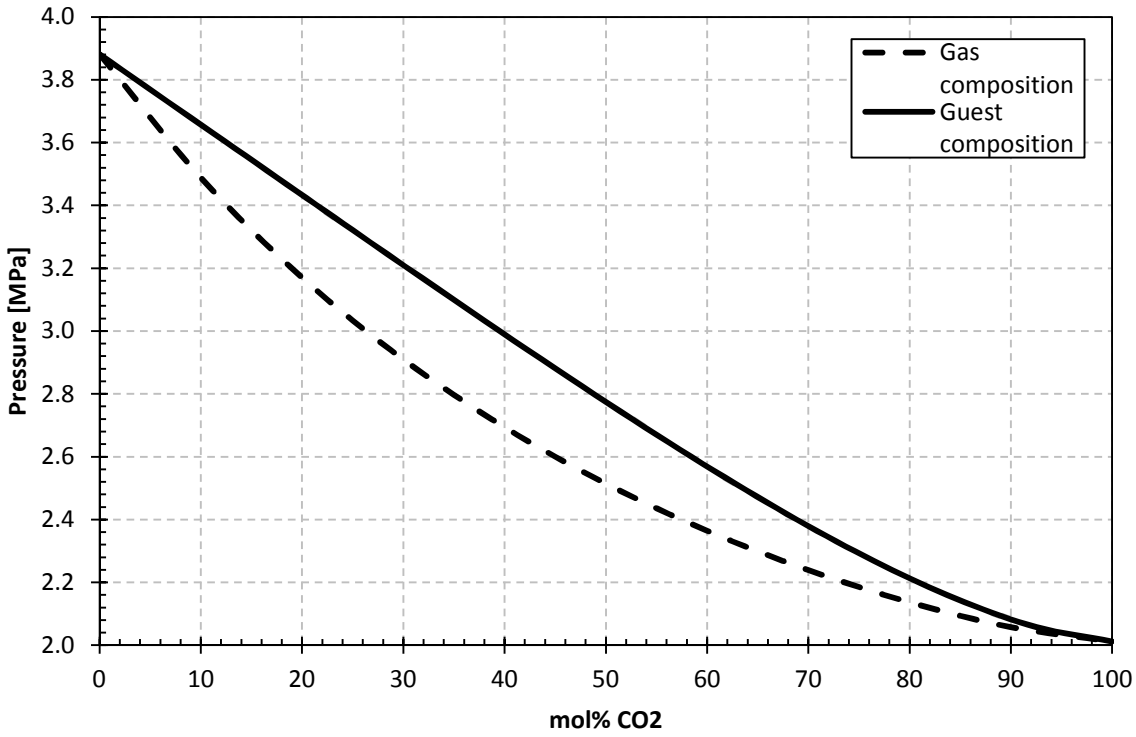

Figure 19 – Gas and guest composition in a P-x diagram at 4°C. Increasing CO_2 concentration in hydrate cavities efficiently reduces the three-phase equilibrium pressure. Data generated using CSMGem (Ballard and Sloan Jr, 2002).

3 NUMERICAL METHODS

Mathematical solutions for complex systems are often approached by discretizing space and time into a finite number of reasonable subdivisions where coupled equations describe the conditions of each subdomain. Elements may be discretized through options such as the finite element method (FEM) and the finite volume method (FVM), but the finite difference method (FDM) is the most common approach in the oil industry. Physical and chemical processes are described through sets of coupled, non-linear partial differential equations that describe fundamental properties such as fluid and heat flow within the reservoir. These coupled equations are solved at discrete points (nodal points) at each time step. The accuracy of the prediction depends on how well defined the problem is, the mathematical solution method (direct or iterative), knowledge of parameters that describe heat flow, chemical interactions and fluid flow, and also the availability of field or laboratory data that can verify the validity of the numerical models.

3.1 Numerical modeling of hydrate bearing sediments

Numerical studies of gas production from hydrates have advanced since the first efforts to evaluate production potential (Holder and Angert, 1982, Burshears et al., 1986, Yousif et al., 1991). A range of numerical models are currently available, where international effort has been made to compare (Wilder et al., 2008) and verify the performance of the different models (Anderson et al., 2011a, Anderson et al., 2011b). Models are generally limited to case studies due to limitations in field studies (Moridis, 2003, Hong et al., 2003, Kurihara et al., 2005, Moridis and Kowalsky, 2005, Moridis et al., 2007, Moridis and Reagan, 2007). Several studies also take advantage of field-specific parameters for evaluation of possible production potential (Moridis, 2004, Moridis et al., 2009, Moridis et al., 2011b, Moridis et al., 2010, Kurihara et al., 2010b, Anderson et al., 2011b, Uddin et al., 2011, Myshakin et al., 2012, Chejara et al., 2013). The common denominator is that most of these models are based on assumptions of phase transitions based on thermodynamic equilibrium, intrinsic kinetic descriptions or minimization of Gibbs free energy.

3.2 TOUGH+HYDRATE

TOUGH+HYDRATE v1.2 (T+H) is a FORTRAN95/2003 code for subsurface simulation of multi-component, multiphase fluid and heat flow (Moridis, 2003, Moridis et al., 2012). 26 different phase combinations are available, where phase transitions are described by equilibrium and kinetic reaction models. Elements are space discretized using integral finite difference method (IFDM) (Edwards, 1972, Narasimhan and Witherspoon, 1976), thereby removing any reference to a global coordinate system which is beneficial for spatial irregular discretization such as the Voronoi tessellation. The model stability is increased by fully implicit time discretization combined with upstream interface weighting of flux terms. The set of strongly coupled nonlinear algebraic equations are solved using Newton-Raphson iterations, where number of iterations required depends on the problem and preset convergence tolerance. Several linear equation solvers are available for solving the Jacobian (either direct solvers or conjugate gradient solvers such as DSLUCS and DLUSTB (van der Vorst, 1992, Sleijpen and Fokkema, 1993)). The properties of the real gas mixtures are computed using the Peng-Robinson EOS (Peng and Robinson, 1976) while implementing interaction parameters from Søreide and Whitson (1992) to account for the effect of salts. Phase relations are preferentially described by a combination of the P_e/T_e derived by Moridis (2003) from data reported by Sloan and Koh (2008) while enthalpy changes are described by Kamath et al. (1984) instead of the Clausius-Clapeyron equation.

3.2.1 The kinetic model

The kinetic model in TOUGH+HYDRATE is based on Kim et al. (1987) and Clarke and Bishnoi (2001), where fugacity is included to describe the rate at which formation and/or dissociation occurs. The mass accumulation term is given by

$$Q_H = \frac{\partial M}{\partial t} = -K_0 e^{\frac{\Delta E_a}{RT}} F_A A\left(f_{eq} - f_v\right)$$

where K_0 is the intrinsic hydration reaction constant [kg/(m^{2}Pas)], ΔE_a is the hydration activation energy [J/mol], R is the universal gas constant [8.314 J/(molK)], T is temperature [K], F_A is an area adjustment factor to correct for irregularities in grain shape and differences in hydrate shape and distribution, A is the active reaction surface area [m^2], f_{eq} is the fugacity [Pa] at equilibrium at temperature T

and f_v is the vapor fugacity [Pa] at temperature T. The intrinsic rate, activation energy and surface area was determined by Moridis et al. (2005) based on experimental results (Kneafsey et al., 2007) and inverse modeling. They concluded that the intrinsic rate was 1.78E+06 [mol/m^2/Pa/s] and the activation energy was 8.97E+04 [J/mol]. The area factor was varied between 0.0832 and 0.1091 to match the experimental data. It is likely that all of these parameters will change as hydrate forms or dissociates, as the pore geometry and reaction interface vary with S_h.

3.2.2 Heat conductivity

Heat transport is believed to be a controlling mechanism during formation and decomposition, and it is therefore important to describe heat transport within the porous media as accurately as possible. The heat flux term in T+H accounts for advection, conduction and radiative heat transfer. Several attempts have been made to measure the thermal conductivity of gas hydrate, and values have been reported to range between 0.25-0.7 (Gupta et al., 2006, Waite et al., 2009, Warzinski et al., 2008, Carrol, 2009). This study has used both 0.45 and 0.57 W/m/K which did not result in significant variation in the mass accumulation term.

3.2.3 Operating the code

The code is operated in a flexible manner, where the user specifies the problem geometry, initial conditions and boundaries, sinks and sources, physical properties of the system and also the computational parameters through one or several ASCII input files. Some sections of the file are free-format, while other sections require fixed format for backward compatibility with the TOUGH2 code (Preuss et al., 2012). The system grid construction (MESH) is generated using an independent FORTRAN program (MeshMaker.f95).

4 EXPERIMENTAL RESULTS AND DISCUSSION

4.1 Hydrate formation

Gas hydrates were formed repeatedly at varying saturations and salinities using the excess gas approach (Chapter 1.3.5). The pore space configuration depends on saturation, where higher S_{wi} is likely to trigger growth in the middle of the pore space at the gas/water interface. This is believed to be the natural growth habitat for gas hydrates as gas-saturated water migrates through the hydrate stable zone.

4.1.1 Mass balance data

Similar response during hydrate formation was generally observed, as illustrated in Figure 20. Hydrate formation was detected as sudden increase in CH_4 delivery from the pumps, as the CH_4 density increases in the hydrate crystal. This resulted in a pressure drop, and the pump compensated by injecting gas to maintain constant pressure. PVT (Pressure, Volume and Temperature) data were therefore monitored for all experiments. The time required for hydrate formation depended upon ion concentration and S_{wi}, as discussed in **Paper 1**, where the formation time was increased for higher initial concentrations. The fraction of crystallized water was reduced for higher salinities because of increased ion interaction with the formation water, as illustrated in Figure 21. *Fill fraction* was defined as (mol CH_4/mol H_2O)*n_H, where the hydration number n_H was set to 5.99 based on measurements from Circone et al. (2005). An experimental n_H=5.99 would therefore induce Fill Fraction=1. CSMGem predict inhibition at 14 wt% NaCl brine at the experimental conditions, illustrated by the red dashed line. The fraction of hydrated water will therefore be less abundant for higher initial ion concentration, and fill fraction is assumed to follow the red theoretical line. Over-estimated fill fraction could indicate lower hydration number (higher degree of cage filling), a small leak, or less salt impact for lower ion concentrations. However, the overall correspondence with predictions from CSMGem is good. The experiments in Figure 20 have been further discussed in **Paper 5**, while some data in Figure 21 have been previously published in (Husebø et al., 2009).

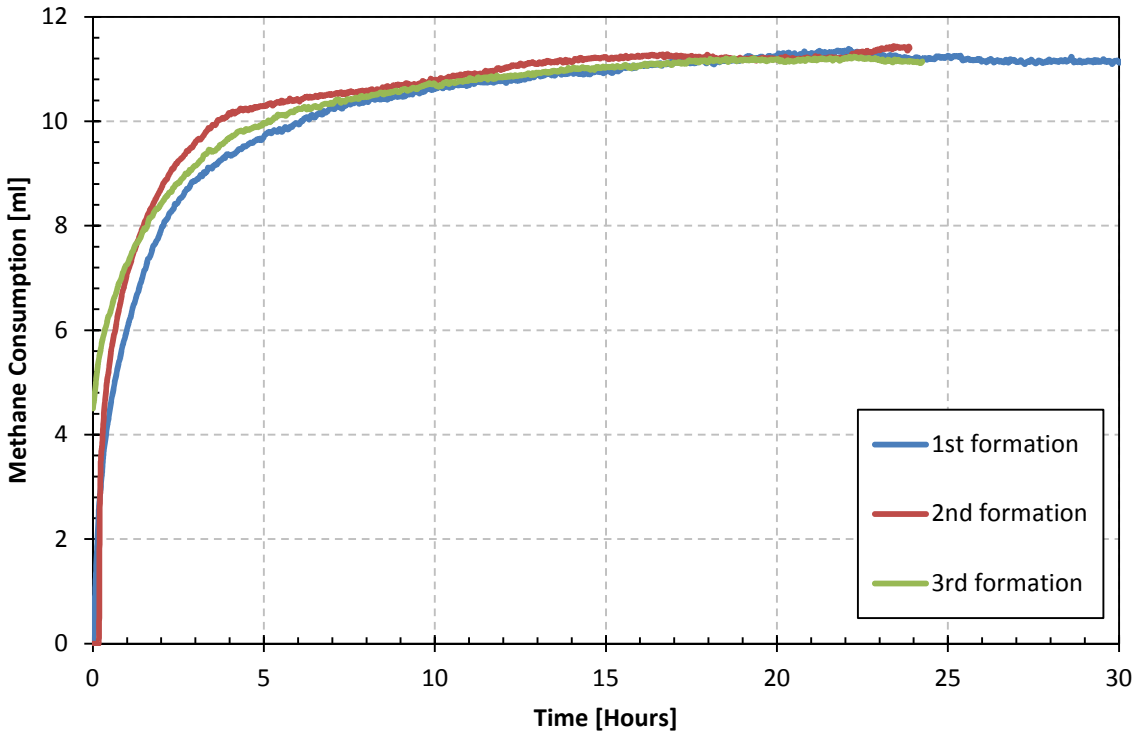

Figure 20 – Comparison of hydrate formation for three experiments at the same sample with S_{wi}=0.3 and 0.1 wt% NaCl brine composition. Higher saturations and higher salinities increased the time required for hydrate formation.

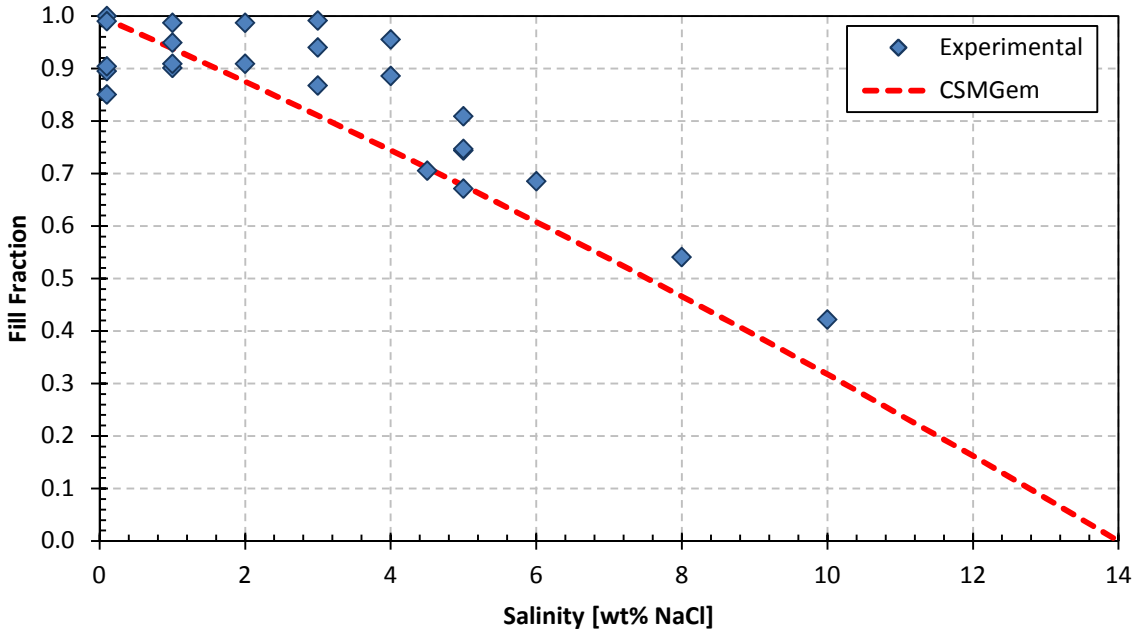

Figure 21 – Salinity impacts during growth appear more pronounced for higher salt concentrations. Fill fraction was defined as the inverse experimental hydration number multiplied by the theoretical hydration number. Hydrate formation is inhibited at 14 wt% ion concentration, and the fill fraction was therefore expected to follow the red dashed line.

4.1.2 MRI saturation data

Hydrogen spin in solid hydrate has short lifetime, as discussed in Chapter 2.2. Hydrate formation was therefore quantified based on loss of signal. Good agreement between mass balance data and MRI was generally observed, as illustrated in Figure 22. The experiment has been further discussed in **Paper 5**. Phase transitions and variations in hydrate growth patterns were spatially resolved using the MRI. Figure 23 shows a sequence of MRI images during growth for a sample at S_{wi}=0.98. Limited guest molecule access restricted initial growth to the transaxial core faces. Hydrate growth progressed at the outer radii, thus indicating that initial growth was limited both by mass and heat transport. The experiment (2-1) has been further described in **Paper 4**.

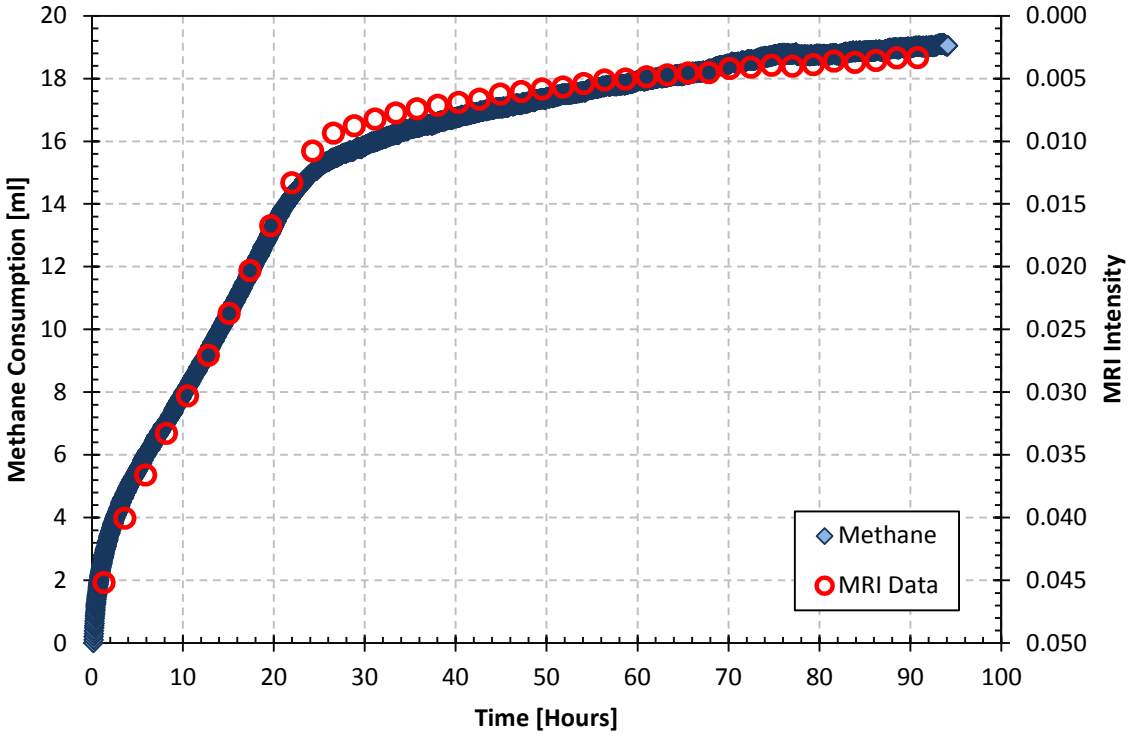

Figure 22 – Comparison of CH_4 consumption and MRI intensity during hydrate formation for an experiment with S_{wi}=0.6 and 0.1 wt% NaCl brine. Mass balance data correspond well with data from MRI, plotted on inverse axis.

4.1 Hydrate formation

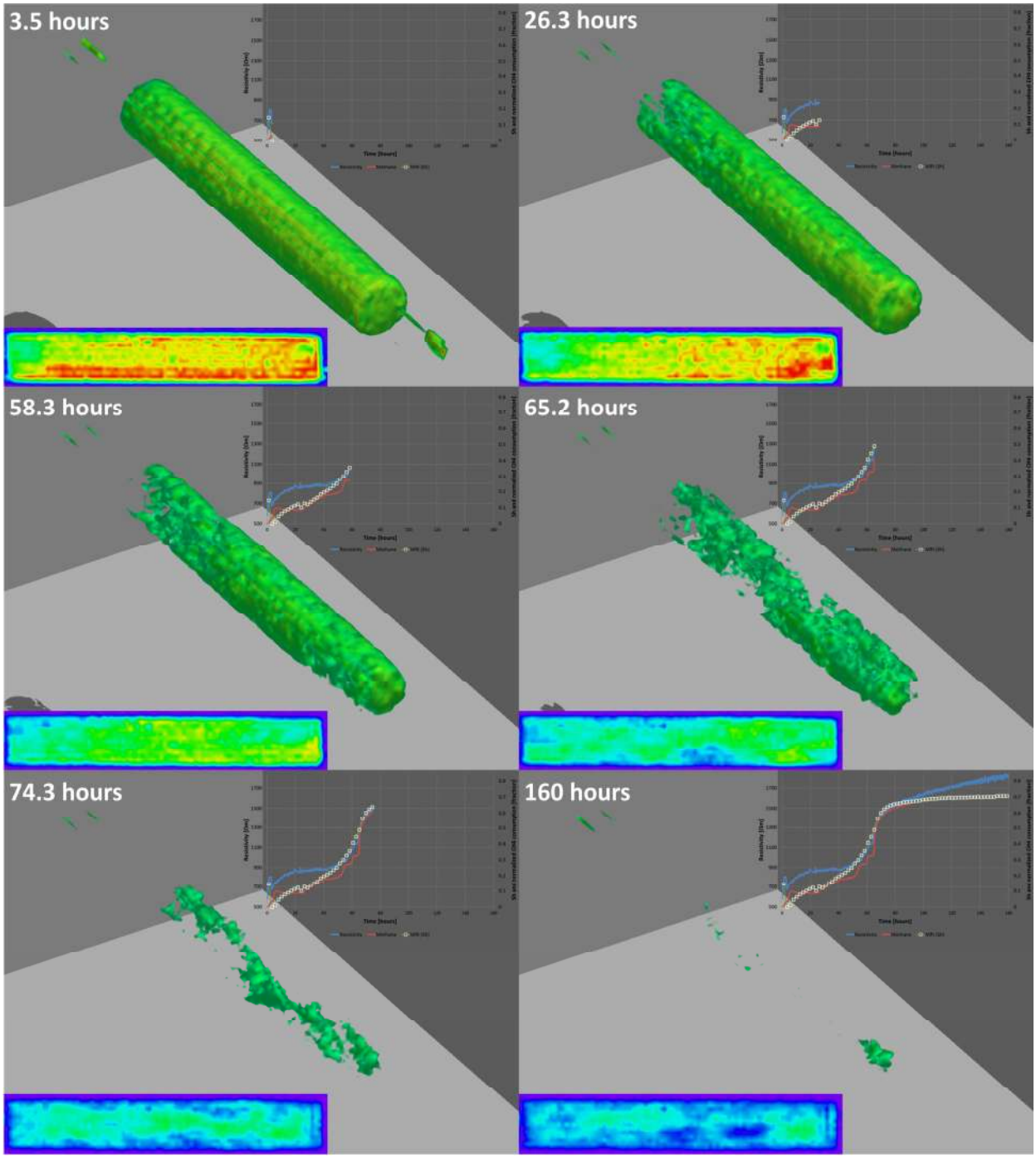

Figure 23 – Spatial 3D saturation data during growth is useful for monitoring differences in growth pattern. Initial growth was focused close to the end pieces and at the outer radii, but progressed in a uniformly manner despite high S_{wi}.

4.1.3 Variations in hydrate growth pattern

Frontal advancement in **Paper 4** was assumed to be a dominating factor for the observed resistivity progression. Growth was initiated at the left core surface in Figure 24 and converged towards the middle section of the core. Slightly non-uniform saturation distribution was observed in the first image, which may provide favorable growth conditions at the left side. Frontal movement may have induced a high-salinity water bank at the hydrate formation front which inhibited further front advancement after 110 hours. However, both heat liberated at the formation front and increased ion concentration result in less favorable growth conditions from a thermodynamic perspective. The piston-like growth pattern therefore appears as an unfavorable growth process.

Similar behavior was observed in a previous single spacer configured experiment, where a piston-like growth pattern emerged after 8 hours (Figure 25). The growth behavior was assumed to be related to variations in initial saturation in **Paper 1**. Yet, the growth process appeared insensitive to the locally lower saturation in the left part of the core and progressed from both directions. Hydrate growth is generally assumed to be heat- or mass transfer limited, as discussed in Chapter 1.2.1. The observed growth behavior in this study was not merely a result of saturation variations, and further evaluation is necessary to fully understand mechanisms involved during hydrate growth in porous media. Variations in hydrate growth pattern will be reflected in physical properties such as geomechanical contribution (**Paper 2**) and electrical resistivity (**Paper 4**), and evaluation of such properties should therefore preferably be supported by *in situ* imaging.

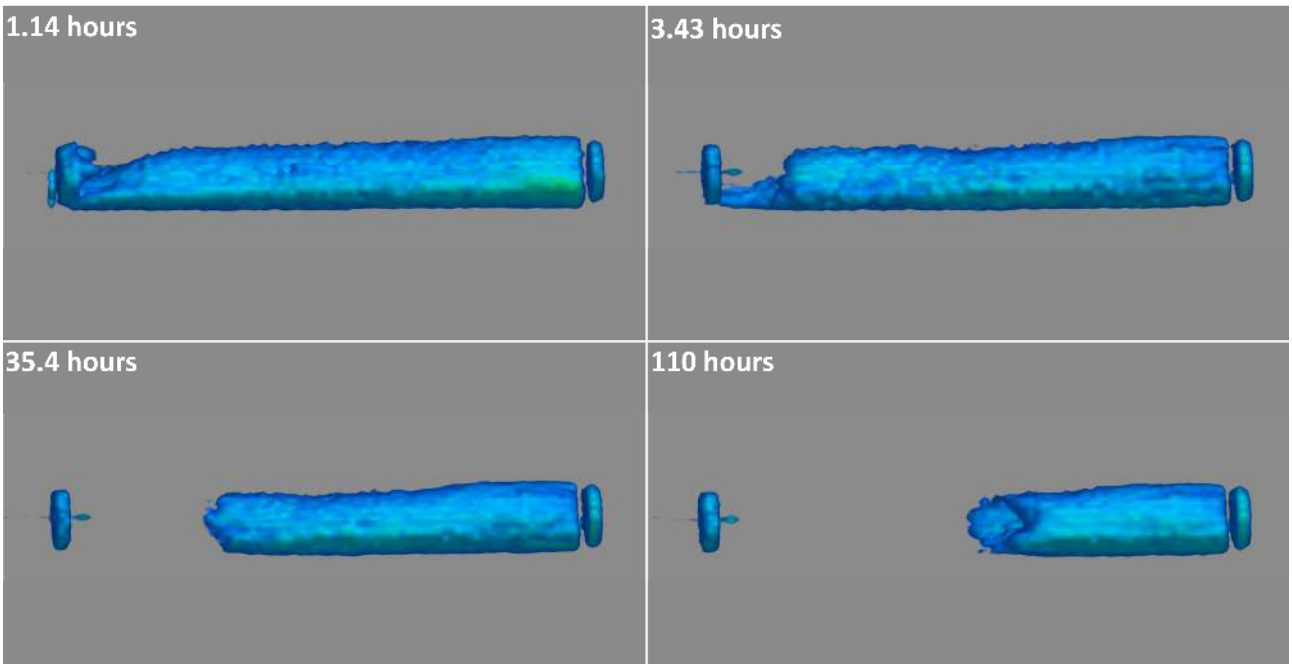

Figure 24 – Frontal advancement was observed from left towards the middle of the core, with minor intensity variations in the remainder of the core. It was assumed that growth was triggered at the left side because non-uniform saturation distribution resulted in more favorable growth conditions.

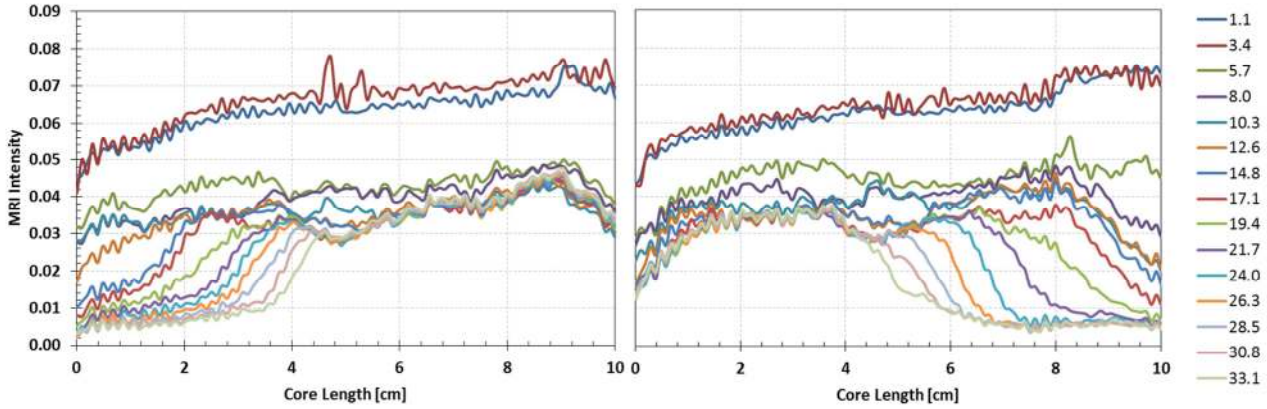

Figure 25 – Frontal advancement was observed in the two core halves, where hydrate growth converged towards the middle section in both core halves. This behavior was initially assumed to be a result of increased reaction interface due to variations in saturation; however, the growth pattern appeared unaffected by global saturation differences. Legend indicates time (hours) for the different images.

4.2 Resistivity measurements

Resistivity is frequently applied to determine saturation in hydrate bearing intervals, but there is a current lack of calibration data. The robustness of the technique was evaluated through a series of experiments that are summarized in **Paper 4** and in an additional paper (Birkedal et al., 2011). The following section will therefore only highlight specific results and provide further discussion on selected subjects.

4.2.1 Preliminary R_o measurements

The sediments response to elevated salinities was determined through a series of preliminary tests, and at the same time served as R_o measurements that were to aid in the resistivity interpretation. Variations in salinity have generally been neglected in the majority of resistivity studies. Salt is excluded during hydrate formation, as there is no space to accommodate salt ions. The local salt concentration is therefore elevated during formation, which enhances the conductivity of the remaining formation brine. An empirical relationship that describes the sediments resistivity response to variations in ion concentration was acquired through regression analysis of R_o measurements. This was implemented in the standard Archie resistivity model, and will be referred to as the dynamic model when applied in this study.

4.2.2 Initial resistivity response

An initial resistivity drop was observed for all experiments in **Paper 4** as hydrates started forming. This has generally been assumed to be a result of adiabatic heating; however, the experiments revealed only minor temperature variations at the initiation of growth (typically <0.5 °C). The thermocouple is positioned at the core surface, and the temperature amplitude may therefore be higher within the porous media. Regression analysis from R_o experiments suggests that a 0.5 °C temperature deflection is not sufficient to explain the overall resistivity drop observed at the initiation of growth. Elevated ion concentration at the water/hydrate/gas interface was assumed to be the main reason for the observed resistivity response in **Paper 4.** The effect is most likely a combination of several physical processes, such as temperature, ion elevation, variations in hydrate morphology related to driving force (i.e. extrusion of needle-like crystals or smooth surface (Servio and Englezos, 2003)) and differences in hydrate growth pattern. As an analogy, ice growth kinetics

is influenced by salinity, where lake ice (low salinity) is characterized by planar progression, while dendrite topologies are observed for sea ice growth (e.g. (Petrich and Eicken, 2010)). The net charge travel length would increase by protrusion of such geometric shapes into the water phase, thus neutralizing the effect of elevated salinity for higher initial salinities.

4.2.3 Effective porosity from Archie

Porosity may be determined through Archie's formation factor, where variations in hydrate saturation have to be accounted for through reduced effective porosity. Changes in salt concentration during hydrate growth should also be accounted for to avoid overestimating the fraction of mobile pore space. Changes in effective porosity ($\phi_{eff}=\phi(1-S_h)$) and R_w were determined through MRI intensity variations. MRI porosity is compared with Archie porosity through static R_w and the dynamic approach in Figure 26. The effective porosity was overestimated by a factor of 2 when neglecting to address growth-induced salinity changes. In comparison, dynamic estimates remained within 1.7 % in porosity units during hydrate growth.

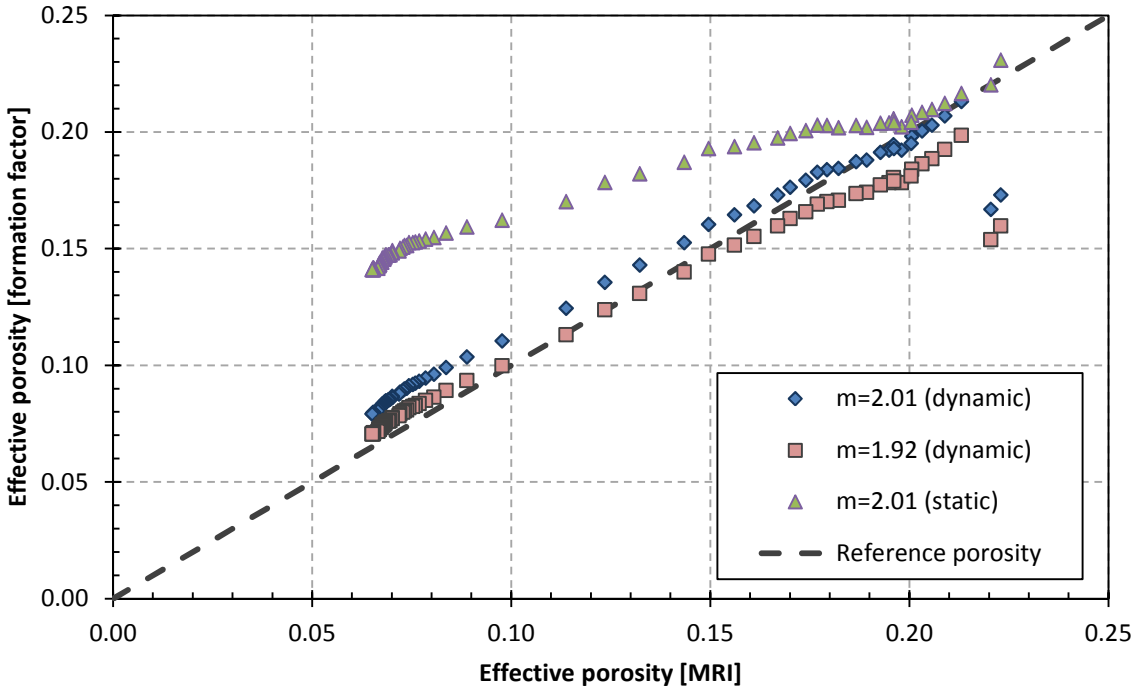

Figure 26 – Comparison of effective porosity from MRI and Archie for different cementation exponents. The static model over-estimated the actual porosity by a factor of 2.

4.2.4 Comparison of data for evaluation of saturation

Determining the accuracy of resistivity-based saturation predictions was the main motivation in this study. Trends in resistivity, CH_4 consumption and MRI intensity were therefore compared in **Paper 4**. Saturation predictions based on resistivity are compared with MRI data and CH_4 consumption in Figure 27. Resistivity-based saturation was estimated through three different approaches; 1) dynamic Resistivity Index (RI) with *n*=1.9386 (Pearson et al., 1983), 2) dynamic RI with average *n* during hydrate formation (2.16), and 3) static RI with *n*=1.9386. Final saturation was underestimated by 11% for the static approach, compared to 2.5% with *n*=1.9386. Impact of variations in *n* will be further elaborated in the next section.

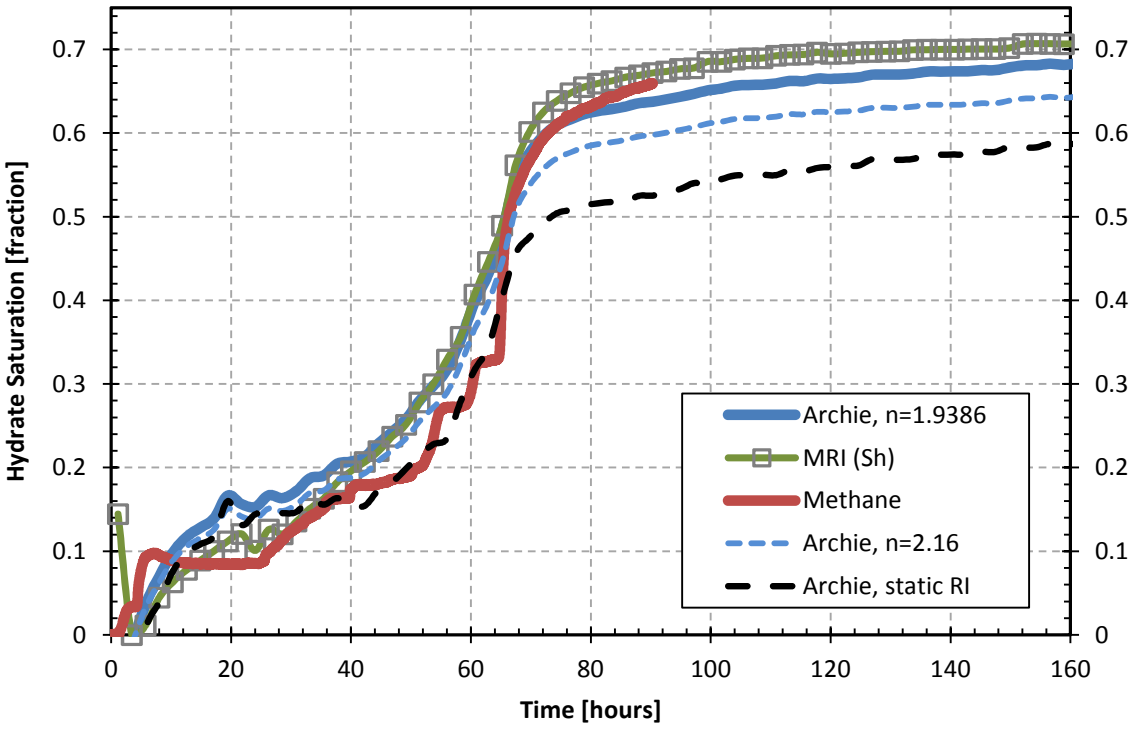

Figure 27 – Comparison of saturation estimates through different methods. Accurate resistivity-based estimates required implementation of a dynamic model that accounted for variable ion concentration.

4.2.5 Variations in saturation exponent *n* during growth

The curve trajectory in RI plots in **Paper 4** was highly variable, which is reflected in dynamic progression of *n* in Figure 28. Experiment 2-2 exhibited trends consistent with expectations for a water-wet sandstone, while 4-3, 2-4 and 2-5 showed deviating trends. Complex pore geometries combined with capillary bound water at the grain surface were documented to result in similar behavior in the oil and gas industry (Worthington et al., 1989, Sen, 1997). The observed trends are also similar to predictions from Spangenberg (2001), where the observed peak was a result of non-cementing growth combined with capillary forces and preservation of a conductive water layer at the mineral surface. In such case, the hydrate bearing sediment may progress into a bi- or multi-modal sediment, where the pore space between the hydrate crystal and mineral surface corresponds to micro-fractures.

Dynamic resistivity trends during hydrate formation coincide with higher concentration formation brine, which indicates that salinity impacts the hydrate morphology within the pore space. In analogy, 10-40% ion retention in microscopic layers between ice structures was observed for sea ice growth (high salinity) while lake ice (low salinity) growth progressed in a planar manner (Petrich and Eicken, 2010). Electrical properties of poly-crystal hydrate separated by microscopic conductive brine layers in inter-granular pore networks may be similar to bi-modal sediments with conductive micro-fractures. These layers will maintain conductivity as the bulk water content is reduced, which may explain the dynamic behaviors in *n*. In comparison, low salinity brine may induce planar progression and only small variations in *n*. Global variations (i.e. piston like advancement) will also impact the inherent resistivity and *n*.

Saturation interpretation for systems with dynamic *n* is complicated, as illustrated in Figure 29. The initial saturation was over-estimated by more than 10 saturation units for average *n* (3.25), while a good agreement was observed for lower S_w. There is a current need for further evaluation and understanding of mechanisms involved in this process.

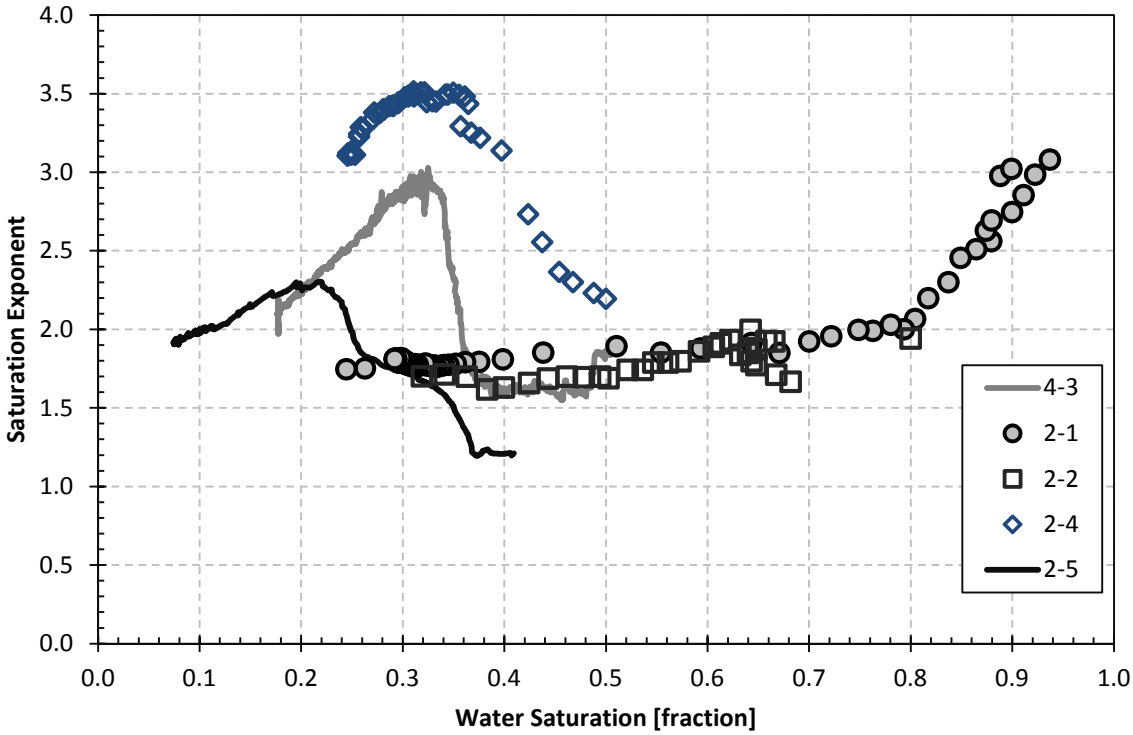

Figure 28 – Variations in saturation exponent during growth for a selection of experiments. The increase in n for lower S_w is similar to observations for sediments with bimodal pore size distribution. This behavior was interpreted as a result of variations in growth pattern in **Paper 4**.

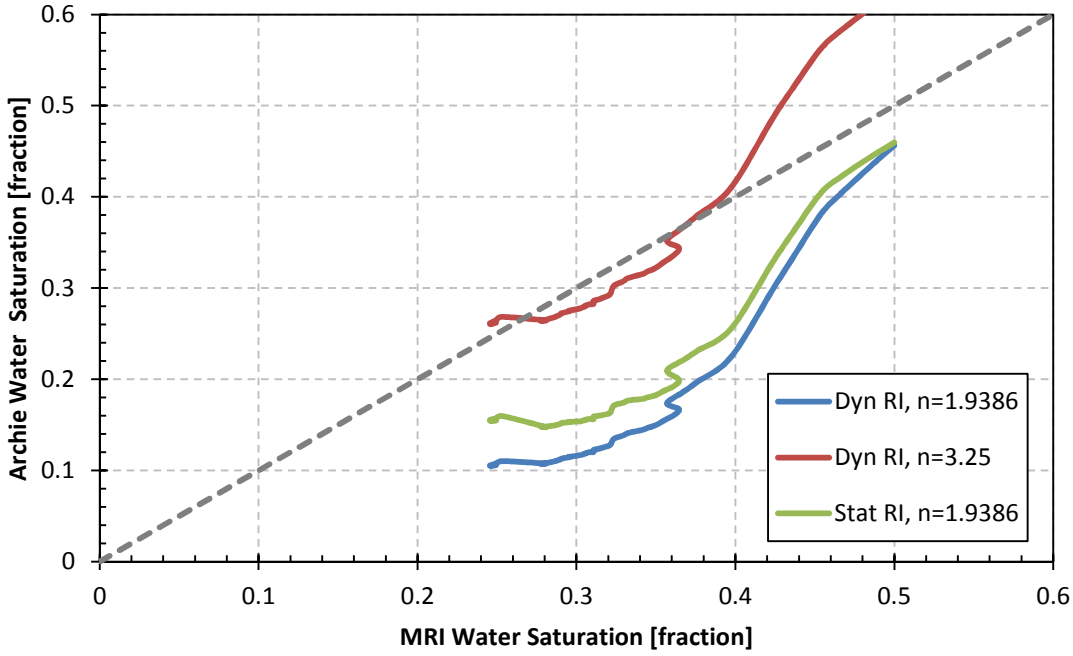

Figure 29 – Comparison of MRI S_w and predictions based on resistivity for experiment 2-4. Significant variations in n during growth complicated the saturation interpretation, where extensive deviations were observed.

4.3 Hydrate depressurization

Depressurization data from previous studies (Husebø et al., 2008, Birkedal, 2009) were further analyzed and discussed in **Paper 1, Paper 2** and **Paper 3**. Permeability was initially assumed to be a controlling mechanism, where hydrate dissociation was restricted to specific core segments and only occurred at the bulk hydrate surface. Film persistence of water at the mineral surface will ensure pressure propagation even at medium high S_h. Permeability was further enhanced by excess gas in this study. Heat transport was established as the main controlling dissociation mechanisms based on extended analysis, as illustrated in Figure 30. The dissociation rate was sensitive to variations in overburden temperature induced by endothermic reactions within the core. Sufficient heat transport is necessitated by the endothermic reaction. Boundary temperature at deflection points corresponded well with statistical equilibrium data from CSMGem, as illustrated in **Paper 3**. The fugacity difference (the driving force) was low, and the system was therefore susceptible to minor temperature variations. Immediate temperature increase after dissociation was observed for Test 1, which corresponds well with previous observations (Kamata et al., 2005, Gupta et al., 2009). Increasing dissociation driving force reduced the temperature sensitivity in both Test 1 and Test 2. Dissociation at higher driving force was therefore employed for Test 3, which will be further elaborated in Chapter 5.2.2.

3D images from the Test 2 depressurization sequence are summarized in Figure 31. Hydrate growth was retained in a core segment despite significant subcooling for 180 hours. Variations in MRI intensity in Figure 32 suggest that this water was active during the decomposition process. Mobilization of under-saturated water or water with elevated salt concentration may explain this behavior, where hydrate decomposes in order to reach equilibrium conditions. This corresponds with observations made by Rehder et al. (2004). Continued decomposition was mainly controlled by heat transfer, as discussed in **Paper 3**. One unique feature in Figure 31 was the loss of signal in the middle core segment between 176.5 and 190.3 hours. Limited heat transfer resulted in reformation while decomposition continued at favorable heat transfer sites adjacent to the end pieces. This behavior was consistent with the sudden temperature drop in Figure 30 (170 hours).

4.3 Hydrate depressurization

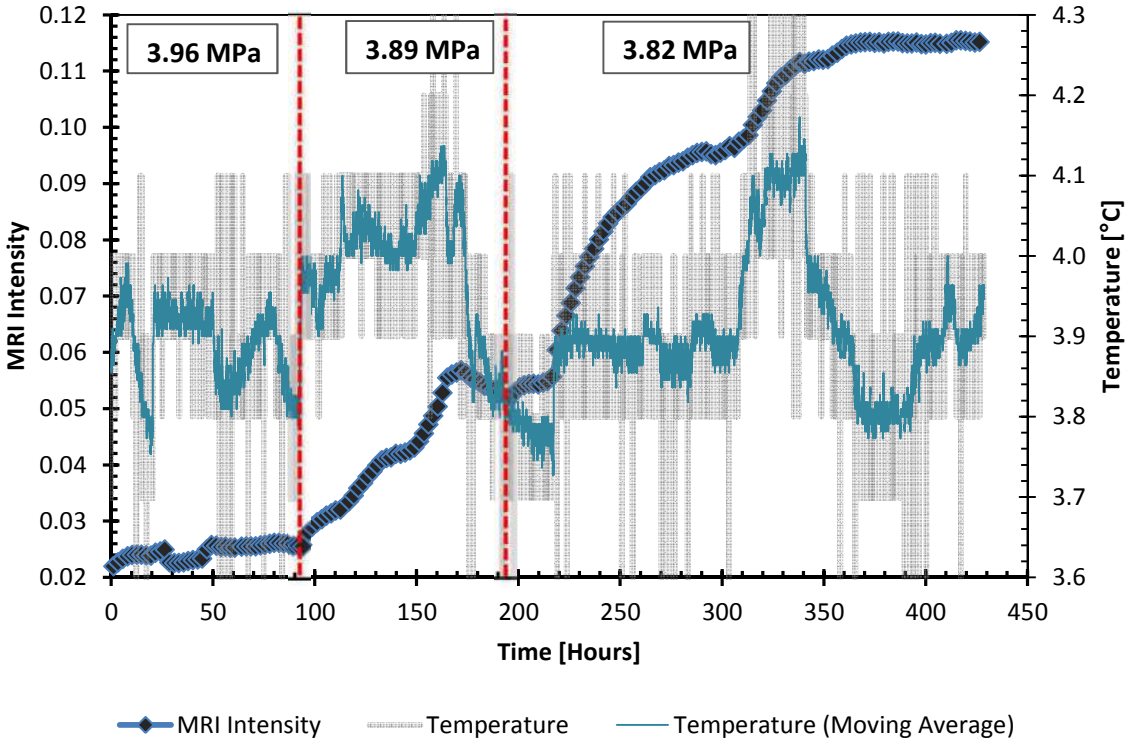

Figure 30 – Changes in MRI intensity and confining temperature during depressurization. Hydrate was decomposed at three pressure steps, where lower pressures increased the dissociation driving force. Decomposition was sensitive to temperature variations, where 0.2-0.3 °C variations shifted the sample into the hydrate stable region after 170 hours.

Release of associated water is one of the inherent limitations with depressurization, and may constitute a significant fraction of the produced fluids. Sample and spacer intensities for Test 2 are compared in Figure 33. Intensity of a CH_4 filled spacer was approximately 0.05, and higher intensities therefore indicate water production into the spacer volume and lines. Water in the front spacer was more abundant, as the pressure drop induces fluid flow towards the producer. Heat transport efficiency will be enhanced by presence of free water in the spacer volume due to favorable thermophysical properties relative to CH_4. Further decomposition may therefore be promoted in vicinity of the end pieces for PT conditions outside the hydrate stable region. Production of excess water has additional environmental consequences, and further reduces the geomechanical stability of the hydrate bearing sediment.

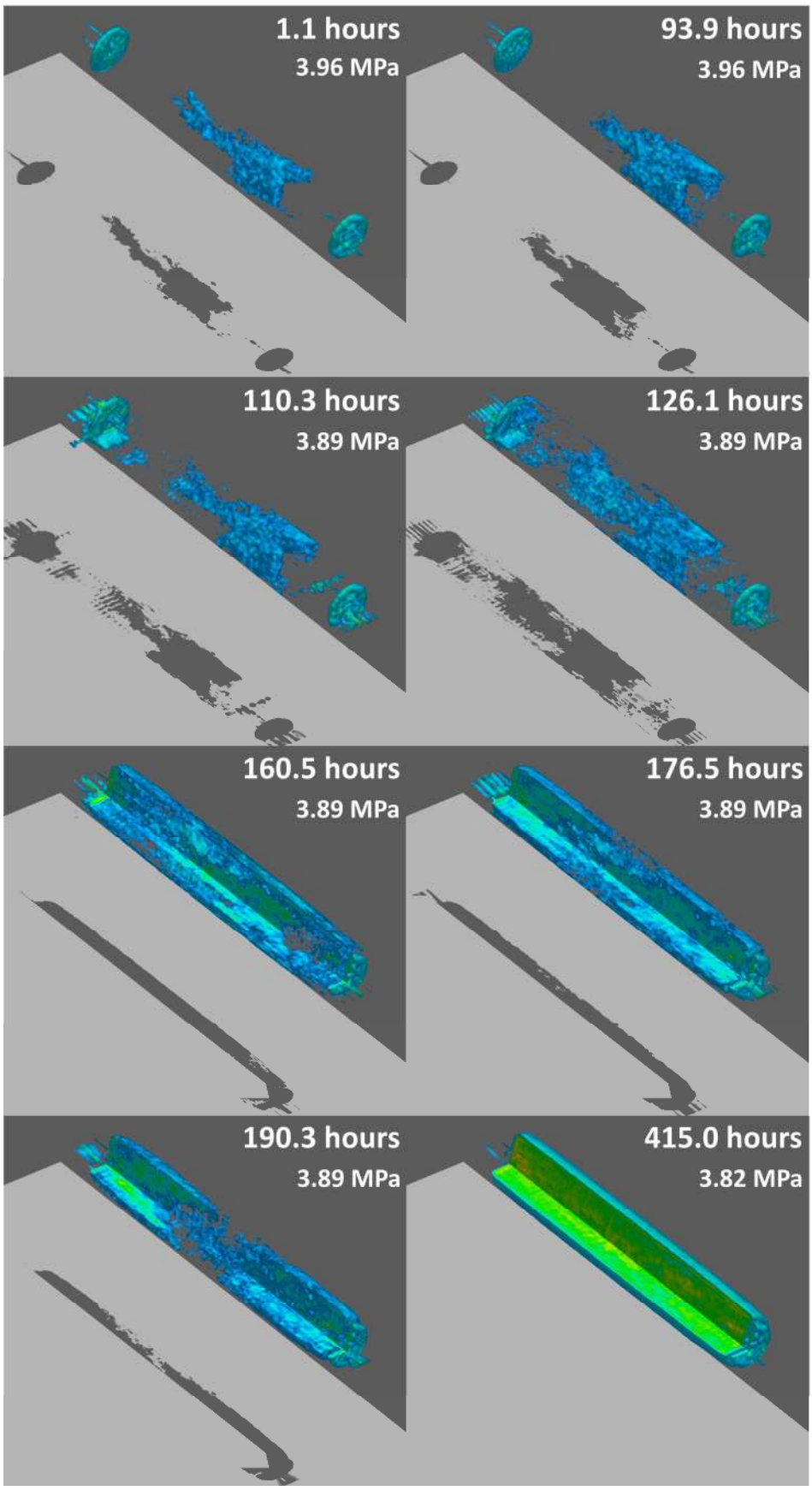

Figure 31 – Depressurization sequence at 3.96, 3.89 and 3.82 MPa.

4.3 Hydrate depressurization

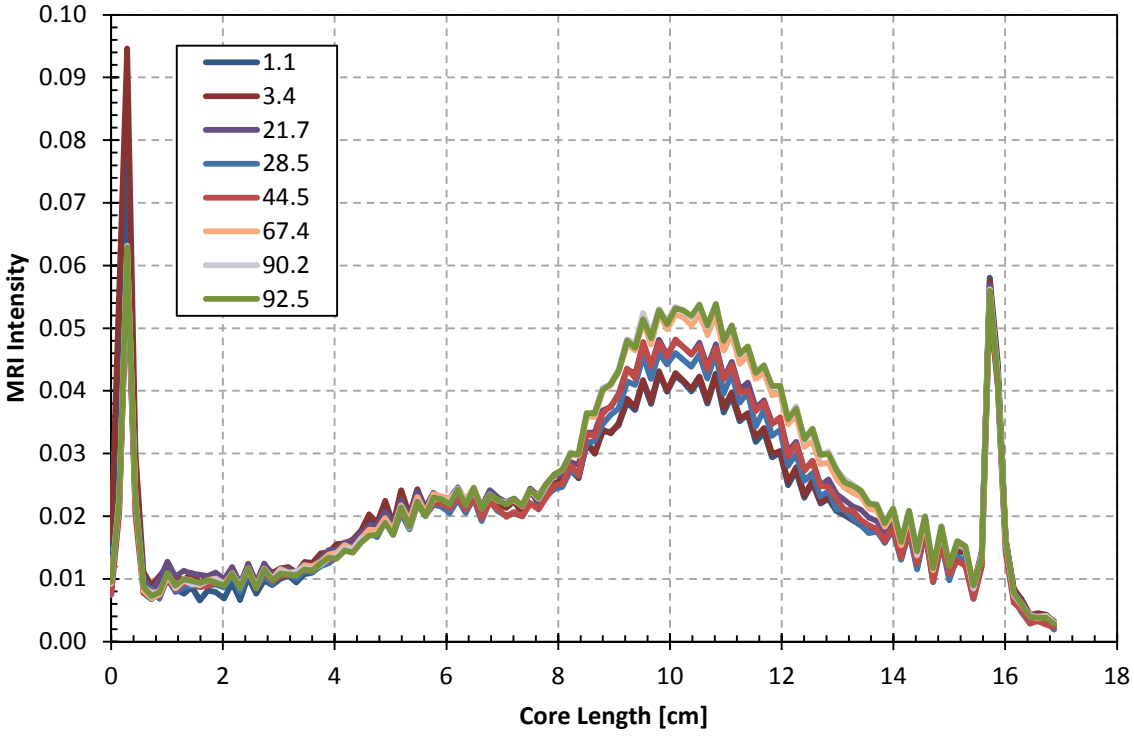

Figure 32 – MRI profiles at 3.96 MPa show decomposition focused in the vicinity of the excess water. Mobilization of suppressed water may trigger dissociation if the chemical composition (solubility of CH_4 or NaCl) results in non-equilibrium conditions. Legend title indicates time in hours.

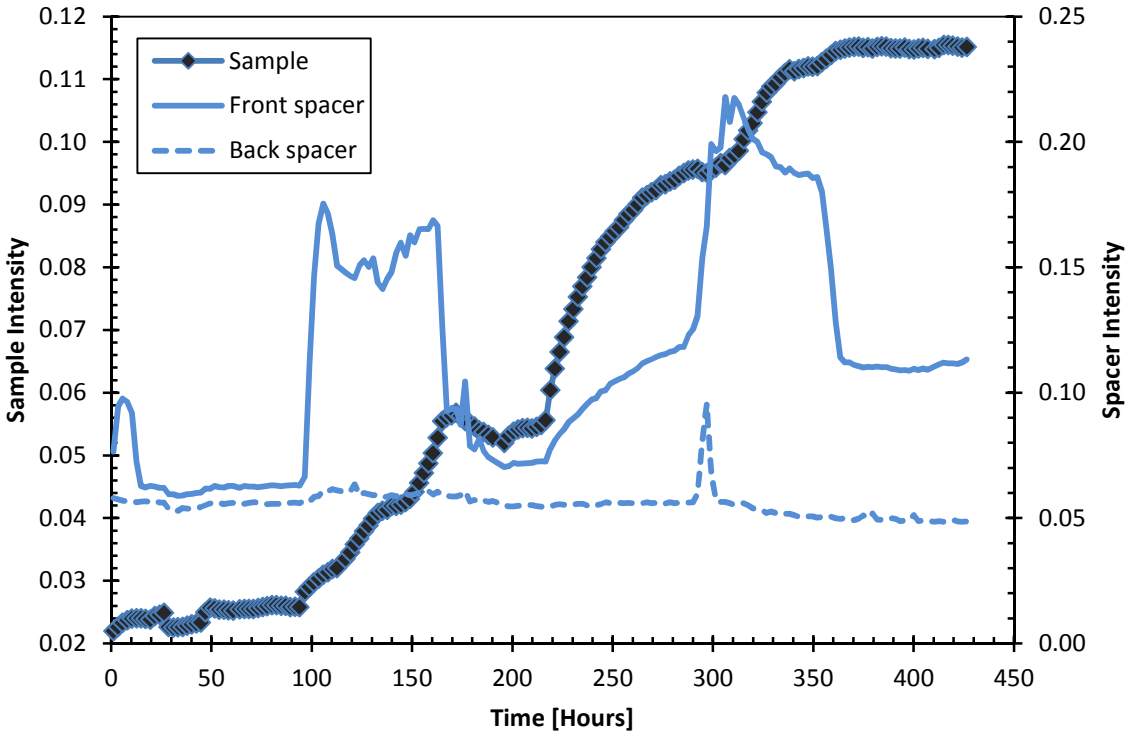

Figure 33 – Sample and spacer intensity variations during decomposition.

4.4 Guest molecule replacement through CO_2 injection

Previous experimental efforts have demonstrated the CO_2-CH_4 exchange feasibility in a single-spacer core configuration, where CH_4 release and accumulation in the spacer volume were monitored *in situ* by MRI (Husebø, 2008, Ersland, 2008). Similar configuration has been applied in this study, but with slight modifications in methodology. Results have been discussed in **Paper 1**, **2**, **4 and 5**, and the following will therefore only outline the overall conclusions and main contributions.

4.4.1 Salt effects during exchange

NaCl is a hydrate inhibitor, and therefore affects both growth and exchange performance. The extent of crystallization in Figure 21 was sensitive to higher salinities, especially when exceeding 4 wt% NaCl brine. The extent of excess water is therefore related to brine salinity, which is important from a mass transfer perspective due to higher diffusivity. Abundance of NaCl results in less favorable conditions in terms of solubility (Duan and Sun, 2003), but the net transportation contribution from NaCl is positive. The intrinsic hydrate stability is also affected by varying salt concentration. CH_4 hydrate formation is inhibited at 14 wt% NaCl (three-phase equilibrium line at 4 °C and 8.38 MPa). In comparison, CO_2 hydrate is more susceptible to variations in salinity, and formation will be retained for lower salinities, as illustrated in Figure 34. This is beneficial from a mass transfer perspective, where excess water crystallization is partially suppressed as the CO_2 advances and diffuses through the high-salinity water film. The importance of a continuous film that coats the mineral grains has been discussed in **Paper 1**, **Paper 2**, **Paper 4** and **Paper 5**.

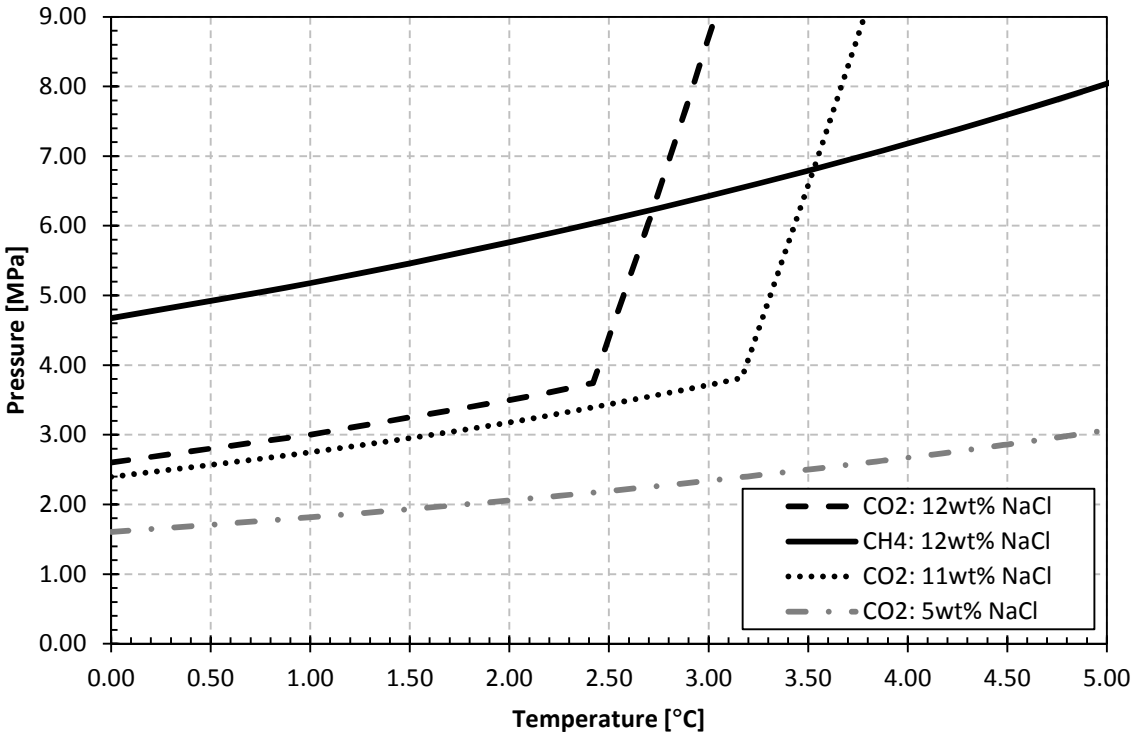

Figure 34 – Hydrate three-phase equilibrium lines at varying salinities for CH_4 and CO_2 guest molecules. CH_4, represented by the solid line, is less susceptible to variations in ion concentration than CO_2. Data generated through CSMGem (Ballard and Sloan Jr, 2002).

4.4.2 Geomechanical stability during exchange

Paper 2 reviewed current opinion on gas hydrates and geomechanical stability, which concluded that gas hydrates significantly enhance sediment stiffness and shear strength. Minor intensity variations have been observed during CO_2 injection and CO_2-CH_4 exchange, and it was therefore assumed that the overall sediment geomechanical stability was maintained during the solid-liquid-solid transition. This has later been confirmed through P-wave measurements (Espinoza and Santamarina, 2011), but should be further addressed in geomechanical tests.

4.4.3 Addressing limitations in driving force

The efficiency of diffusion-driven CO_2 transport and CO_2-CH_4 exchange driving force are both related to the CO_2 composition in the gas/liquid phase, and will therefore be sensitive to dilution during CH_4 release. Initial CO_2 transport into the core segments was not necessarily a slow process, but dilution may have inhibited transport to radially more distant positions, as illustrated in **Paper 5**. This limitation

was targeted in a series of six experiments, where CO_2 was injected at constant rate to maintain high CO_2 concentration. Limitations in exchange kinetics were addressed by varying saturation and exposure time.

Shifting hydration pressure for varying guest composition was used to determine the final hydrate composition, as discussed in Chapter 2.4.6. Exchange results from one non-fractured (w1) and six single-spacer (c1-c6) experiments are compared in Figure 35, where changes in dissociation pressure are reflected in guest composition (mol% CO_2). The MRI intensity is normalized, where 1 indicates no hydrate.

The CO_2-CH_4 exchange efficiency was enhanced through constant CO_2 injection and required less soaking time relative to the huff and puff approach (c1). The exchange efficiency ranged between 59-83% for uniformly saturated samples, where final conversion was related to soaking time (between 2-5 days). Recovery was enhanced by 10% by extending injection from 2 to 3 days. The exchange was also slightly more efficient for lower S_h, as illustrated by differences between c3 (S_{wi}=0.3) and c6 (S_{wi}=0.6) in Figure 35.

CO_2 mass transport in c2-c6 was maximized by continuous CO_2 injection, as the diffusive flux in Fick's law relates to concentration. The mass transfer process may be envisioned as a counter-current flow process, where CO_2 diffuses from the spacer while CH_4 diffuses from the sample. In theory, favorable mass transportation may be achieved through constant injection in a non-fractured sample where CO_2 displaces released CH_4 while advancing towards the producer. The CO_2-CH_4 exchange driving force is maximized by abundant CO_2 concentration as the guest composition relates to the gas composition (e.g. Figure 19). The exchange efficiency in w1 (sample 2-4) was inefficient because of non-uniform saturation distribution. Reduced CO_2-CH_4 exchange efficiency and multi-compositional hydrate structures were generally detected for non-fractured samples due to anisotropic flow conditions and plugging. These problems will be further elaborated in Chapter 4.4.6. However, exchange in non-fractured samples should be further addressed.

Spatial variations in hydrate composition

S_{wi} was increased to 0.6 for c4-c6 by injecting a specified brine volume into the spacer. c4 was characterized by non-uniform saturation distribution, as illustrated in Figure 36, where local S_{wi} exceeded 80-90%. Diffusivity of CO_2 in bulk hydrate is approximately three orders of magnitude slower than diffusivity in water (Chapter

1.3.8). Exchange performance is facilitated by presence of a non-frozen water layer that coats mineral grains, but mass transfer in bulk hydrate necessitates extended soaking times. A multi-compositional hydrate with varying hydration pressure was reflected by the six pressure steps that were required for hydrate decomposition. Exchange kinetics was assumed to be limited by mass transfer, as initial dissociation in c4 was focused in areas characterized by high S_{wi} and subsequent high S_h.

Volume expansion during decomposition redistributed the water phase and generated a uniformly saturated sample for the remaining two cycles. The conversion efficiency difference between the uniformly (c6) and non-uniformly (c4) saturated sample was in the 30-40% range, and mass transport is therefore believed to be a dominating mechanism.

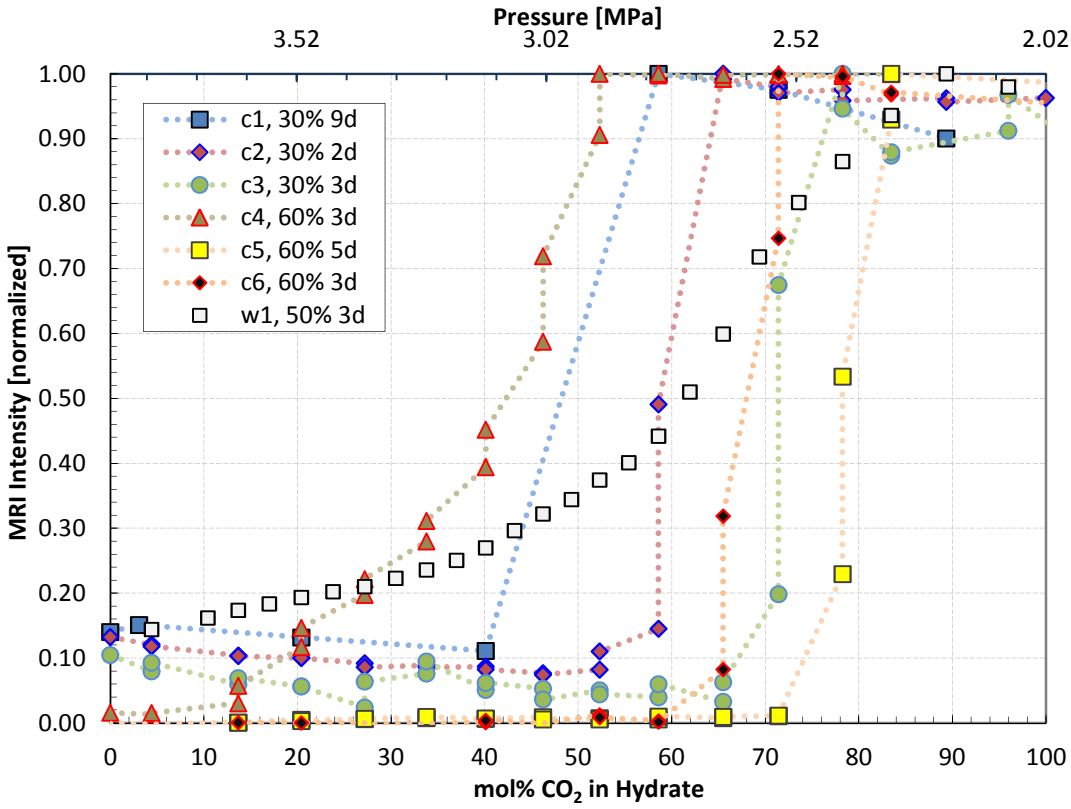

Figure 35 – The overall exchange efficiency was dependent upon soaking time and continuous replenishment of CO_2. Mass transfer was retained by local saturation variations, which were observed for experiment c4. The results demonstrate how mass transfer is a limiting mechanism in exchange kinetics. Legend explanation: c1, 30% 9d = cycle 1, S_{wi}=0.3, 9 days soaking. 3.5 wt% NaCl was used for w1, and pressures on the secondary x-axis does therefore not apply for this experiment. Figure inspired by Hester et al. (2011).

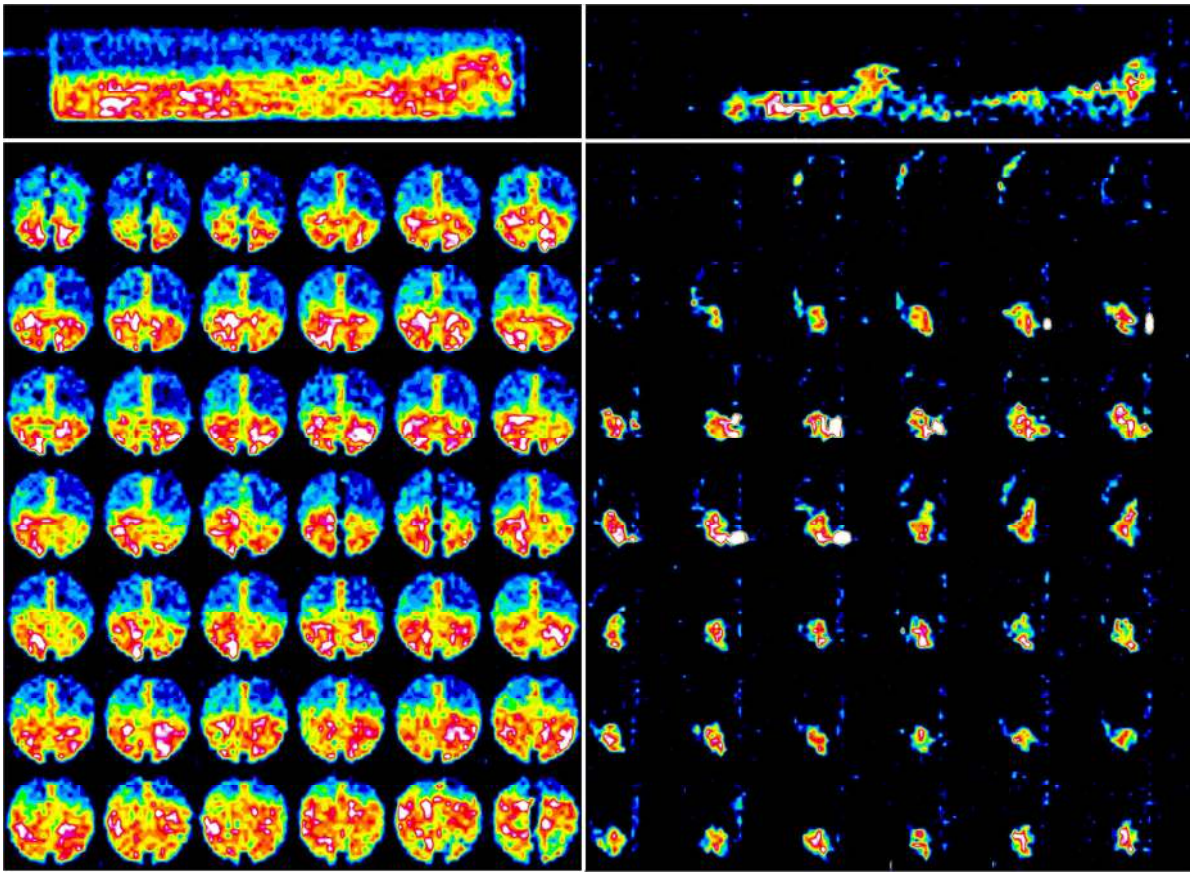

Figure 36 – c4 was characterized by non-uniform initial saturation distribution, as illustrated in the left part of the figure. The upper images are sagittal slices of the sample, while the lower circular images show transverse slices at different positions along the core length. The bottom section of the core was characterized by consistently higher water saturation, where saturation in local areas exceeded 80-90%.The right section of the figure shows initial dissociation focused in areas characterized by high S_{wi}.

4.4.4 Temperature effects

Heat liberated at the reaction site will facilitate further CO_2-CH_4 exchange because of net positive enthalpy change during exchange. Some PT regimes may provide favorable exchange conditions as the heat liberation effect is dependent upon the degree of subcooling. This was investigated in **Paper 5** through a series of experiments at temperatures between 0.5 and 10.4 °C, but data were inconsistent in terms of final conversion because of varying flow conditions. The experiments were mainly conducted on non-fractured samples, and were therefore susceptible to heterogeneities in fluid distribution.

4.4.5 Excess water and flow control

The native hydrate state of the sample in Figure 24 included a section with significant excess brine, and therefore offered a unique opportunity for investigating potential wellbore effects during CO_2 injection. CO_2 injection from right resulted in immediate plugging, which was reflected in both resistivity and differential pressure (see **Paper 4**). The hydrate film at the core interface ruptured as the differential pressure exceeded 0.8 MPa, and CO_2 advanced through the sample. A non-uniform final hydrate composition was illustrated in the depressurization sequence in Figure 37, where high concentration CH_4 hydrate decomposed at the left end. Poorly consolidated hydrate reservoirs limit the injection pressure, and plugging can therefore have severe consequences in a reservoir-scale production test.

4.4.6 Remediation of plugged samples

Plugged samples were treated through thermal stimulation, injection of chemical additives and binary gas injection (75/25 mol% N_2/CO_2). The last approach was most efficient, and may offer favorable conditions in terms of continued exchange for specific gas mixtures (Park et al., 2008). Our findings in **Paper 4** suggest significant rearrangement of hydrate crystals due to non-equilibrium with subsequent partial decomposition. A softening sediment response and enhanced permeability were observed during co-injection (77/23 mol% N_2/CO_2) in a CH_4 hydrate saturated sand-pack (Kneafsey et al., 2013), which corroborates observations from this study. However, changes in effluent composition were monitored *in situ* by an in line GC in **Paper 5**. The CO_2 mol fraction was consistently lower than the injected mol fraction which indicates a CO_2 sink within the sample. CO_2 hydrate formation is therefore a reasonable assumption. The overall change in hydrate saturation was not quantified due to lack of imaging possibilities, but results from this study and from the Ignik Sikumi field test indicate that binary CO_2/N_2 injection is favorable in terms of sustained flow and CO_2-CH_4 exchange.

4.4 Guest molecule replacement through CO2 injection

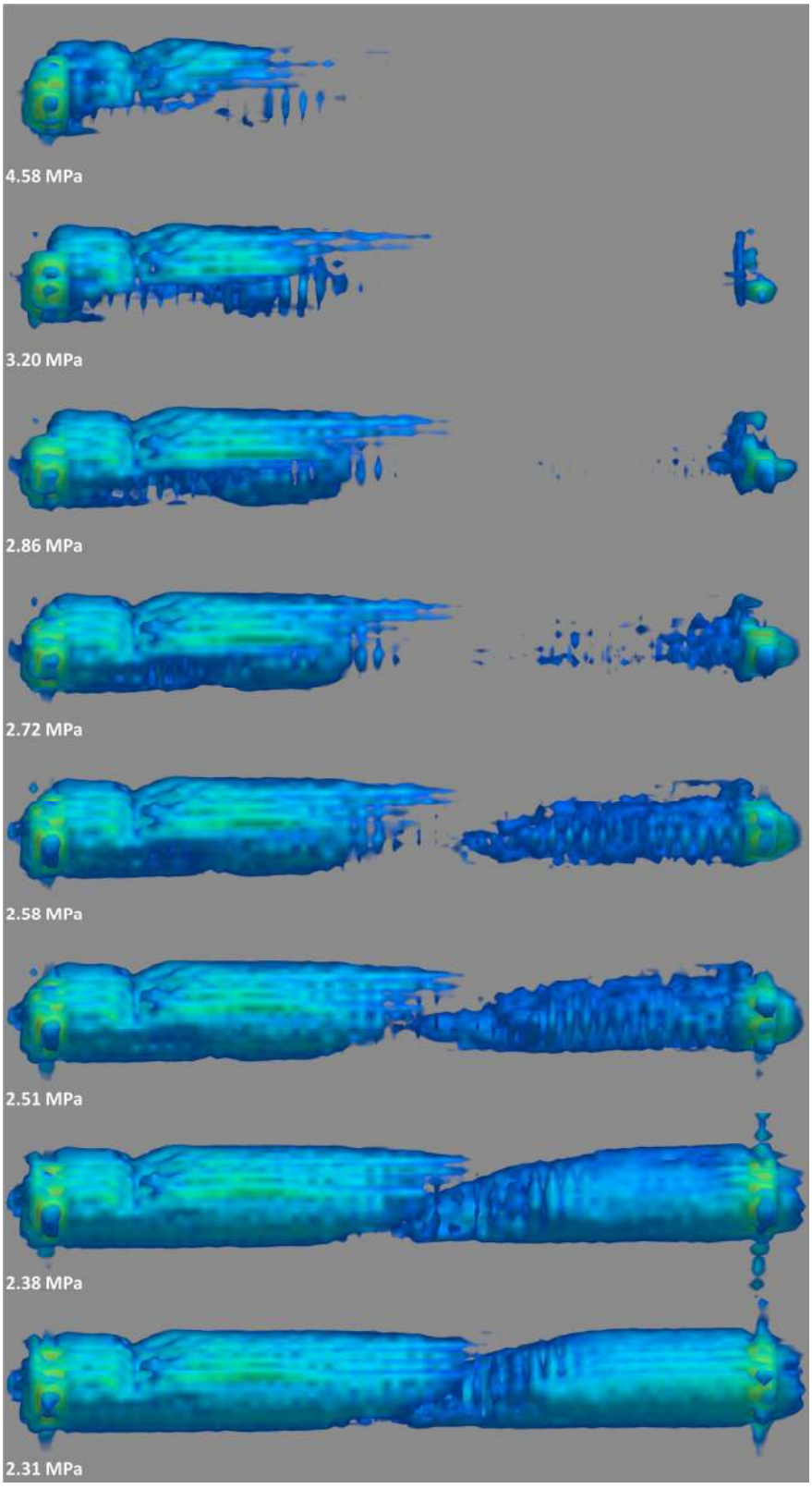

Figure 37 – Depressurization sequence for experiment 2-4 revealed significant spatial differences in terms of hydrate composition. The left core half was characterized by abundance of CH_4 hydrate, while the right core half was mainly composed of CO_2 hydrate.

4.4.7 Effluent evaluation during CO_2 injection

The gas effluent was continuously sampled through an *in line* GC to prepare for exchange, depressurization and to evaluate exchange efficiency. Effluent profiles during CO_2 injection for CO_2-CH_4 exchange are illustrated in Figure 38. The CH_4 peak was delayed due to excess line volume between sample outlet and GC. A steep increase in CH_4 and N_2 composition were observed after approximately 0.3 hours. The samples were not fully evacuated prior to saturation, and N_2 therefore serves as a tracer for production of free gas. Temperature increase at the core outlet in a previous experiment indicated CO_2 breakthrough after 5.2 hours of injection. This corresponds well with trends observed for this experiment. The CH_4 composition was low (~1 mol%) for the remaining injection period.

The results have not been quantified in terms of conversion efficiency due to variations in volumetric flow rates. This short-coming has recently been addressed through implementation of a mass flow meter and additional volume control units for improved control of produced gas. However, GC measurements have been an important part of the experimental work and necessary during gas injection.

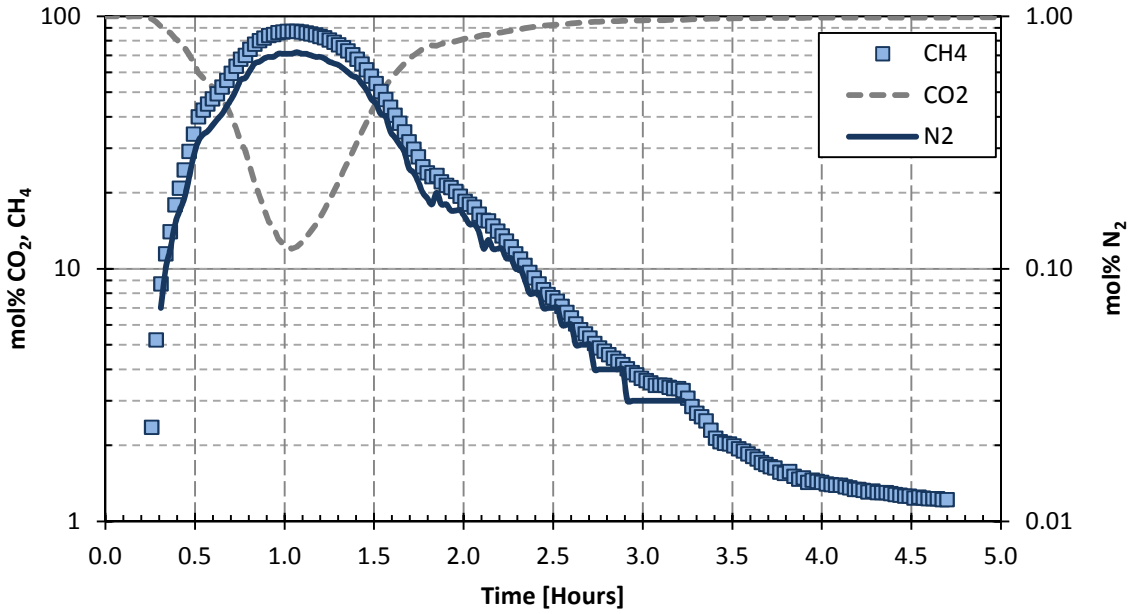

Figure 38 – Gas composition of produced gas. The production delay is a result of line volume between the sample and in-line GC. N_2 is a tracer for production of free gas. The CH_4 peak was high (87 mol%), but was quickly reduced after breakthrough.

5 NUMERICAL RESULTS

Numerical tools have aided in the interpretation of empirical trends and increased the understanding of mechanisms involved during hydrate dissociation. The following section will outline the work and summarize conclusions based on T+H, which are further described in **Paper 5**.

5.1 Discretization and initial conditions

The numerical mesh was discretized according to sediment intrinsic properties (i.e. geometry, porosity, permeability, thermal conductivity and specific heat capacity) for experiments described in Chapter 4.3. MRI saturation data were implemented and used as initial condition for the numerical model. A time-variable temperature boundary was defined based on empirical observations.

5.1.1 Cartesian 2D model

The 2D model was discretized according to a 2D sagittal MRI slice, as illustrated in **Paper 5**. Accurate predictions of heat and fluid flow within the sample were achieved by discretizing the problem into 8765 subdomains for well-defined heat conductivity towards the constant temperature boundary. Material specific heat properties (specific heat capacity and thermal conductivity) for the pressure vessel and end-pieces were implemented in the model. The gas saturated spacer volume was initialized with linear relative permeability and no capillary pressure to define capillary discontinuity across the core surface. A sink/source was positioned inside the spacer volume, which maintained constant pressure without any heat transfer.

5.1.2 Voronoi tessellation

Irregular Voronoi tessellation was required to fully take advantage of MRI data and maintain well-defined boundaries. The tessellation process has been described in **Paper 5**, and Figure 39 visualizes a quadrant section of the tetrahedral Voronoi mesh. 137,054 elements with 537,331 connections reproduced the physical system as accurately as possible.

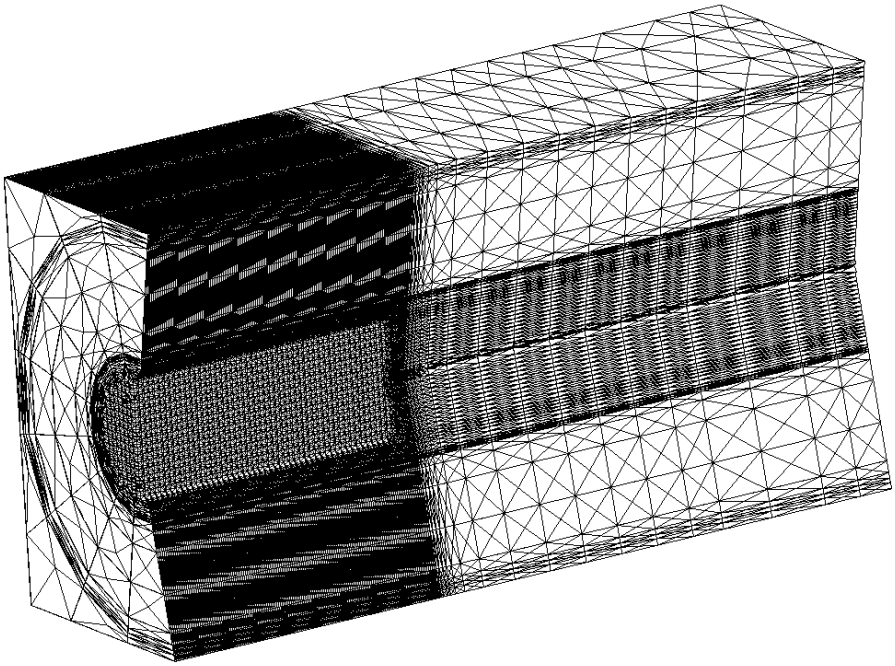

Figure 39 – The hydrate sample is represented by rectilinear mesh corresponding to MRI voxel elements, while cylindrical rings surrounding the sample were used as tessellation generation points for a pseudo-cylindrical region outside of the sample. Figure generated by Matt Freeman.

5.2 Numerical reproduction of empirical results

The overall objective of the numerical study was to investigate the quality of predictions and to enhance our understanding of empirical behaviors. Similar trends were observed in two identical experiments, where gas hydrates appeared to re-form during the dissociation process. Numerical modeling was conducted in an attempt to reproduce these processes and aid in the interpretation of empirical data.

5.2.1 Temperature dependency during decomposition

Inherently strong temperature dependency was observed in a series of preliminary equilibrium simulations with varying boundary temperature conditions, where decomposition time was increased from 13 to 27 hours for temperatures 4.2 and 4.15 °C. Small temperature variations in vicinity of the three-phase equilibrium line were therefore expected to significantly impact the decomposition time.

5.2 Numerical reproduction of empirical results

For Test 2, empirical behaviors were accurately reproduced at all pressure steps by implementing and applying temperature variations from Figure 30 as a time-variable temperature boundary. Deflection points in decomposition rate were reproduced, which demonstrates how decomposition was limited by heat transfer. Temperature variations were not employed for Test 3, but empirical data demonstrated how temperature variations affected decomposition rate even for higher driving force. Immediate temperature response was observed in numerical predictions in Figure 40, in close agreement with empirical results. The sensitivity analysis included 17 different combinations of kinetic parameters, where the two combinations illustrated in Figure 40 resulted in overall good correspondence at all pressure steps. Similar temperature response was observed for the two sets of kinetic parameters, but fluctuations were amplified at higher intrinsic rate.

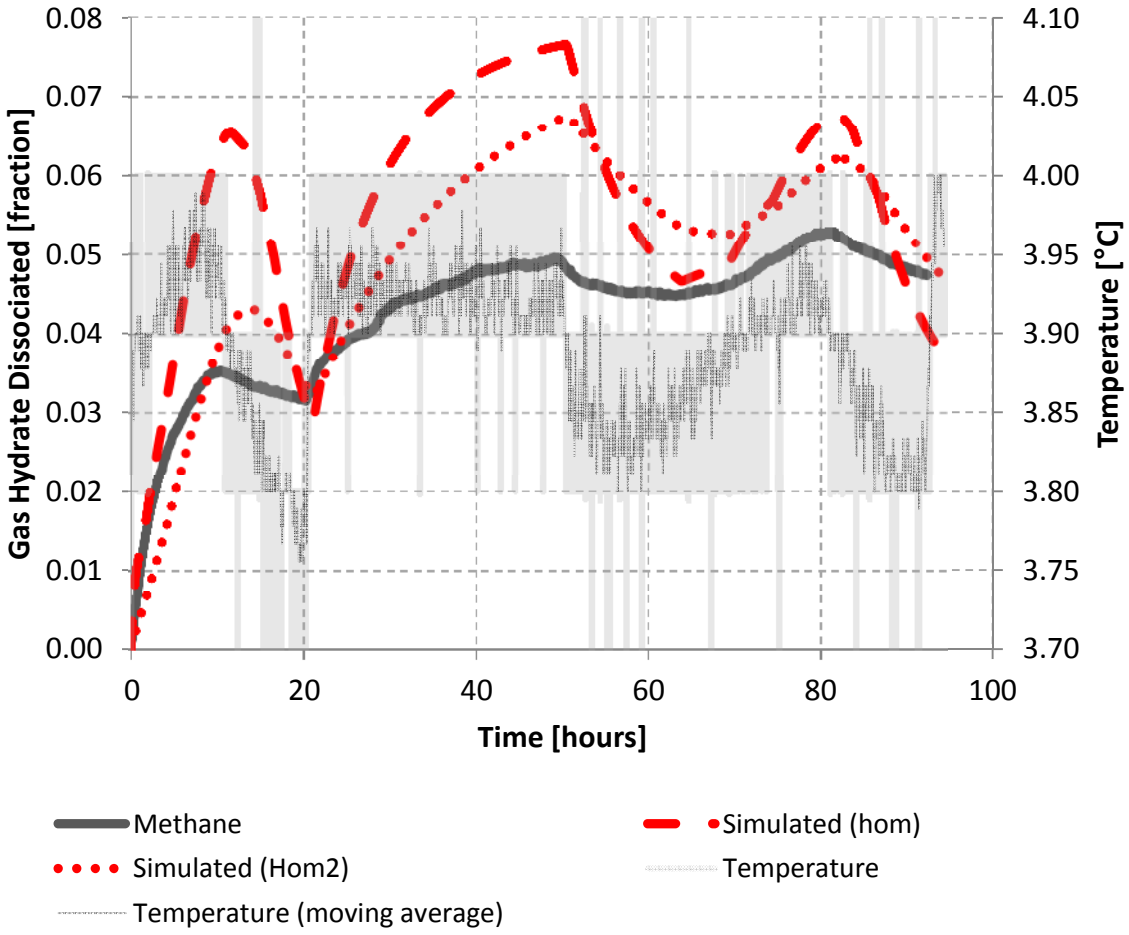

Figure 40 – Comparison of experimental and numerical results at 3.96 MPa for the experiment in Figure 31. Dissociation performance was affected by small temperature variations, which were reflected in all three datasets. The numerical results apply two different sets of kinetic parameters and therefore exhibit slightly different trends.

Predictions were more sensitive to variations in kinetic parameters than anticipated. Minor short-term variations between the equilibrium and kinetic reaction model on reservoir scale became more pronounced on a rapid small-scale (1.5m) test in a previous study (Kowalsky and Moridis, 2007). Test 1 and 2 had limited driving force, and was therefore not as susceptible to deviations between the two reaction models. Differences between the reaction models were substantiated through a third dissociation test at higher driving force in order to evaluate the simulator performance. The experimental design and procedure were based on preliminary numerical predictions.

5.2.2 Equilibrium and kinetic predictions at higher driving force

Empirical trends were reproduced by both reaction models at 3.96 MPa in vicinity of the equilibrium line, as illustrated in **Paper 5**. Differences between the reaction models were more pronounced at 3.2 MPa, where decomposition occurred over 30 hours. The equilibrium decomposition time was six times less than experimental observations in Figure 41. Empirical trends were consistently reproduced with kinetic combinations 4-0, and resulted in excellent agreement for Test 3. The equilibrium model required extensive number of iterations to solve the problem, and was therefore computationally more demanding than the kinetic model. The physical geometry of the problem should therefore be decisive for the choice of reaction model, where rapid small-scale decomposition requires kinetic modeling.

5.2.3 Limiting mechanisms during decomposition

Fluid flow, heat transfer and intrinsic kinetics may all be controlling mechanisms during decomposition. In Figure 42, decomposition was initially controlled by pressure propagation (fluid mobility). Convective heat flow impacted further dissociation as cooled fluids from the middle core segment were mobilized and advanced towards the sink. Finally, heat conductivity controlled the dissociation trend. Favorable thermophysical properties of the POM spacer and Teflon shrink tubing relative to CH_4 resulted in less abundance of gas hydrates adjacent to corner elements. Heat transfer and kinetic limitations were assumed to be controlling decomposition mechanisms in this study based on observations in Figure 40 and Figure 41.

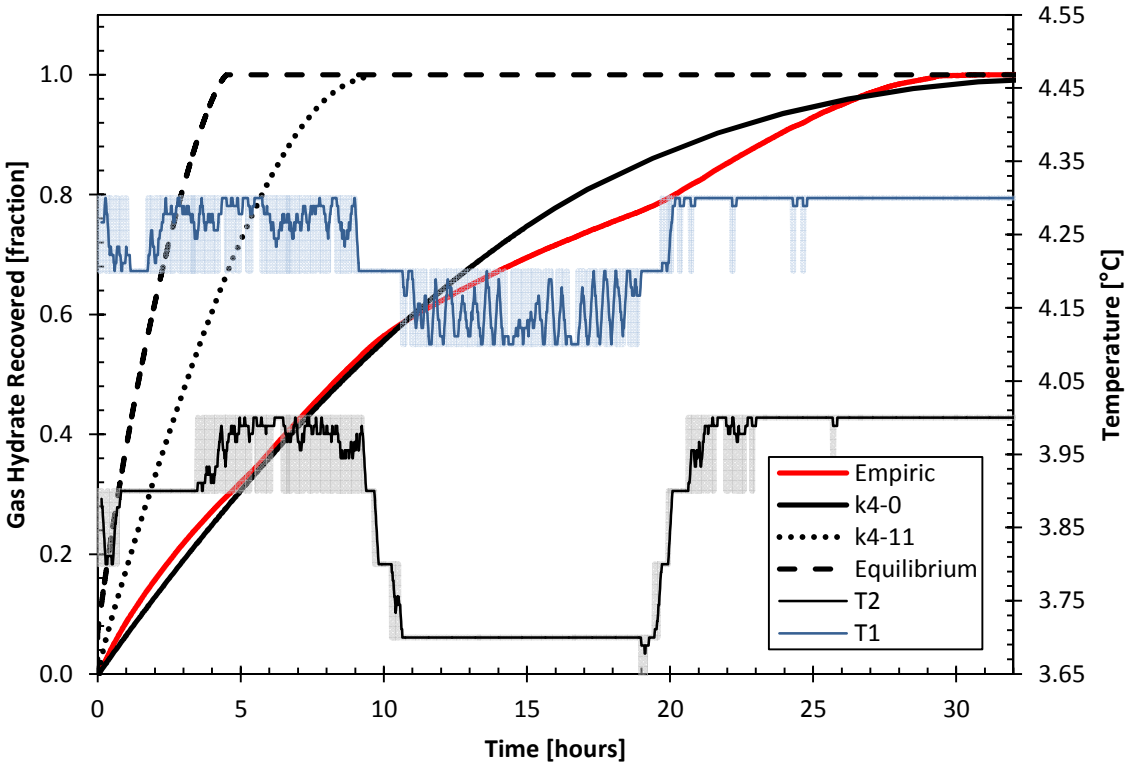

Figure 41 – Empirical and numerical decomposition at 3.2 MPa. The decomposition time was reduced by an order of magnitude, which corresponded well with the numerical predictions from k4-0.

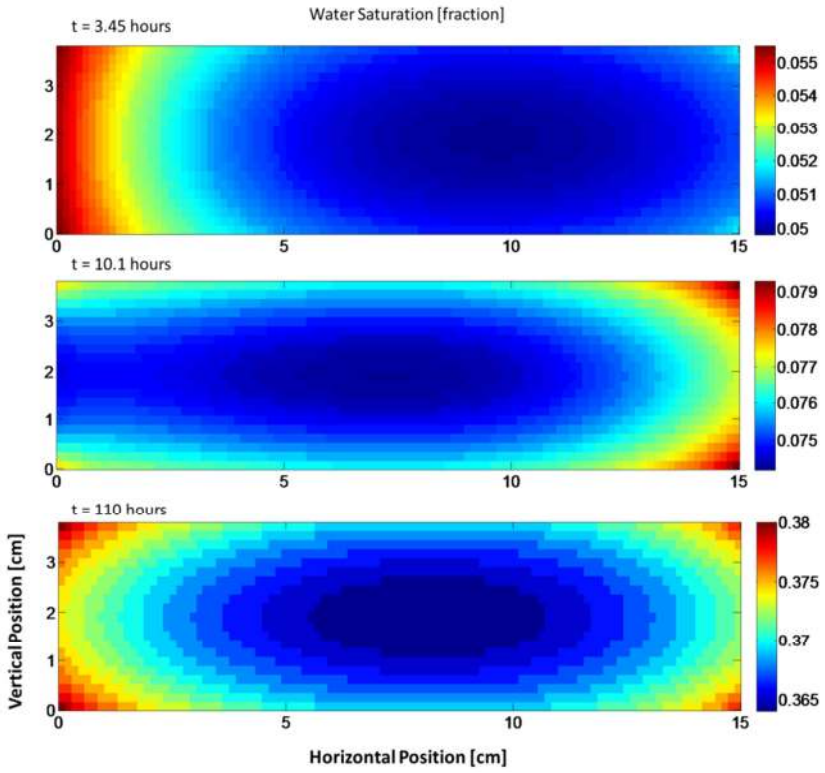

Figure 42 – Variations in S_w during dissociation.

5.3 Upscaling to small reservoir

A simple 2D Class III reservoir (10m*1m*40m) was designed in order to remove boundary effects from the core holder and investigate the decomposition response at larger scale. The reservoir was initialized with hydrostatic pressure (9.795 kPa/m) and a high temperature gradient (0.05 °C/m) with S_H=0.5. The sand interval was confined by non-permeable shale sections. Only the lower section of the hydrate interval was perforated, and initial decomposition was therefore focused adjacent to the sink, as illustrated in Figure 43. Dissociation preferentially progressed in the horizontal direction, which is a result of favorable heat transport conditions and high permeability. These trends therefore correspond well with heat limiting behavior observed in the laboratory. Kinetic limitations were less dominant on larger scale.

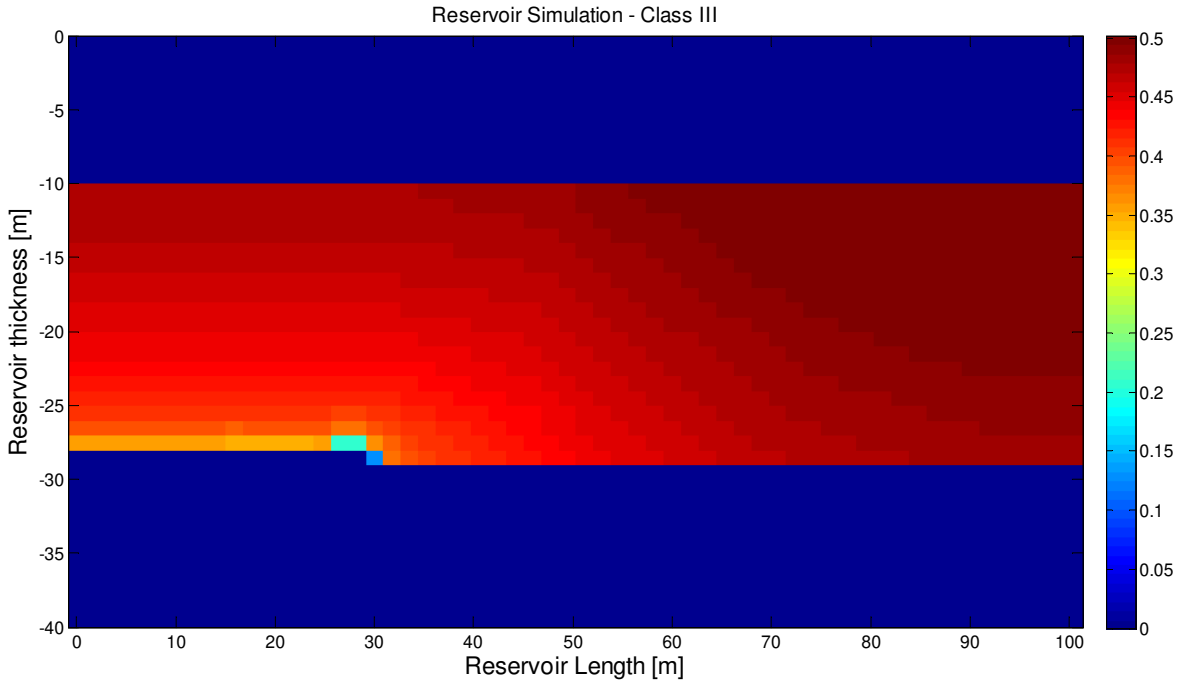

Figure 43 – Reservoir scale depressurization corresponded with trends observed on smaller scale, where heat transfer is one of the main controlling mechanisms for hydrate dissociation kinetics.

6 CONCLUSIONS

Improved understanding of controlling mechanisms during hydrate growth was targeted through a series of hydrate formation experiments while preparing for subsequent lab-scale production tests. Consistent trends in terms of CH_4 hydrate growth rate and patterns were confirmed through PVT data and corroborated by *in situ* MRI measurements. Relatively uniform growth patterns were observed for the majority of experiments, which is consistent with previous measurements.

The robustness of Archie's resistivity model for gas hydrates was determined through a series of resistivity experiments. A resistivity drop was detected at the onset of hydrate formation for all experiments. Resistivity increased for continued growth due to increased tortuosity. The effective porosity and saturation interpretation was improved by employing an empirical R_o function which accounted for the sediment response to elevated ion concentration.

Differences in growth pattern within the pore space were reflected in the saturation exponent *n*, which ranged between 1.36 and 3.25 in this study. Variations in hydrate morphology, inter-granular micro-layers of brine, and capillary forces may explain these differences. Improved accuracy in saturation estimates was generally observed for low concentration brine.

Gas hydrates were dissociated through depressurization at a series of consecutive pressure steps (3.96, 3.89 and 3.82 MPa) or at a single pressure step of 3.2 MPa. Dissociation time was reduced by an order of magnitude at lower pressure. Heat transfer was a controlling mechanism in these experiments, where minor temperature variations shifted the dissociation rate.

Empirical trends were reproduced numerically, which confirmed that temperature variations at the core boundary were decisive for observed variations in dissociation rate. Both reaction models were employed, where the kinetic model was preferable in terms of accuracy and CPU time. Kinetic limitations may be present in short-term small scale dissociation, as deviations between predictions for the reaction models were more pronounced at higher dissociation driving force. The validity of the T+H code for core-scale depressurization was demonstrated in this study.

CONCLUSIONS

Spontaneous CO_2-CH_4 exchange occurred during CO_2 injection, thus creating a synergy between energy production and safe CO_2 storage with reduced negative feedback from CH_4 seepage. CO_2 concentration in the gas/liquid phase affected the rate of exchange kinetics, where higher concentrations provided favorable conditions in terms of diffusion and exchange driving force. Exchange efficiency was related to soaking time and hydrate saturation. Continuous CO_2 flow induced a binary gas hydrate consisting of 59-83 mol% CO_2 guests for uniformly saturated samples. The replacement efficiency was improved for continuous injection relative to huff and puff. Frequent plugging was observed when employing constant CO_2 injection in non-fractured samples. In comparison, excellent flow conditions were achieved through binary gas injection (75/25 mol% N_2/CO_2). CO_2-CH_4 exchange was sustained, but the overall change in hydrate saturation was unknown.

Some of the main conclusions from this study were:

- CO_2-CH_4 exchange efficiency was enhanced through constant CO_2 injection, which maximized the mass transfer and exchange driving force.
- CH_4 was produced while 59-83% CO_2 remained stored within hydrate cavities.
- Kinetic modeling was required to reproduce empirical small-scale dissociation. Kinetic limitations may therefore be present in laboratory studies.
- An empirical R_o function improved the resistivity interpretation accuracy.
- Differences in hydrate growth were reflected in variable *n*. Neglecting to account for these deviations will induce errors in saturation estimates.

Experiments in this study have been part of a joint effort towards a pilot test in Alaska. Improved understanding of coexisting processes during exchange and resistivity measurements have been addressed in order to acquire data and prepare for the field test. Ignik Sikumi validated the CO_2-CH_4 exchange technology on reservoir scale, where CO_2 and N_2 were injected through huff and puff with subsequent depressurization and flow-back after 5 days of soaking. Initial reports suggest that approximately 60% of the injected CO_2 remained stored within the hydrate bearing sediment while benefitting from CH_4 production. The CO_2-CH_4 exchange technology may therefore hold promise of a cleaner energy future.

7 FUTURE PERSPECTIVE

Improved understanding of mechanisms that affect hydrate growth, resistivity progression, hydrate dissociation and exchange should be targeted through further micro-scale experiments. Preliminary studies have been initiated where time-lapse photography combined with microscopy may provide insight into salt-dependent variations in hydrate morphology. This setup should also be assisted by resistivity measurements in order to further address resistivity trends observed at the onset of hydrate growth and variations in *n*.

Improved understanding of mechanisms at larger scale is also necessary for validation of production technology on larger scale. A block-scale setup has been designed and built as part of this thesis. Boundary effects will be reduced on this setup, which could have significant impact on processes occurring within the pore space. Up-scaling is important in order to further compare diffusion-driven CO_2 transport and constant injection for CO_2-CH_4 exchange, and also to acquire decomposition data for further evaluation of numerical tools.

Paper 2 concluded that CO_2 exchange is preferable to depressurization from a geomechanical perspective. This assumption was based on lack of intensity increase during exchange, and assumed that the solid-liquid-solid transition is short-lived. Sediment stability should be addressed through simple compaction tests for pure and mixed compositions in future geomechanical studies. This is assumed to be one of the main advantages with CO_2-CH_4 exchange, but quantitative results are needed.

Exchange kinetics for varying temperatures should be further investigated. The single-spacer configuration offers favorable flow conditions, and could be utilized to minimize contribution from unknown parameters such as flow pattern.

Future studies should further investigate the impact of binary gas injection, preferentially supported by *in situ* imaging to verify potential phase transitions. Furthermore, other gas fractions may provide favorable conditions, which should be approached through an extended study.

NOMENCLATURE

A_p	Surface area of particle [m^2], active reaction surface
Å	Angström, 10^{-10}m
$\Delta E=\Delta E_a$	Activation energy for gas hydrate decomposition [J/mol]
F_A	Area adjustment factor
Δf	Fugacity difference [Pa]
f_{eg}	Fugacity at equilibrium conditions [Pa]
f_{exp}	Fugacity at experimental conditions [Pa]
f_g^v	Fugacity of hydrate former in the gas phase [Pa]
ΔG	Gibbs free energy
K_d	Decomposition rate constant [mol/m^2*Pa*s]
$K_d^0=K_0$	Intrinsic decomposition rate constant [mol/m^2*Pa*s]
M_0	Magnetization, from Curie's law
n	Saturation exponent
n_H	Hydration number
$\left(\frac{\partial n}{\partial t}\right)_p=\frac{\partial M}{\partial t}=Q_H$	Decomposition rate
P_e	Equilibrium pressure [Pa]
R	Universal gas constant, 8.314 [J/molK]
R_o	Resistivity of fully water saturated sample
S_h	Hydrate saturation
$S_{h,CH4}$	Hydrate saturation
S_w	Water saturation
S_{wi}	Initial water saturation
T	Temperature [K]
T_e	Equilibrium temperature [K]

NOMENCLATURE

ϕ	Intrinsic porosity
ϕ_{eff}	Effective porosity

ABBREVIATIONS

EM	Electro Magnetic
FDM	Finite Difference Method
FEM	Finite Element Method
FVM	Finite Volume Method
HEN	Heterogeneous Nucleation
HON	Homogeneous Nucleation
IFDM	Integral Finite Difference Method
LWD	Logging While Drilling
MRI	Magnetic Resonance Imaging
MSCF	Thousand standard cubic feet
NMR	Nuclear Magnetic Resonance
PEEK	Polyetheretherketone
POM	Polyoxymethylene
PVT	Pressure Volume Temperature
RI	Resistivity Index
sI	Structure I hydrate cavity
STP	Standard Temperature and Pressure
TCD	Thermal Conductivity Detector
THF	Tetrahydrofuran hydrate
TSCF	Trillion standard cubic feet

REFERENCES

ANDERSON, B., HANCOCK, S., WILSON, S., ENGER, C., COLLETT, T., BOSWELL, R. & HUNTER, R. 2011a. Formation pressure testing at the Mount Elbert Gas Hydrate Stratigraphic Test Well, Alaska North Slope: Operational summary, history matching, and interpretations. *Marine and Petroleum Geology,* 28**,** 478-492.

ANDERSON, B. I., COLLETT, T. S., LEWIS, R. E. & DUBOURG, I. 2008. Using Open Hole And Cased-Hole Resistivity Logs to Monitor Gas Hydrate Dissociation During a Thermal Test In the Mallik 5L-38 Research Well, Mackenzie Delta, Canada. *PetroPhysics,* 49.

ANDERSON, B. J., KURIHARA, M., WHITE, M. D., MORIDIS, G. J., WILSON, S. J., POOLADI-DARVISH, M., GADDIPATI, M., MASUDA, Y., COLLETT, T. S., HUNTER, R. B., NARITA, H., ROSE, K. & BOSWELL, R. 2011b. Regional long-term production modeling from a single well test, Mount Elbert Gas Hydrate Stratigraphic Test Well, Alaska North Slope. *Marine and Petroleum Geology,* 28**,** 493-501.

ANDERSON, G. K. 2003. Enthalpy of dissociation and hydration number of carbon dioxide hydrate from the Clapeyron equation. *The Journal of Chemical Thermodynamics,* 35**,** 1171-1183.

ANDERSON, G. K. 2004. Enthalpy of dissociation and hydration number of methane hydrate from the Clapeyron equation. *The Journal of Chemical Thermodynamics,* 36**,** 1119-1127.

ANDERSON, W. G. 1986. Wettability Literature Survey-Part 3: The Effects of Wettability on the Electrical Properties of Porous Media. *SPE Journal of Petroleum Technology,* 38.

ARCHER, D. 2007. Methane hydrate stability and anthropogenic climate change. *Biogeosciences,* 4**,** 521-544.

ARCHIE, G. E. 1942. The electrical resistivity log as an aid in determining some reservoir characteristics. *J. Pet. Technol,* 5**,** 1-8.

BALDWIN, B. A., MORADI-ARAGHI, A. & STEVENS, J. C. 2003. Monitoring hydrate formation and dissociation in sandstone and bulk with magnetic resonance imaging. *Magnetic Resonance Imaging,* 21**,** 1061-1069.

BALLARD, A. L. & SLOAN JR, E. D. 2002. The next generation of hydrate prediction: I. Hydrate standard states and incorporation of spectroscopy. *Fluid Phase Equilibria,* 194–197**,** 371-383.

BIRKEDAL, K. A. 2009. *Hydrate Formation and CH4 Production from Natural Gas Hydrates - Emphasis on Boundary Conditions and Production Methods.* Master Thesis, University of Bergen.

BIRKEDAL, K. A., ERSLAND, G., HAUGE, L. P. Ø., GRAUE, A., HESTER, K., STEVENS, J. & HOWARD, J. Electrical Resistivity Measurements of CH4-Hydrate Bearing Sandstone During Formation. 7th International Conference on Gas Hydrates, July 17-21 2011 Edinburgh, Scotland.

BLOCH, F. 1946. Nuclear Induction. *Physical Review,* 70**,** 460-474.

BONA, N., ROSSI, E., CAPACCIOLI, S. & LUCCHESI, M. 2008. Electrical measurements: Considerations on the performance of 2- and 4- contact systems. *International Symposium of the SCA.* Abu Dhabi, UAE.

BOSWELL, R. & COLLETT, T. S. 2006. The Gas Hydrate Resource Pyramid. *Fire in the ice, NETL Fall Newsletter,* 5-7.

BOSWELL, R., FRYE, M., SHELANDER, D., SHEDD, W., MCCONNELL, D. R. & COOK, A. 2012. Architecture of gas-hydrate-bearing sands from Walker Ridge 313, Green Canyon 955, and Alaminos Canyon 21: Northern deepwater Gulf of Mexico. *Marine and Petroleum Geology,* 34**,** 134-149.

BOSWELL, R., SHELANDER, D., LEE, M., LATHAM, T., COLLETT, T., GUERIN, G., MORIDIS, G., REAGAN, M. & GOLDBERG, D. 2009. Occurrence of gas hydrate in Oligocene Frio sand: Alaminos Canyon Block 818: Northern Gulf of Mexico. *Marine and Petroleum Geology*.

BRYN, P., BERG, K., FORSBERG, C. F., SOLHEIM, A. & KVALSTAD, T. J. 2005. Explaining the Storegga Slide. *Marine and Petroleum Geology,* 22**,** 11-19.

BUFFETT, B. & ARCHER, D. 2004. Global inventory of methane clathrate: sensitivity to changes in the deep ocean. *Earth and Planetary Science Letters,* 227**,** 185-199.

BUGGE, T., BEFRING, S., BELDERSON, R. H., EIDVIN, T., JANSEN, E., KANYON, N. H., HOLTEDAHL, H. & SEJRUP, H. P. 1987. A giant three-stage submarine slide off Norway. *Geo-Marine Letters,* 7**,** 191-198.

BURSHEARS, M., O'BRIEN, T. J. & MALONE, R. D. 1986. A Multi-Phase, Multi-Dimensional, Variable Composition Simulation of Gas Production From a Conventional Gas Reservoir in Contact With Hydrates. *SPE Unconventional Gas Technology Symposium.* Louisville, Kentucky.

CARROL, J. 2009. *Natural Gas Hydrates - A Guide for Engineers,* Oxford, UK, Elsevier.

CHEJARA, A., KVAMME, B., VAFAEI, M. T. & JEMAI, K. 2013. Simulations of long term methane hydrate dissociation by pressure reduction using an extended RetrasoCodeBright simulator. *Energy Conversion and Management,* 68**,** 313-323.

CHEN, M. P., RIEDEL, M., SPENCE, G. D. & HYNDMAN, R. D. Data report: a downhole electrical resistivity study of northern Cascadia marine gas hydrate. Proceedings of the Integrated Ocean Drilling Program, 2008.

CHU, S. & MAJUMDAR, A. 2012. Opportunities and challenges for a sustainable energy future. *Nature,* 488**,** 294-303.

CIRCONE, S., KIRBY, S. & STERN, L. A. 2005. Direct Measurement of Methane Hydrate Composition along the Hydrate Equilibrium Boundary. *The Journal of Physical Chemistry,* 109**,** 9468-9475.

CLARKE, M. & BISHNOI, P. R. 2001. Determination of the activation energy and intrinsic rate constant of methane gas hydrate decomposition. *The Canadian Journal of Chemical Engineering,* 79**,** 143-147.

CLARKE, M. A. & BISHNOI, P. R. 2005. Determination of the intrinsic kinetics of CO gas hydrate formation using in situ particle size analysis. *Chemical Engineering Science,* 60**,** 695-709.

CLENNELL, M. B., HOVLAND, M., BOOTH, J. S., HENRY, P. & WINTERS, W. J. 1999. Formation of natural gas hydrates in marine sediments - 1. Conceptual model of gas hydrate growth conditioned by host sediment properties. *Journal of Geophysical Research,* 104**,** 22,985-23,003.

COATES, G. R., XIAO, L. & PRAMMER, M. G. 1999. *NMR Logging - Principles & applications,* Texas, Halliburton Energy Services.

COLLETT, T. 2001. A Review of Well-Log Analysis Techniques Used to Assess Gas-Hydrate-Bearing Reservoirs. *In:* PAULL, C. K. & DILLON, W. P. (eds.) *Natural Gas Hydrates - Occurrence, Distribution and Detection.* Washington, DC: American Geophysical Union.

COLLETT, T., RIEDEL, M., COCHRAN, J. R., BOSWELL, R., KUMAR, P. & SATHE, A. V. Indian Continental Margin Gas Hydrate Prospects: Results of the Indian National Gas Hydrate Program (NGHP) Expedition 01. 6th International Conference on Gas Hydrates, 2008a Vancouver, BC, Canada.

COLLETT, T. S. 1998. WELL LOG EVALUATION OF GAS HYDRATE SATURATIONS. Society of Petrophysicists & Well Log Analysts.

COLLETT, T. S., AGENA, W. F., LEE, M. W., ZYRIANOVA, M. V., BIRD, K. J., CHARPENTIER, T. C., HOUSEKNECT, D. W., KLETT, T. R., POLLASTRO, R. M. & SCHENK, C. J. 2008b. Assessment of gas hydrate resources on the North Slope, Alaska, 2008. *U.S. Geological Survey Fact Sheet 2008-3073*.

COLLETT, T. S., BOSWELL, R., LEE, M. W., ANDERSON, B. J., ROSE, K. & LEWIS, K. A. 2012a. Evaluation of Long-Term Gas-Hydrate-Production Testing Locations on the Alaska North Slope. *SPE Reservoir Evaluation & Engineering,* 15**,** pp. 243-264.

COLLETT, T. S. & LADD, J. 2000. Detection of gas hydrate with downhole logs and assessment of gas hydrate concentration (saturations) and gas volumes on the blake ridge with electrical resistivity log data. *In:* PAULL, C. K., MATSUMOTO, R., WALLACE, P. J. & DILLON, W. P. (eds.) *Proceedings of the Ocean Drilling Program, Scientific Results.* College Station, TX.

COLLETT, T. S., LEE, M. W., AGENA, W. F., MILLER, J. J., LEWIS, K. A., ZYRIANOVA, M. V., BOSWELL, R. & INKS, T. L. 2011. Permafrost-associated natural gas hydrate occurrences on the Alaska North Slope. *Marine and Petroleum Geology,* 28**,** 279-294.

COLLETT, T. S., LEE, M. W., ZYRIANOVA, M. V., MROZEWSKI, S. A., GUERIN, G., COOK, A. E. & GOLDBERG, D. S. 2012b. Gulf of Mexico Gas Hydrate Joint Industry Project Leg II logging-while-drilling data acquisition and analysis. *Marine and Petroleum Geology,* 34**,** 41-61.

DALLIMORE, S. R. & COLLETT, T. 2005. Scientific Results from the Mallik 2002 Gas Hydrate Production Research Well Program, Mackenzie Delta, Northwest Territories, Canada. *GSC Bulletin,* 585.

DALLIMORE, S. R., UCHIDA, T. & COLLETT, T. 1999. Scientific Results From JAPEX/JNOC/GSC Mallik 2L-38 Gas Hydrate Research Well, Mackenzie Delta, Northwest Territories, Canada. *Geological Survey of Canada Bulletin,* 544.

DAVIDSON, D. W., GARG, S. K., GOUGH, S. R., HANDA, Y. P., RATCLIFFE, C. I., RIPMEESTER, J. A., TSE, J. S. & LAWSON, W. F. 1986. Laboratory analysis of a naturally occurring gas hydrate from sediment of the Gulf of Mexico. *Geochimica et Cosmochimica Acta,* 50**,** 619-623.

DAVIES, S. R., LACHANCE, J. W., SLOAN, E. D. & KOH, C. A. A novel approach to measuring methane diffusivity through a hydrate film using differential scanning calorimetry. 6th International Conference on Gas Hydrates, 2008 Vancouver, BC, Canada.

DAVIES, S. R., SELIM, M. S., SLOAN, E. D., BOLLAVARAM, P. & PETERS, D. J. 2006. Hydrate plug dissociation. *AIChE Journal,* 52**,** 4016-4027.

DAWSON, A. G., LONG, D. & SMITH, D. E. 1988. The Storegga slides: Evidence from eastern Scotland for a possible tsunami. *Marine Geology,* 82**,** 271-276.

DEMUROV, A., RADHAKRISHNAN, R. & TROUT, B. L. 2002. Computations of diffusivities in ice and CO2 clathrate hydrates via molecular dynamics and Monte Carlo simulations. *Journal of Chemical Physics,* 116**,** 702-709.

DONALDSON, E. C. & SIDDIQUI, T. K. 1989. Relationship Between the Archie Saturation Exponent and Wettability. *SPE Formation Evaluation,* 4**,** 359-362.

DUAN, Z. & SUN, R. 2003. An improved model calculating CO2 solubility in pure water and aqueous NaCl solutions from 273 to 533 K and from 0 to 2000 bar. *Chemical Geology,* 193**,** 257-271.

DUNN, K. J., BERGMAN, D. J. & LATORRACA, G. A. 2002. *Nuclear Magnetic Resonance Petrophysical and Logging Applications*, Elsevier Science.

EBINUMA, T., KAMATA, Y., MINAGAWA, H., OHMURA, R., NAGAO, J. & NARITA, H. Mechanical properties of sandy sediment containing methane hydrate. Proceedings of the 5th International Conference on Gas Hydrates, June 12-16 2005 Trondheim, Norway.

EDWARDS, A. L. 1972. TRUMP: A computer program for transient and steady-state temperature distributions in multidimensional systems. *Mathematics and Computers.* Livermore, CA: Lawrence Livermore National Laboratory.

EDWARDS, R. 1997. On the resource evaluation of marine gas hydrate deposits using sea-floor transient electric dipole-dipole methods. *GEOPHYSICS,* 62**,** 63-74.

EDWARDS, R. N., SCHWALENBERG, K., WILLOUGHBY, E. C., MIR, R. & SCHOLL, C. 2010. Marine Controlled-Source Electromagnetics and the Assessment of Seafloor Gas Hydrate. *In:* RIEDEL, M., WILLOUGHBY, E. C. & CHOPRA, S. (eds.) *In: Geophysical Characterization of Gas Hydrates.* Tulsa, OK, USA: Society of Exploration Geophysicists.

ELLIS, D. V. & SINGER, J. M. 2007. *Well Logging for Earth Scientists,* Ridgefield, Springer Netherlands.

ENGLEZOS, P., KALOGERAKIS, N., DHOLABHAI, P. D. & BISHNOI, P. R. 1987a. Kinetics of formation of methane and ethane gas hydrates. *Chemical Engineering Science,* 42**,** 2647-2658.

ENGLEZOS, P., KALOGERAKIS, N., DHOLABHAI, P. D. & BISHNOI, P. R. 1987b. Kinetics of gas hydrate formation from mixtures of methane and ethane. *Chemical Engineering Science,* 42**,** 2659-2666.

ERSLAND, G. 2008. *Studies of flow mechanisms and hydrate phase transitions in fractured rocks.* PhD Thesis, University of Bergen.

ERSLAND, G., HUSEBØ, J., GRAUE, A., BALDWIN, B. A., HOWARD, J. & STEVENS, J. 2010. Measuring gas hydrate formation and exchange with CO2 in Bentheim sandstone using MRI tomography. *Chemical Engineering Journal,* 158**,** 25-31.

ESPINOZA, D. N. & SANTAMARINA, J. C. 2011. P-wave monitoring of hydrate-bearing sand during CH4–CO2 replacement. *International Journal of Greenhouse Gas Control,* 5**,** 1031-1038.

FLEYFEL, F. & DEVLIN, J. P. 1988. FT-IR spectra of 90 K films of simple, mixed, and double clathrate hydrates of trimethylene oxide, methyl chloride, carbon dioxide, tetrahydrofuran, and ethylene oxide containing decoupled water-d2. *The Journal of Physical Chemistry,* 92**,** 631-635.

FRANKS, F. 1972. *Water: A Comprehensive Treatise,* New York, Plenum Press.

FREER, E. M., SELIM, M. S. & SLOAN, E. D. 2001. Methane hydrate film growth kinetics. *Fluid Phase Equilibria,* 185**,** 65-75.

FRYE, M. 2008. Preliminary Evaluation of In-Place Gas Hydrate Resources: Gulf of Mexico Outer Continental Shelf. *OCS Report MMS 2008-004.* Washington, DC: US DOI, Minerals Management Service.

FRYE, M., SHEDD, W. & BOSWELL, R. 2012. Gas hydrate resource potential in the Terrebonne Basin, Northern Gulf of Mexico. *Marine and Petroleum Geology,* 34**,** 150-168.

FUJII, T., SAEKI, T., KOBAYASHI, T., INAMORI, T., HAYASHI, M., TAKANO, O., TAKAYAMA, T., KAWASAKI, T., NAGAKUBO, S., NAKAMIZU, M. & YOKOI, K. 2008. Resource Assessment of Methane Hydrate in the Eastern Nankai Trough, Japan. *Offshore Technology Conference.* Houston, Texas, USA.

GOLDBERG, D. S., KLEINBERG, R. L., WEINBERGER, J. L., MALINVERNO, A., MCLELLAN, P. J. & COLLETT, T. S. 2010. Evaluation of Natural Gas-Hydrate Systems Using Borehole Logs. *In:* RIEDEL, M., WILLOUGHBY, E. C. & CHOPRA, S. (eds.) *Geophysical Characterization of Gas Hydrates.* Tulsa, OK, USA: Society of Exploration Geophysicists.

GRACE, J., COLLETT, T. S., COLWELL, F. S., ENGLEZOS, P., JONES, E., MANSELL, R., MEEKISON, J. P., OMMER, R., POOLADI-DARVISH, M., RIEDEL, M., RIPMEESTER, J. A., SHIPP, C. & WILLOUGHBY, E. 2008. *Energy from gas hydrates: Assessing the opportunities & challenges for Canada*.

GRAUE, A., KVAMME, B., BALDWIN, B., STEVENS, J., HOWARD, J. J., ASPENES, E., ERSLAND, G., HUSEBO, J. & ZORNES, D. 2008. MRI Visualization of Spontaneous Methane Production From Hydrates in Sandstone Core Plugs When Exposed to CO2. *SPE Journal,* 13**,** 146-152.

GUPTA, A. 2007. *Methane Hydrate Dissociation Measurements and Modeling: The Role of Heat Transfer and Reaction Kinetics.* PhD Thesis, Colorado School of Mines.

GUPTA, A., DEC, S. F., KOH, C. A. & SLOAN, E. D. 2007. NMR Investigation of Methane Hydrate Dissociation. *The Journal of Physical Chemistry C,* 111**,** 2341-2346.

GUPTA, A., KNEAFSEY, T. J., MORIDIS, G., SEOL, Y., KOWALSKY, M. B. & SLOAN, E. D. Estimation of Composite Thermal Conductivity of a Heterogeneous Methane Hydrate Sample using iTOUGH2. TOUGH Symposium, 2006 Berkeley, USA.

GUPTA, A., MORIDIS, G. J., KNEAFSEY, T. J. & SLOAN, E. D. 2009. Modeling Pure Methane Hydrate Dissociation Using a Numerical Simulator from a Novel Combination of X-ray Computed Tomography and Macroscopic Data. *Energy & Fuels,* 23**,** 5958-5965.

HAHN, E. L. 1950. Spin Echoes. *Physical Review,* 80**,** 580-594.

HAMMERSCHMIDT, G. G. 1934. Formation of Gas Hydrates in Natural Gas Transmission Lines. *Industrial & Engineering Chemistry,* 26**,** 851-855.

HEARST, J. R., NELSON, P. H. & PAILLET, F. 2000. *Well logging for Physical Properties: A Handbook for Geophysicists, Geologists and Engineers,* West Sussex, England, John Wiley & Sons Ltd.

HELGERUD, M. B. 2001. *Wave speeds in gas hydrate and sediments containing gas hydrate: A laboratory and modeling study.* PhD Thesis, Stanford University.

HESTER, K. 2007. *Probing Hydrate Stability and Structural Characterization of both Natural and Synthetic Clathrate Hydrates.* PhD Thesis, Colorado School of Mines.

HESTER, K. & BREWER, P. G. 2009. Clathrate Hydrates in Nature. *Annual Reviews of Marine Science,* 1**,** 303-327.

HESTER, K. C., STEVENS, J. C. & HOWARD, J. J. Composition Studies to Determine Rate and Extent of CO2 Exchange in a Hydrate-Bearing Core. 7th International Conference on Gas Hydrates, July 17-21 2011 Edinburgh, Scotland.

HOLDER, G. D. & ANGERT, P. F. 1982. Simulation of Gas Production From a Reservoir Containing Both Gas Hydrates and Free Natural Gas. *SPE Annual Technical Conference and Exhibition.* New Orleans, Louisiana: Society of Petroleum Engineers of AIME.

HONG, H., POOLADI-DARVISH, M. & BISHNOI, P. R. 2003. Analytical Modelling of Gas Production From Hydrates in Porous Media. *Journal of Canadian Petroleum Technology,* 42**,** 45-56.

HUNTER, R. B., COLLETT, T. S., BOSWELL, R., ANDERSON, B. J., DIGERT, S. A., POSPISIL, G., BAKER, R. & WEEKS, M. 2011. Mount Elbert Gas Hydrate Stratigraphic Test Well, Alaska North Slope: Overview of scientific and technical program. *Marine and Petroleum Geology,* 28.

HUSEBØ, J. 2008. *Monitoring depressurization and CO2-CH4 exchange production scenarios for natural gas hydrates.* PhD Thesis, University of Bergen.

HUSEBØ, J., ERSLAND, G., GRAUE, A. & KVAMME, B. 2009. Effects of salinity on hydrate stability and implications for storage of CO2 in natural gas hydrate reservoirs. *Energy Procedia,* 1**,** 3731-3738.

HUSEBØ, J., GRAUE, A., KVAMME, B., STEVENS, J., HOWARD, J. J. & BALDWIN, B. A. Experimental investigation of methane release from hydrate formation in sandstone through both hydrate dissociation and CO2 sequestration. 6th International Conference on Gas Hydrates, July 6-10 2008 Vancouver, Canada.

HUSEBØ, J., KVAMME, B. & GRAUE, A. 2007. In-Situ Hydrate Formation and Reformation Kinetics Measured by Magnetic Resonance Imaging. *WSEAS Transactions on Systems and Control,* 2**,** 59-66.

HYNDMAN, R. D., YUAN, T. & MORAN, K. 1999. The concentration of deep sea gas hydrates from downhole electrical resistivity logs and laboratory data. *Earth and Planetary Science Letters,* 172**,** 167-177.

IEA 2011. World Energy Outlook 2011. International Energy Agency.

ISRAELACHVILI, J. N. 2011. *Intermolecular and Surface Forces,* San Diego, CA, USA, Elsevier.

JADHAWAR, P., YANG, J., JADHAWAR, J. & TOHIDI, B. 2005. Preliminary Experimental Investigation on Replacing Methane in Hydrate Structure with Carbon Dioxide in Porous Media. *Proceedings of the 5th International Conference on Gas Hydrates.* Trondheim, Norway.

JUNG, J.-W. & SANTAMARINA, J. C. 2012. Hydrate formation and growth in pores. *Journal of Crystal Growth,* 345**,** 61-68.

JUNG, J. W., ESPINOZA, D. N. & SANTAMARINA, J. C. 2010. Properties and phenomena relevant to CH4-CO2 replacement in hydrate-bearing sediments. *Journal of Geophysical Research: Solid Earth,* 115**,** B10102.

KAMATA, Y., EBINUMA, T., OMURA, R., MINAGAWA, H., NARITA, H., MASUDA, Y. & KONNO, Y. Decomposition Behavior of Artificial Methane Hydrate Sediment by Depressurization. 5th International Conference on Gas Hydrates, June 13-16 2005 Trondheim, Norway.

KAMATH, V. A., HOLDER, G. D. & ANGERT, P. F. 1984. Three phase interfacial heat transfer during the dissociation of propane hydrates. *Chemical Engineering Science,* 39**,** 1435-1442.

KASHCHIEV, D. & FIROOZABADI, A. 2002. Nucleation of gas hydrates. *Journal of Crystal Growth,* 243**,** 476-489.

KENNETT, J. P., CANNARIATO, K. G., HENDY, I. L. & BEHL, R. J. 2003. *Methane Hydrates in Quaternary Climate Change: The Clathrate Gun Hypothesis,* Washington, DC, American Geophysical Union.

KIM, H. C., BISHNOI, P. R., HEIDEMANN, R. A. & RIZVI, S. S. H. 1987. Kinetics of methane hydrate decomposition. *Chemical Engineering Science,* 42**,** 1645-1653.

KLAUDA, J. B. & SANDLER, S. I. 2005. Global Distribution of Methane Hydrate in Ocean Sediment. *Energy & Fuels,* 19**,** 459-470.

KLEINBERG, R. L., FLAUM, C., GRIFFIN, D. D., BREWER, P. G., MALBY, G. E., PELTZER, E. T. & YESINOWSKI, J. P. 2003. Deep Sea NMR: Methane Hydrate Growth Habit in Porous Media and its Relationship to Hydraulic Permeability, Deposit Accumulation, and Submarine Slope Stability. *Journal of Geophysical Research B.*

KLEINBERG, R. L. & GRIFFIN, D. D. 2005. NMR measurements of permafrost: unfrozen water assay, pore-scale distribution of ice, and hydraulic permeability of sediments. *Cold Regions Science and Technology,* 42**,** 63-77.

KNEAFSEY, T. J., LU, H., WINTERS, W., BOSWELL, R., HUNTER, R. & COLLETT, T. S. 2011. Examination of core samples from the Mount Elbert Gas Hydrate Stratigraphic Test Well, Alaska North Slope: Effects of retrieval and preservation. *Marine and Petroleum Geology,* 28**,** 381-393.

KNEAFSEY, T. J., NAKAGAWA, S. & BORGLIN, S. E. 2013. Properties of Hydrate-Bearing Sediments Subjected to Changing Gas Compositions. *In:* KNEAFSEY, T. J. (ed.). Berkeley: Lawrence Berkeley National Laboratory.

KNEAFSEY, T. J., TOMUTSA, L., MORIDIS, G. J., SEOL, Y., FREIFELD, B. M., TAYLOR, C. E. & GUPTA, A. 2007. Methane hydrate formation and dissociation in a partially saturated core-scale sand sample. *Journal of Petroleum Science and Engineering,* 56**,** 108-126.

KOWALSKY, M. B. & MORIDIS, G. J. 2007. Comparison of kinetic and equilibrium reaction models in simulating gas hydrate behavior in porous media. *Energy Conversion and Management,* 48**,** 1850-1863.

KURIHARA, M., FUNATSU, K., OUCHI, H., MASUDA, Y., YASUDA, M., YAMAMOTO, K., NUMASAWA, M., FUJII, T., NARITA, H., DALLIMORE, S. R. & WRIGHT, F. Analysis of the JOGMEC/NRCAN/AURORA Mallik gas hydrate production test through numerical simulation. 6th International Conference on Gas Hydrates, July 6-10 2008 Vancouver, BC, Canada.

KURIHARA, M., KUNIHIRO, F., OUCHI, H., MASUDA, Y. & NARITA, H. Investigation on applicability of methane hydrate production methods to reservoirs with diverse characteristics. 5th International Conference on Gas Hydrates, June 13-17 2005 Trondheim, Norway.

KURIHARA, M., SATO, A., FUNATSU, K., OUCHI, H., MASUDA, Y., NARITA, H. & COLLETT, T. S. 2011. Analysis of formation pressure test results in the Mount Elbert methane hydrate reservoir through numerical simulation. *Marine and Petroleum Geology,* 28**,** 502-516.

KURIHARA, M., SATO, A., FUNATSU, K., OUCHI, H., YAMAMOTO, K., NUMASAWA, M., EBINUMA, T., NARITA, H., MASUDA, Y., DALLIMORE, S. R., WRIGHT, F. & ASHFORD, D. I. 2010a. Analysis of Production Data for 2007/2008 Mallik Gas Hydrate Production Tests in Canada. *International Oil and Gas Conference and Exhibition in China.* Beijing, China: Society of Petroleum Engineers.

KURIHARA, M., SATO, A., OUCHI, H., NARITA, H., EBINUMA, T., SUZUKI, K., MASUDA, Y., SAEKI, T., YAMAMOTO, K. & FUJII, T. 2010b. Prediction of Production Test Performances in Eastern Nankai Trough Methane Hydrate Reservoirs Using 3D Reservoir Model. *Offshore Technology Conference.* Houston, Texas, USA.

KVAMME, B. 2002. Kinetics of Hydrate Formation from Nucleation Theory. *International Journal of Offshore and Polar Engineering,* 12.

KVAMME, B., GRAUE, A., BUANES, T., KUZNETSOVA, T. & ERSLAND, G. 2007. Storage of CO2 in natural gas hydrate reservoirs and the effect of hydrate as an extra sealing in cold aquifers. *International Journal of Greenhouse Gas Control,* 1**,** 236-246.

KVENVOLDEN, K. A. 1988. Methane Hydrate - a major reservoir of carbon in the shallow geosphere? *Chemical Geology,* 71**,** 41-51.

LEDERHOS, J. P., LONG, J. P., SUM, A., CHRISTIANSEN, R. L. & SLOAN, E. D. 1995. Effective kinetic inhibitors for natural gas hydrates. *Chemical Engineering Science,* 51**,** 1221-1229.

LEE, H., SEO, Y., SEO, Y.-T., KIM, D. Y., MOUDRAKOVSKI, I. L., RIPMEESTER, J. A., SANG-EON PARK, J.-S. C. & KYU-WAN, L. 2004. Replacement of methane hydrate by carbon dioxide: 13C NMR study for studying a limit to the degree of substitution. *Studies in Surface Science and Catalysis.* Volume 153 ed.: Elsevier.

LEE, H., SEO, Y., SEO, Y.-T., MOUDRAKOVSKI, I. L. & RIPMEESTER, J. A. 2003. Recovering Methane from Solid Methane Hydrate with Carbon Dioxide. *Angewandte Chemie,* 115**,** 5202-5205.

LEE, M. W. & COLLETT, T. S. 2011. In-situ gas hydrate hydrate saturation estimated from various well logs at the Mount Elbert Gas Hydrate Stratigraphic Test Well, Alaska North Slope. *Marine and Petroleum Geology,* 28**,** 439-449.

LELIEVELD, J., CRUTZEN, P. J. & DENTENER, F. J. 1998. Changing concentration, lifetime and climate forcing of atmospheric methane. *Tellus B,* 50**,** 128-150.

LI, F.-G., SUN, C.-Y., LI, S.-L., CHEN, G.-J., GUO, X.-Q., YANG, L.-Y., PAN, H., LI, S. & ZHANG, K. 2012. Experimental Studies on the Evolvement of Electrical Resistivity during Methane Hydrate Formation in Sediments. *Energy & Fuels,* 26**,** 6210-6217.

LI, S., XIA, X., XUAN, J., LIU, Y. & LI, Q. 2010. Resistivity in Formation and Decomposition of Natural Gas Hydrate in Porous Medium. *Chinese Journal of Chemical Engineering,* 18**,** 39-42.

LU, W., CHOU, I. M. & BURRUSS, R. C. 2008. Determination of methane concentrations in water in equilibrium with sI methane hydrate in the absence of a vapor phase by in situ Raman spectroscopy. *Geochimica et Cosmochimica Acta,* 72**,** 412-422.

MAKOGON, Y. F. 1997. *Hydrates of Hydrocarbons,* Tulsa, Oklahoma, PennWell Books.

MAKOGON, Y. F., MAKOGON, T. Y. & HOLDITCH, S. A. Gas Hydrate Formation and Dissociation with Thermodynamic and Kinetic Inhibitors. SPE annual Technical Conference and Exhibition, October 3-6 1999 Houston, Texas, USA. SPE.

MALEGAONKAR, M. B., DHOLABHAI, P. D. & BISHNOI, P. R. 1997. Kinetics of carbon dioxide and methane hydrate formation. *The Canadian Journal of Chemical Engineering,* 75**,** 1090-1099.

MASUDA, Y., YAMAMOTO, K., TADAAKI, S., EBINUMA, T. & NAGAKUBO, S. 2009. Japan's Methane Hydrate R&D Program Progresses to Phase 2. *Fire in the Ice,* 9**,** 1-6.

MATHEWS, M. 1986. Logging Characteristics Of Methane Hydrate. *The Log Analyst,* XXVII.

MILKOV, A. V. 2004. Global estimates of hydrate-bound gas in marine sediments: how much is really out there? *Earth-Science Reviews,* 66**,** 183-197.

MILKOV, A. V. 2005. Molecular and stable isotope compositions of natural gas hydrates: A revised global dataset and basic interpretations in the context of geological settings. *Organic Geochemistry,* 36**,** 681-702.

MOCHIZUKI, T. & MORI, Y. H. 2006. Clathrate-hydrate film growth along water/hydrate-former phase boundaries—numerical heat-transfer study. *Journal of Crystal Growth,* 290**,** 642-652.

MORGAN, W. B. & PIRSON, S. J. 1964. THE EFFECT OF FRACTIONAL WETTABILITY ON THE ARCHIE SATURATION EXPONENT. Society of Petrophysicists & Well Log Analysts.

MORI, Y. H. 2001. Estimating the thickness of hydrate films from their lateral growth rates: application of a simplified heat transfer model. *Journal of Crystal Growth,* 223**,** 206-212.

MORIDIS, G. & COLLETT, T. 2003. Strategies for gas production from hydrate accumulations under various geologic conditions. *TOUGH Symposium.* Berkeley, CA, USA.

MORIDIS, G., COLLETT, T. S., POOLADI-DARVISH, M., HANCOCK, S. H., SANTAMARINA, C., BOSWELL, R., KNEAFSEY, T. J., RUTQVIST, J., KOWALSKY, M. B., REAGAN, M. T., SLOAN, E. D., SUM, A. & KOH, C. 2011a. Challenges, Uncertainties, and Issues Facing Gas Production From Gas-Hydrate Deposits. *SPE Reservoir Evaluation & Engineering,* 14**,** pp. 76-112.

MORIDIS, G., SEOL, Y. & KNEAFSEY, T. J. Studies of Reaction Kinetics of Methane Hydrate Dissocation in Porous Media. ICGH 5, 2005 Trondheim, Norway.

MORIDIS, G. J. 2003. Numerical Studies of Gas Production From Methane Hydrates. *SPE Journal,* 8**,** 359-370.

MORIDIS, G. J. 2004. Numerical Studies of Gas Production From Class 2 and Class 3 Hydrate Accumulations at the Mallik Site, Mackenzie Delta, Canada. *SPE Reservoir Evaluation & Engineering,* 7**,** 175-183.

MORIDIS, G. J., COLLETT, T. S., BOSWELL, R., KURIHARA, M., REAGAN, M. T., KOH, C. & SLOAN, E. D. Toward Production From Gas Hydrates: Current Status, Assessment of Resources, and Model-Based Evaluation of Technology and Potential. SPE Unconventional Reservoirs Conference, February 10-12 2008 Keystone, Colorado, USA. SPE.

MORIDIS, G. J., COLLETT, T. S., DALLIMORE, S. R., SATOH, T., HANCOCK, S. & WEATHERILL, B. 2004. Numerical studies of gas production from several CH4 hydrate zones at the Mallik site, Mackenzie Delta, Canada. *Journal of Petroleum Science and Engineering,* 43**,** 219-238.

MORIDIS, G. J. & KOWALSKY, M. B. 2005. Gas Production from Unconfined Class 2 Hydrate Accumulations in the Oceanic Subsurface. *In:* MAX, M. D. (ed.) *Economic Geology of Natural Gas Hydrates.* Kluwer Academic/Plenum Publishers.

MORIDIS, G. J., KOWALSKY, M. B. & PREUSS, K. 2012. TOUGH+HYDRATE v1.2 Users Manual: A Code for the Simulation of System Behavior in Hydrate-bearing Geologic Media. Berkeley, CA, USA: Lawrence Berkeley National Laboratory.

MORIDIS, G. J., KOWALSKY, M. B. & PRUESS, K. 2007. Depressurization-Induced Gas Production From Class 1 Hydrate Deposits. *SPE Reservoir Evaluation & Engineering,* 10**,** 458-481.

MORIDIS, G. J. & REAGAN, M. T. 2007. Gas Production From Oceanic Class 2 Hydrate Accumulations. *Offshore Technology Conference.* Houston, Texas.

MORIDIS, G. J., REAGAN, M. T., BOSWELL, R., COLLETT, T. S. & ZHANG, K. 2010. Preliminary Evaluation of the Production Potential of Recently Discovered Hydrate Deposits in the Gulf of Mexico. *Offshore Technology Conference.* Houston, Texas, USA.

MORIDIS, G. J., REAGAN, M. T., KIM, S. J., SEOL, Y. & ZHANG, K. 2009. Evaluation of the Gas Production Potential of Marine Hydrate Deposits in the Ulleung Basin of the Korean East Sea. *SPE Journal,* 14**,** 759-781.

MORIDIS, G. J., SILPNGARMLERT, S., REAGAN, M. T., COLLETT, T. & ZHANG, K. 2011b. Gas production from a cold, stratigraphically bounded hydrate deposit at the Mount Elbert site, North Slope, Alaska. *Marine and Petroleum Geology,* 28**,** 517-534.

MOUDRAKOVSKI, I. L., MCLAURIN, G. E., RATCLIFFE, C. I. & RIPMEESTER, J. A. 2004. Methane and Carbon Dioxide Hydrate Formation in Water Droplets: Spatially Resolved Measurements from Magnetic Resonance Microimaging. *Journal of Physical Chemistry B,* 108**,** 17591-17595.

MYSHAKIN, E. M., GADDIPATI, M., ROSE, K. & ANDERSON, B. J. 2012. Numerical simulations of depressurization-induced gas production from gas hydrate reservoirs at the Walker Ridge 313 site, northern Gulf of Mexico. *Marine and Petroleum Geology,* 34**,** 169-185.

NARASIMHAN, T. N. & WITHERSPOON, P. A. 1976. An integrated finite difference method for analyzing fluid flow in porous media. *Water Resources Research,* 12**,** 57-64.

NITAO, J. J. & BEAR, J. 1996. Potentials and their role in transport in porous media. *Water Resources Research,* 32**,** 225-250.

ODLAND, J. 2009. *Hydratdannelse og metanproduksjon fra gasshydrat - produksjonsmetoder og resistivitetsutvikling.* Master Thesis, University of Bergen.

OHMURA, R., SHIGETOMI, T. & MORI, Y. H. 1999. Formation, growth and dissociation of clathrate hydrate crystals in liquid water in contact with a hydrophobic hydrate-forming liquid. *Journal of Crystal Growth,* 196**,** 164-173.

OTA, M., MOROHASHI, K., ABE, Y., WATANABE, M., SMITH, J. R. L. & INOMATA, H. 2005. Replacement of CH4 in the hydrate by use of liquid CO2. *Energy Conversion and Management,* 46**,** 1680-1691.

PARK, K. P. Gas Hydrate Exploration Activities in Korea. 6th International Conference on Gas Hydrates, July 6-10 2008 Vancouver, BC, Canada.

PARK, Y., CHA, M., CHA, J. H., SHIN, K., LEE, H., PARK, K. P., HUH, D. G., LEE, H. Y., KIM, S. J. & LEE, J. Swapping Carbon Dioxide for Complex Gas Hydrate Structures. Preoceedings of the 6th International Conference on Gas Hydrates, 2008 Vancouver, BC, Canada. 6.

PARSHALL, J. 2012. Production Method for Methane Hydrate Sees Scientific Success. *Journal of Petroleum Technology,* August**,** 50-51.

PEARSON, C., MURPHY, J. & HERMES, R. 1986. Acoustic and Resistivity Measurements on Rock Samples Containing Tetrahydrofuran Hydrates: Laboratory Analogues to Natural Gas Hydrate Deposits. *J. Geophys. Res.,* 91.

PEARSON, C. F., HALLECK, P. M., MCGUIRE, P. L., HERMES, R. & MATHEWS, M. 1983. Natural Gas Hydrate Deposits: A Review of in Situ Properties. *Journal of Physical Chemistry,* 87**,** 4180-4185.

PENG, D. Y. & ROBINSON, D. B. 1976. A New Two-Constant Equation of State. *Ind. Eng. Chem. Fundam.,* 15**,** 59-64.

PETRICH, C. & EICKEN, H. 2010. Growth, Structure and Properties of Sea Ice. *Sea Ice.* Wiley-Blackwell.

PHALE, H. A., ZHU, T., WHITE, M. D. & MCGRAIL, B. P. 2006. Simulation study on injection of CO2-Microemulsion for Methane Recovery From Gas-Hydrate Reservoirs. *SPE Gas Technology Symposium.* Calgary, Alberta, Canada: Society of Petroleum Engineers.

POOLADI-DARVISH, M. & HONG, H. 2011. Use of formation pressure test results over a hydrate interval for long-term production forecasting at the Mount Elbert Gas Hydrate Stratigraphic Test Well, Alaska North Slope: Implications of uncertainties. *Marine and Petroleum Geology,* 28**,** 535-545.

PREUSS, K., OLDENBURG, C. M. & MORIDIS, G. 2012. TOUGH2 User's Guide, Version 2.

PURCELL, E. M. 1946. Resonance Absorption by Nuclear Magnetic Moments in a Solid. *Physical Review,* 69**,** 37-38.

REHDER, G., KIRBY, S. H., DURHAM, W. B., STERN, L. A., PELTZER, E. T., PINKSTON, E. & BREWER, P. G. 2004. Dissolution rates of pure methane hydrate and carbon-dioxide hydrate in undersaturated seawater at 1000-m depth. *Geochimica et Cosmochimica Acta,* 68**,** 285-292.

REN, S. R., LIU, Y., LIU, Y. & ZHANG, W. 2010. Acoustic velocity and electrical resistance of hydrate bearing sediments. *Journal of Petroleum Science and Engineering,* 70**,** 52-56.

RIEDEL, M., COLLETT, T. S., MALONE, M. J. & SCIENTISTS, T. E. Cascadia Margin Gas Hydrate. IODC Management International, 2005.

RIEDEL, M., WILLOUGHBY, E. C. & CHOPRA, S. 2010. *Geophysical Characterization of Gas Hydrates,* Tulse, OK, USA, Society of Exploration Geophysicists.

RIPMEESTER, J. A. & RATCLIFFE, C. I. 1999. On the contributions of NMR spectroscopy to clathrate science. *Journal of Structural Chemistry,* 40**,** 654-662.

ROSE, K., BOSWELL, R. & COLLETT, T. 2011. BPXA-DOE-USGS Mount Elbert gas hydrate stratigraphic test well: coring operations, core sedimentology and lithostratigraphy. *Marine and Petroleum Geology,* 28**,** 311-331.

SCHODERBEK, D. & BOSWELL, R. 2011. Ignik Sikumi #1, Gas Hydrate Test Well, Successfully Installed on the Alaska North Slope. *Fire in the Ice,* 11**,** 1-5.

SCHODERBEK, D., SMITH, B. & HESTER, K. 2012. Progress Report First Half 2012 - ConocoPhillips Gas Hydrate Production Test. *In:* SCHODERBEK, D. (ed.) *Oil & Natural Gas Technology.* Anchorage, AK: ConocoPhillips.

SELIM, M. S. & SLOAN, E. D. 1990. Hydrate Dissociation in Sediment. *SPE Reservoir Engineering,* 5**,** 245-251.

SEN, P. 1997. Resistivity of partially saturated carbonate rocks with microporosity. *GEOPHYSICS,* 62**,** 415-425.

SEO, Y.-T. & LEE, H. 2001. Multiple-Phase Hydrate Equilibria of the Ternary Carbon Dioxide, Methane, and Water Mixtures. *The Journal of Physical Chemistry B,* 105**,** 10084-10090.

SERRA, O. 1986. *Fundamentals of Well-Log Interpretation 2. The Interpretation of Logging Data*, Elsevier.

SERVIO, P. & ENGLEZOS, P. 2003. Morphology of methane and carbon dioxide hydrates formed from water droplets. *AIChE Journal,* 49**,** 269-276.

SHANKAR, U. & RIEDEL, M. 2011. Gas hydrate saturation in the Krishna-Godavari basin from P-wave velocity and electrical resistivity logs. *Marine and Petroleum Geology,* 28**,** 1768-1778.

SKOVBORG, P. & RASMUSSEN, P. 1994. A mass transport limited model for the growth of methane and ethane gas hydrates. *Chemical Engineering Science,* 49**,** 1131-1143.

SLEIJPEN, G. L. G. & FOKKEMA, D. R. 1993. BiCGSTAB(m) for Linear Equations Involving Unsymmetric Matrices with Complex Spectrum. *Electronic Transactions on Numerical Analysis.,* 1**,** 11-32.

SLOAN, E. D. 2003. Fundamental principles and applications of natural gas hydrates. *Nature,* 426**,** 353-363.

SLOAN, E. D. & KOH, C. A. 2008. *Clathrate Hydrates of Natural Gases,* Boca Raton, CRC Press.

SPANGENBERG, E. 2001. Modeling of the influence of gas hydrate content on the electrical properties of porous sediments. *J. Geophys. Res.,* 106**,** 6535-6548.

SPANGENBERG, E. & KULENKAMPFF, J. 2006. Influence of methane hydrate content on electrical sediment properties. *Geophys. Res. Lett.,* 33**,** L24315.

SPANGENBERG, E., KULENKAMPFF, J., NAUMANN, R. & ERZINGER, J. 2005. Pore space hydrate formation in a glass bead sample from methane dissolved in water. *Geophys. Res. Lett.,* 32**,** L24301.

STERN, L. A., CIRCONE, S., KIRBY, S. H. & DURHAM, W. B. 2001. Anomalous Preservation of Pure Methane Hydrate at 1 atm. *The Journal of Physical Chemistry B,* 105**,** 1756-1762.

STERN, L. A., CIRCONE, S., KIRBY, S. H. & DURHAM, W. B. 2003. Temperature, pressure, and compositional effects on anomalous or "self" preservation of gas hydrates. *Can. J. Phys.,* 81**,** 271-283.

STERN, L. A., KIRBY, S. H. & DURHAM, W. B. 1996. Peculiarities of Methane Clathrate Hydrate Formation and Solid-State Deformation, Including Possible Superheating of Water Ice. *Science,* 273**,** 1843-1848.

STERN, L. A., KIRBY, S. H. & DURHAM, W. B. 1998. Polycrystalline Methane Hydrate: Synthesis from Superheated Ice, and Low-Temperature Mechanical Properties. *Energy & Fuels,* 12**,** 201-211.

STERN, L. A., LORENSON, T. D. & PINKSTON, J. C. 2011. Gas-hydrate characterization and grain-scale imaging of recovered cores from the BPXA-DOE-USGS Mount Elbert Gas-Hydrate Stratigraphic Test Well, Milne Point, Alaska. *Marine and Petroleum Geology,* 28**,** 394-403.

STEVENS, J. C., BALDWIN, B. A., GRAUE, A., ERSLAND, G., HUSEBØ, J. & HOWARD, J. J. Measurements of Hydrate Formation in Sandstone. International Symposium of the Society of Core Analysts, 2007 Calgary, Canada.

STILLINGER, F. H. & RAHMAN, A. 1974. Improved simulation of liquid water by molecular dynamics. *The Journal of Chemical Physics,* 60**,** 1545-1557.

SULTAN, N., COCHONAT, P., FOUCHER, J. P. & MIENERT, J. 2004. Effect of gas hydrates melting on seafloor slope instability. *Marine Geology,* 213**,** 379-401.

SUM, A. K., BURRUSS, R. C. & SLOAN, E. D. 1997. Measurement of Clathrate Hydrates via Raman Spectroscopy. *The Journal of Physical Chemistry B,* 101**,** 7371-7377.

SUN, Y., GOLDBERG, D., COLLETT, T. & HUNTER, R. 2011. High-resolution well-log derived dielectric properties of gas-hydrate-bearing sediments, Mount Elbert Gas Hydrate Stratigraphic Test Well, Alaska North Slope. *Marine and Petroleum Geology,* 28**,** 450-459.

SUN, Y. F. & GOLDBERG, D. 2005. Dielectric method of high-resolution gas hydrate estimation. *Geophys. Res. Lett.,* 32**,** L04313.

SVANDAL, A., KUZNETSOVA, T. & KVAMME, B. 2006. Thermodynamic properties and phase transitions in the H2O/CO2/CH4 system. *Fluid Phase Equilibria,* 246**,** 177-184.

SVANDAL, A., KVAMME, B., GRÀNÀSY, L. & PUSZTAI, T. 2005. The influence of diffusion on hydrate growth. *Journal of Phase Equilibria and Diffusion,* 26**,** 534-538.

SWEENEY, S. A. & JENNINGS, H. Y. 1960. Effect of Wettability on the Electrical Resistivity of Carbonate Rock from a Petroleum Reservoir. *The Journal of Physical Chemistry,* 64**,** 551-553.

SØREIDE, I. & WHITSON, C. H. 1992. Peng-Robinson predictions for hydrocarbons, CO2, N2, and H2 S with pure water and NaCI brine. *Fluid Phase Equilibria,* 77**,** 217-240.

TAKEYA, S., EBINUMA, T., UCHIDA, T., NAGAO, J. & NARITA, H. 2002. Self-preservation effect and dissociation rates of CH4 hydrate. *Journal of Crystal Growth,* 237–239, Part 1**,** 379-382.

TAYLOR, C. J., MILLER, K. T., KOH, C. A. & SLOAN JR, E. D. 2007. Macroscopic investigation of hydrate film growth at the hydrocarbon/water interface. *Chemical Engineering Science,* 62**,** 6524-6533.

THOMAS, W. J. & ADAMS, M. J. 1965. Measurement of the diffusion coefficients of carbon dioxide and nitrous oxide in water and aqueous solutions of glycerol. *Transactions of the Faraday Society,* 61**,** 668-673.

TOHIDI, B., ANDERSON, R., CLENNELL, M. B., BURGASS, R. W. & BIDERKAB, A. B. 2001. Visual observation of gas-hydrate formation and dissociation in synthetic porous media by means of glass micromodels. *Geology,* 29**,** 867-870.

TORRES, M. E., COLLETT, T., ROSE, K., SAMPLE, J. C., AGENA, W. & ROSENBAUM, E. 2011. Pore fluid geochemistry from the Mount Elbert gas hydrate stratigraphic test well, Alaska North Slope. *Marine and Petroleum Geology,* 28**,** 332-342.

TORRES, M. E., TRÉHU, A. M., CESPEDES, N., KASTNER, M., WORTMANN, U. G., KIM, J. H., LONG, P., MALINVERNO, A., POHLMAN, J. W., RIEDEL, M. & COLLETT, T. 2008. Methane hydrate formation in turbidite sediments of northern Cascadia, IODP Expedition 311. *Earth and Planetary Science Letters,* 271**,** 170-180.

UCHIDA, T., EBINUMA, T., KAWABATA, J. I. & NARITA, H. 1999. Microscopic observations of formation processes of clathrate-hydrate films at an interface between water and carbon dioxide. *Journal of Crystal Growth,* 204**,** 348-356.

UCHIDA, T., TAKEYA, S., EBINUMA, T. & NARITA, H. Replacing Methance with CO2 in Clathrate Hydrate: Observations using Raman Spectroscopy. *In:* DURIE, R. A., MCMULIAN, P., PAULSON, C. A. J., SMITH, A. Y. & WILLIAMS, D. J., eds. 5th International Conference on Greenhouse Gas Control Technologies, 2000 Caims, East Melbourne, Australia. CSIRO Publishing.

UDDIN, M., WRIGHT, F. & COOMBE, D. A. 2011. Numerical Study of Gas Evolution and Transport Behaviours in Natural Gas-Hydrate Reservoirs. *Journal of Canadian Petroleum Technology,* 50**,** pp. 70-89.

VALIULLIN, R. & FURO, I. 2002. The morphology of coexisting liquid and frozen phases in porous materials as revealed by exchange of nuclear spin magnetization followed by ^{1}H nuclear magnetic resonance. *The Journal of Chemical Physics,* 117**,** 2307-2316.

VAN DER VORST, H. A. 1992. BI-CGSTAB: a fast and smoothly converging variant of BI-CG for the solution of nonsymmetric linear systems. *SIAM J. Sci. Stat. Comput.,* 13**,** 631-644.

VYSNIAUSKAS, A. & BISHNOI, P. R. 1983. A kinetic study of methane hydrate formation. *Chemical Engineering Science,* 38**,** 1061-1072.

WAALS, J. H. V. D. & PLATTEEUW, J. C. 1959. Clathrate Solutions. *Advances in Chemical Physics.* John Wiley & Sons, Inc.

WAITE, W. F., SANTAMARINA, J. C., CORTES, D. D., DIUGAN, B., ESPINOZA, D. N., GERMAINE, J., JANG, J., JUNG, J. W., KNEAFSEY, T. J., SHIN, H., SOGA, K., WINTERS, W. J. & YUN, T. S. 2009. Physical properties of hydrate-bearing sediments. *Rev. Geophys.,* 47.

WARZINSKI, R. P., GAMWO, I. K., ROSENBAUM, E. J., MYSHAKIN, E. M., JIANG, H., JORDAN, K. D., ENGLISH, N. J. & SHAW, D. W. Thermal Properties of Methane Hydrate by Experiment and Modeling and Impacts upon Technology. 6th International Conference on Gas Hydrates, July 6-10 2008 Vancouver, Canada.

WEI, J.-Z. & LILE, O. B. 1991. Influence of Wettability on Two- and Four-Electrode Resistivity Measurements on Berea Sandstone Plugs. *SPE Formation Evaluation,* 6**,** 470-476.

WEITEMEYER, K. A., CONSTABLE, S. C., KEY, K. W. & BEHRENS, J. P. 2006. First results from a marine controlled-source electromagnetic survey to detect gas hydrates offshore Oregon. *Geophys. Res. Lett.,* 33**,** L03304.

WHITE, M. D., WURSTNER, S. K. & MCGRAIL, B. P. 2011. Numerical studies of methane production from Class 1 gas hydrate accumulations enhanced with carbon dioxide injection. *Marine and Petroleum Geology,* 28**,** 546-560.

WILDER, J. W., MORIDIS, G. J., WILSON, S. J., KURIHARA, M., WHITE, M. D., MASUDA, Y., ANDERSON, B. J., COLLETT, T. S., HUNTER, R. B., NARITA, H., POOLADI-DARVISH, M., ROSE, K. & BOSWELL, R. An international effort to compare gas hydrate reservoir simulators. ICGH 2008, July 6-10 2008 Vancouver BC, Canada.

WILSON, S. J., HUNTER, R. B., COLLETT, T. S., HANCOCK, S., BOSWELL, R. & ANDERSON, B. J. 2011. Alaska North Slope regional gas hydrate production modeling forecasts. *Marine and Petroleum Geology,* 28**,** 460-477.

WINTERS, W. J., WALKER, M., HUNTER, R., COLLETT, T., BOSWELL, R., ROSE, K., WAITE, W. F., TORRES, M. E., PATIL, S. & DANDEKAR, A. 2011. Physical properties of sediment from the BPXA-DOE-USGS Mount Elbert gas hydrate stratigraphic test well. *Marine and Petroleum Geology,* 28**,** 361-380.

WORTHINGTON, P. F. & PALLATT, N. 1992. Effect of Variable Saturation Exponent on the Evaluation of Hydrocarbon Saturation. *SPE Formation Evaluation,* 7**,** 331-336.

WORTHINGTON, P. F., PALLATT, N. & TOUSSAINT-JACKSON, J. E. 1989. Influence of Microporosity on the Evaluation of Hydrocarbon Saturation. *SPE Formation Evaluation,* 4**,** 203-209.

YAMAMOTO, K. & DALLIMORE, S. R. 2008. Aurora-JOGMEC-MRCan Mallik 2006-2008 Gas Hydrate Research Project Progress. *Fire in the ice,* 8**,** 1-5.

YAMAMOTO, K., INADA, N., KUBO, S., FUJII, T., SUZUKI, K. & KONNO, Y. 2012. Pressure Core Sampling in the Eastern Nankai Trough. *Fire in the Ice,* 12.

YANG, S., ZHANG, H., WU, N., SU, X., SCHULTHEISS, P., HOLLAND, M., ZHANG, G., LIANG, J., LU, J. & ROSE, K. High Concentration Hydrate in Disseminated Forms Obtained in Shenhu Area, North Slope of South China Sea. 6th International Conference on Gas Hydrates, 2008 Vancouver, BC, Canada.

YOUSIF, M. H., ABASS, H. H., SELIM, M. S. & SLOAN, E. D. 1991. Experimental and theoretical investigation of Methane-Gas-Hydrate Dissociation in Porous Media. *SPE Reservoir Engineering,* 6**,** 69-76.

YUAN, Q., SUN, C.-Y., LIU, B., WANG, X., MA, Z.-W., MA, Q.-L., YANG, L.-Y., CHEN, G.-J., LI, Q.-P., LI, S. & ZHANG, K. 2013. Methane recovery from natural gas hydrate in porous sediment using pressurized liquid CO2. *Energy Conversion and Management,* 67**,** 257-264.

ZHOU, D. & STENBY, E. H. 1997. A Percolation Study of Wettability Effect on the Electrical Properties of Reservior Rocks. *Transport in Porous Media,* 29**,** 85-98.

Appendix A – Additional Experimental Setups

A microscopy setup combined with time-lapse photography has been slightly modified to prepare for hydrate formation tests, as there is a current need for enhanced understanding of mechanisms involved on pore-scale. This setup may be able to provide information related to hydrate growth pattern and impact on resistivity and exchange efficiency.

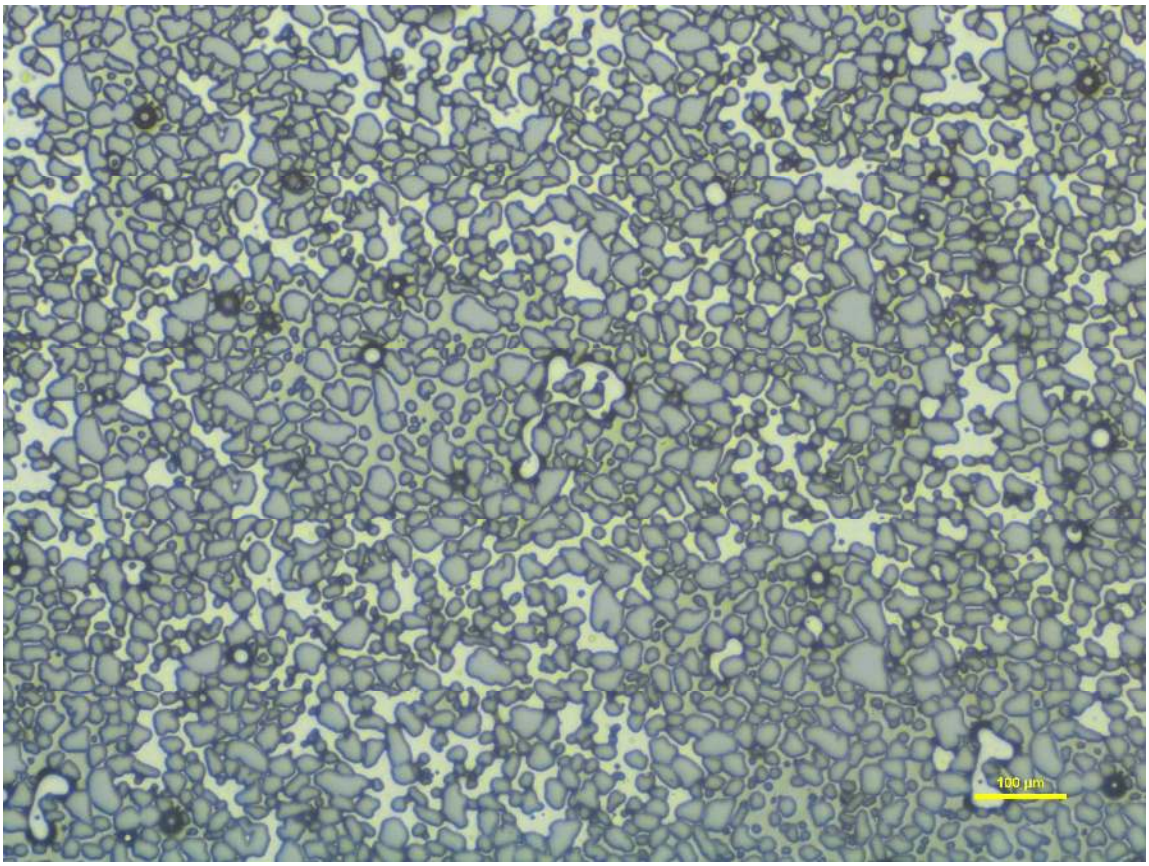

Figure I – Etched silicon wafer micro model partially saturated with water and CH_4. Grey indicates minerals, while lighter grey is water and bright color is CH_4. Water occupies smaller pores and occluded sections, such as the middle left section. This was bypassed during drainage because of extensive capillary pressure.

A second setup was designed and built in an attempt to minimize contribution from boundary effects and to prepare for up-scaling. The block setups is compatible with large blocks (20cm*10cm*6cm) or sand-packs (up to 5.4 l), which will be used for continued evaluation of exchange efficiency. A combined resistivity and seismic evaluation study is currently planned.

Figure II – A high pressure vessel has been designed and built. The larger volume and additional connections are useful for up-scaling of future gas hydrate experiments.

Scientific Papers